



UNIL | Université de Lausanne

Unicentre

CH-1015 Lausanne

<http://serval.unil.ch>

---

Year : 2019

## NUMERICAL MODELLING OF THERMO-MECHANICAL COUPLING: EFFECTS OF STRAIN HEATING ON THE ICE FLOW

Licul Aleksandar

Licul Aleksandar, 2019, NUMERICAL MODELLING OF THERMO-MECHANICAL COUPLING:  
EFFECTS OF STRAIN HEATING ON THE ICE FLOW

Originally published at : Thesis, University of Lausanne

Posted at the University of Lausanne Open Archive <http://serval.unil.ch>

Document URN : urn:nbn:ch:serval-BIB\_1010104D48793

### **Droits d'auteur**

L'Université de Lausanne attire expressément l'attention des utilisateurs sur le fait que tous les documents publiés dans l'Archive SERVAL sont protégés par le droit d'auteur, conformément à la loi fédérale sur le droit d'auteur et les droits voisins (LDA). A ce titre, il est indispensable d'obtenir le consentement préalable de l'auteur et/ou de l'éditeur avant toute utilisation d'une oeuvre ou d'une partie d'une oeuvre ne relevant pas d'une utilisation à des fins personnelles au sens de la LDA (art. 19, al. 1 lettre a). A défaut, tout contrevenant s'expose aux sanctions prévues par cette loi. Nous déclinons toute responsabilité en la matière.

### **Copyright**

The University of Lausanne expressly draws the attention of users to the fact that all documents published in the SERVAL Archive are protected by copyright in accordance with federal law on copyright and similar rights (LDA). Accordingly it is indispensable to obtain prior consent from the author and/or publisher before any use of a work or part of a work for purposes other than personal use within the meaning of LDA (art. 19, para. 1 letter a). Failure to do so will expose offenders to the sanctions laid down by this law. We accept no liability in this respect.

Faculté des géosciences et de l'environnement  
Institut des dynamiques de la surface terrestre

NUMERICAL MODELLING OF THERMO-MECHANICAL  
COUPLING: EFFECTS OF STRAIN HEATING ON THE ICE  
FLOW

THÈSE DE DOCTORAT

présentée à la Faculté des géosciences et de l'environnement de l'Université de Lausanne  
pour l'obtention du grade de Docteur en sciences de la Terre par

ALEKSANDAR LICUL

Maîtrise ès physique et géophysique de l'Université de Zagreb

Jury

Prof. Dr. Frédéric Herman	Université de Lausanne	Directeur de thèse
Prof. Dr. Yury Y. Podladchikov	Université de Lausanne	Expert interne
Dr. Thomas Zwinger	Finnish IT Center for Science	Expert externe
Prof. Dr. Christian Kull	Université de Lausanne	Président du jury

Lausanne, 2019





UNIL | Université de Lausanne  
Faculté des géosciences et de l'environnement  
bâtiment Géopolis bureau 4631

## IMPRIMATUR

Vu le rapport présenté par le jury d'examen, composé de

Président de la séance publique :	M. le Professeur Christian Kull
Président du colloque :	M. le Professeur Christian Kull
Directeur de thèse :	M. le Professeur Frédéric Herman
Expert interne :	M. le Professeur Yury Podladchikov
Expert externe :	M. le Docteur Thomas Zwinger

Le Doyen de la Faculté des géosciences et de l'environnement autorise l'impression de la thèse de

### **Monsieur Aleksandar LICUL**

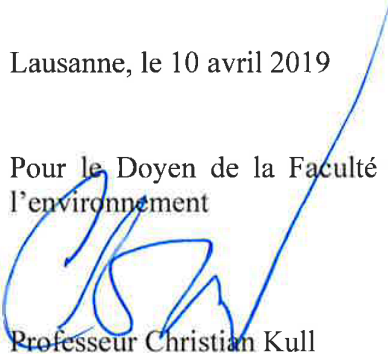
Titulaire d'un  
*Master in Physics and Geophysics*  
*de l'Université de Zagreb*

intitulée

### **Numerical Modelling of Thermo-Mechanical Coupling: Effects of Strain Heating on the Ice Flow**

Lausanne, le 10 avril 2019

Pour le Doyen de la Faculté des géosciences et de  
l'environnement

  
Professeur Christian Kull



*In dedication to my wife Ivana*



---

## Contents

---

<b>1</b>	<b>Introduction</b>	<b>1</b>
1.1	General . . . . .	2
1.2	First order physics and a mathematical model . . . . .	3
1.3	Numerical modelling and numerical model development . . . . .	4
1.4	Research questions . . . . .	5
<b>2</b>	<b>Modelling the coupled thermo-mechanical ice flow using the implicit pseudo-transient method on the computer graphics cards</b>	<b>17</b>
2.1	Introduction . . . . .	19
2.2	Model . . . . .	20
2.2.1	Mathematical model . . . . .	20
2.2.2	Numerical implementation . . . . .	23
2.3	Implementation of the method on computer graphic cards . . . . .	27
2.4	Model configuration . . . . .	29
2.5	Results and performance . . . . .	31
2.5.1	Experiments results . . . . .	31
2.5.2	Computational performance . . . . .	48
2.6	Discussion . . . . .	52
2.7	Conclusions . . . . .	54

---

<b>3</b>	<b>The effect of strain heating on the ice flow</b>	<b>65</b>
3.1	General introduction: Towards an effective boundary condition . . . . .	67
3.2	Literature review on the effects of strain heating on ice flow . . . . .	68
3.3	Model . . . . .	72
3.3.1	Mathematical model . . . . .	72
3.3.2	Numerical model setup . . . . .	74
3.4	Results . . . . .	77
3.5	Parametrization of 1D numerical profiles of velocity and temperature . . . . .	83
3.6	Effects of strain heating for typical ice mass parameters . . . . .	92
3.7	Discussion and summary . . . . .	95
3.7.1	Discussion of the results . . . . .	95
3.7.2	Comparison to previous literature . . . . .	98
3.8	Conclusions . . . . .	101
<b>4</b>	<b>Perspectives</b>	<b>113</b>
4.1	General remarks . . . . .	114
4.2	Future work . . . . .	115





## Abstract

Observations of ice velocity on ice sheets and glaciers suggest two significantly different modes of ice flow: slow and fast flow, with up to three orders of magnitude differences in flow velocity between the two. Understanding the physical processes governing the ice flow is of crucial importance if one wishes to predict the future sea level rise due to the global warming. This heterogeneity in flow velocities can be often explained by the thermo-mechanical coupling and the so called creep instability mechanics. Creep instability or thermal runaway mechanism is a process which revolves around a simple concept of a positive feedback between deformation rate of ice and temperature. Increasing the deformation rate, rises the ice temperature, through strain heating, which further increases the ice deformation rate. Unfortunately, most current ice flow models are known for their inability to predict and model this strong heterogeneity observed in ice flow velocities. This is mostly because current Stokes solvers are computationally demanding and often require the use of modern supercomputers and sophisticated algorithms. Additionally, most of the ice flow models are based on simplifying approximations of the mechanical solver, while often neglecting the energy coupling. Nevertheless, most of the current ice flow models are not very well adapted to all modern trends in the hardware industry based around many core architectures. Further, they are to a large extent mostly serial and not easily parallelizable.

In this thesis I address these challenges by developing an ice flow model based on the iterative pseudo-transient (PT) continuation method. The method relies on the usage of matrix-free stencil based method, therefore ensuring minimal, local and regular memory access. This algorithm properties are well suited for modern massively parallel hardware accelerators like the computer graphic cards. To numerically couple the thermal and mechanical solver an implicit coupling method is used. Our results show that two orders of magnitude increase in performance can be obtained over the vectorised CPU version of the algorithm on a single GPU, in turn enabling us to perform high resolution three dimensional modelling of the thermo-mechanically coupled ice flow on a personal computer. Additionally, we have shown that, in order to fully resolve the non linearities associated with the ice flow rheology a high spatial and temporal resolution is needed.

Finally, I have further investigated how important heat source strain heating can be. I found during the course of this thesis that strain heating is the main internal volumetric heat source in the conservation of energy. Its influence is dynamic and it is primarily dependent on the distribution of stress, ice velocity and temperature. Hence it can vary significantly both in space and time. It can be a significant heat source in some situations, while non important in others, nevertheless it should never be discarded since it provides a crucial balance needed for a proper conservation of mass, energy and momentum. Additionally, my results shown that strain heating is a process which operates on different time scales and that two distinctive

regimes are usually associated with the strain heating; transient and steady state. Hence, if one wishes to determine the importance of strain heating as a volumetric heat source it needs to take both regimes into consideration.



## Résumé

L'observation de la vitesse de la glace sur les calottes glaciaires et les glaciers suggère deux modes d'écoulement glaciaire très différents : l'écoulement lent et l'écoulement rapide, avec des différences jusqu'à trois ordres de grandeur de vitesse d'écoulement entre les deux. Comprendre les processus physiques régissant l'écoulement de la glace est d'une importance cruciale si l'on souhaite prédire l'élévation future du niveau de la mer due au réchauffement de la planète. Cette hétérogénéité des vitesses d'écoulement est souvent expliquée par le couplage thermomécanique et par la mécanique d'instabilité liée au fluage. L'instabilité de fluage, ou mécanisme d'emballage thermique, est un processus qui repose sur un concept simple de rétroaction positive entre le taux de déformation de la glace et la température. En augmentant le taux de déformation, la température de la glace augmente, en chauffant la base, ce qui augmente encore le taux de déformation de la glace.

Malheureusement, les modèles actuels d'écoulement de la glace sont connus pour leur incapacité à prédire et à modéliser cette forte hétérogénéité observée dans les vitesses d'écoulement de la glace. Cela est principalement dû au fait que les solveurs Stokes actuels exigent des calculs complexes et nécessitent souvent l'utilisation de supercalculateurs modernes et d'algorithmes sophistiqués. En outre, la plupart des modèles d'écoulement de la glace reposent sur la simplification des approximations du solveur mécanique, tout en négligeant souvent le couplage énergétique. Néanmoins, la plupart des modèles d'écoulement de glace actuels ne sont pas très adaptés aux tendances modernes de l'industrie du matériel basées sur de nombreuses architectures de base. En outre, ils sont dans une large mesure principalement en série et difficilement parallélisables.

Dans cette thèse, j'aborde ces défis en développant un modèle d'écoulement de la glace basé sur la méthode de continuation pseudo-transitoire (PT) itérative. Cette méthode repose sur l'utilisation d'une méthode sans matrice basée sur le gabarit, garantissant ainsi un accès mémoire minimal, local et régulier. Les propriétés de cet algorithme sont bien adaptées aux accélérateurs matériels massivement parallèles modernes tels que les cartes graphiques d'ordinateur. Pour coupler numériquement le solveur thermique et mécanique, une méthode de couplage implicite est utilisée. Nos résultats montrent qu'il est possible d'obtenir une augmentation de deux ordres de grandeur des performances par rapport à la version CPU de l'algorithme vectorisée sur un seul GPU. Cela nous permet ainsi de réaliser une modélisation tridimensionnelle à haute résolution de la circulation de la glace couplée thermo-mécaniquement sur un ordinateur personnel. De plus, je montre que, pour résoudre complètement les non-linéarités associées à la rhéologie des écoulements de glace, une résolution spatiale et temporelle élevée est nécessaire.

Finalement, j'ai également étudié à quel point le chauffage par contrainte de source de chaleur peut être important. J'ai pu établir que le chauffage par contrainte est la principale source de

---

chaleur volumétrique interne dans la conservation de l'énergie. Son influence est dynamique et dépend principalement de la répartition des contraintes, de la vitesse de la glace et de la température. Par conséquent, il peut varier considérablement dans l'espace et dans le temps. Il peut constituer une source de chaleur importante dans certaines situations, mais pas dans d'autres. Néanmoins, il ne faut jamais le rejeter car il constitue un équilibre crucial nécessaire à la conservation appropriée de la masse, de l'énergie et de la quantité de mouvement. De plus, nos résultats ont montré que le chauffage par contrainte est un processus qui fonctionne à différentes échelles de temps et que deux régimes distincts sont généralement associés au chauffage par contrainte; état transitoire et stable. Par conséquent, si l'on souhaite déterminer l'importance du chauffage par déformation en tant que source de chaleur volumétrique, il convient de prendre en compte les deux régimes.



# CHAPTER 1

---

Introduction

---

## 1.1 General

Ice sheets and glaciers represent a major component of the Earth climate system and are tightly coupled to both the ocean and the atmosphere dynamics. Understanding the dynamics of the ice flow therefore is of special interest in today's global warming world. This is mostly because of the large volume of water contained in the glaciers and ice sheets and can hence represent a potential hazard on both the human life and property (Solomon et al., 2007). This applies to both the coastal regions and the high mountainous regions. The coastal regions are affected by potential, worldwide sea level rise associated with the melting of ice sheets. On the other hand, the mountainous regions are at risk of both the abrupt floods and glacier collapses. Both can have catastrophic environmental and socio-economic consequences.

Sea level rise is mostly associated to the ice discharge from both the Antarctic and Greenland ice sheets. Observations of ice velocity obtained from the satellite measurements, reveal two distinct ice flow regimes, slow and fast. The typical velocity range for the slow flow is between a few meters per year ( $\frac{\text{m}}{\text{yr}}$ ) to up to a  $100 \frac{\text{m}}{\text{yr}}$ . Fast ice flow is usually associated with basal sliding and the typical velocity range can be found anywhere between  $100 \frac{\text{m}}{\text{yr}}$  and  $10 \frac{\text{km}}{\text{yr}}$ . On both ice sheets, slow ice flow can be found on the largest part of the ice sheet surface. In contrast, the fast flow is usually associated with the ice streams. The fast flow can be found on less than 10% of ice sheet surface, but it can carry even up to 90% of ice discharge into the ocean (Bamber et al., 2000). For example, we show this ice flow velocity heterogeneity in Figure 1.1 for Greenland and Antarctica ice sheets. Explanations for this ice flow heterogeneity are often attributed to the topographic and/or geologic control. In example, significant basal topography can direct the flow into the steep narrow channels, therefore significantly affecting the stress state and focusing all the ice flow into the channel. On the other hand, geology affects the properties of the bed itself (Clarke, 2005). For example, the transition from slow to fast flow can coincide with the transition from hard bed to the soft bed. The existence and temporal variability of some of the ice streams cannot be explained by either the topographic or geologic control. These are known as pure ice streams and can mostly be found in the Siple Coast region of Antarctica, hence a different physical mechanism needs to be invoked to explain and predict spontaneous generation and evolution of pure ice streams. This has long been recognized as a crucial task in the glaciology community (Brinkerhoff and Johnson, 2015; Bueler and Brown, 2009; Haseloff et al., 2018; Kyrke-Smith et al., 2015; Payne and Dongelmans, 1997; Suckale et al., 2014). Often, two different physical mechanisms are invoked to explain the striking difference in the ice flow velocities between stream and sheet flow. The first one is the thermal runaway (Clarke et al., 1977; Yuen and Schubert, 1979b), often also called creep instability, while the other is hydraulic runaway or instability (Fowler and Johnson, 1996). The former is related to the non-linear feedbacks between the ice temperature and velocity. The later is associated with melt-water drainage

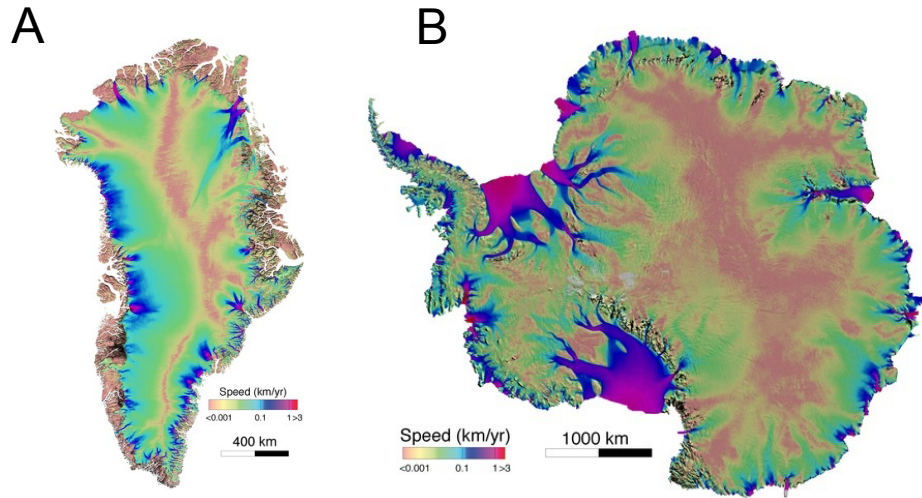


**Figure 1.1:** A) Greenland velocity field B) Antarctica velocity field. Figure modified from Mougnot et al.(2017)

system (distributed or channelized) and non-linear feedbacks between the ice velocity and basal water pressure through a phenomenological sliding law dependent on the effective pressure. Interestingly, these two distinct mechanisms are not exclusive of each other since they are linked through the production of basal melt-water. Similarly, both physical mechanisms are often invoked to explain, still unresolved, glacier surging phenomena. It is therefore often speculated that streaming and surging can arise solely as a result of thermo-mechanical feedbacks (Clarke et al., 1977; Payne and Dongelmans, 1997; Schubert and Yuen, 1982; Yuen and Schubert, 1979b). Surging is explained as a temporal variation occurring when an ice flow is constrained to flow in one direction, while the streaming occurs in the three dimensions when the flow is horizontally free (Fowler and Johnson 1996, Payne 1997).

## 1.2 First order physics and a mathematical model

Since the 1950s, it is a well-established fact in glaciology that at the first order physics of the ice flow is best described by a mathematical model for gravity-driven viscous fluid with a strong temperature dependence of viscosity (Grigoryan et al., 1976; Hutter, 1983; Morland, 1984; Robin, 1955). This results in a mathematical model which is described by a set of highly non-linear coupled mathematical equations not susceptible to an analytical treatment.

The strongest nonlinearities inherent to the ice flow are associated with the ice rheology. The ice rheology is given by a stress-strain rate relation which describes the secondary creep rate of ice (also called steady state creep). It is usually described by a power law with a power law exponent (Glen, 1955, 1952; Steinemann, 1958) or by a hyperbolic flow law (Garofalo,

1963; Wong and Jonas, 1968). The value of the power law exponent is still heavily debated in the glaciology community (Bons et al., 2018). However, the commonly used value in ice flow modelling is 3. In both cases, the rate factor varies with temperature and is described by an Arrhenius type exponential dependence. Hence, ice velocity strongly depends, through ice viscosity, on temperature, while the temperature depends on strain heating. How strong is this coupling and how important strain heating is for the ice flow is still elusive. Although this was a topic of numerous previous studies opposing conclusions were made (Clarke et al., 1977; Fowler et al., 2010; Grigoryan et al., 1976; Yuen and Schubert, 1979b).

It is a well established fact that multi-coupled nonlinear problems, such as the ice flow, can result in a highly localized multi scale problem, both in space and time. Additionally, it is unknown a priori where and when this localization will occur. Therefore, the ice flow is a multi-physics and multi-scale problem and to resolve all the physics a high numerical spatial and temporal resolution is needed.

### 1.3 Numerical modelling and numerical model development

The publication of the fourth Intergovernmental Panel on Climate Change (IPCC) assessment report (Solomon et al., 2007) revealed that ice sheet flow models did not provide an accurate description of polar ice sheet discharge due to their inability to model slow and fast ice flow simultaneously and their inability to correctly capture marine ice sheet dynamics (Bueler and Brown, 2009; Gagliardini et al., 2013; Pattyn et al., 2008). This was attributed to the fact that at the time most ice flow models were based on simplified asymptotic approximations of the Stokes flow. Since then, the main focus of ice flow modelling community has been on the mechanics of the ice flow either through development of more computationally tractable shallow models or through the development of the Stokes flow models. Additionally, extensive effort was invested into the development of more physics based enthalpy based model (Aschwanden et al., 2012; Gilbert et al., 2014; Hewitt and Schoof, 2017; Schoof and Hewitt, 2016) and the investigation of its numerical properties (Kleiner et al., 2015). Unfortunately, these studies are concentrated on a single model, i.e. either mechanical model or temperature/energy model, and no feedbacks were explored. Hence, even though a variety of energy/thermo-mechanically coupled models exist little investigation is done into the verification of the obtained numerical solutions. This is mostly due to the lack of analytical solutions. Meanwhile model benchmarks are often concentrated on verifying the implementation of the mechanical model only, i.e. EISMINT (Huybrechts and Payne, 1996) and ISMIP-HOM (Pattyn et al., 2008) benchmark experiments, while only a single model inter-comparison investigating the physical thermo-mechanical coupling exist, i.e. EISMINT 2 (Payne et al., 2000). Unfortunately, the experiments in EISMINT 2 are usually performed using a thermo-coupled shallow approximation model, i.e. shallow ice model or a first order model. Therefore, aforementioned studies

reveal that thermo-mechanically coupled models do not converge below the grid refinement. Numerically resolving the first order physics governing the ice flow is imperative to properly model and predict the complex behaviour of real ice sheets and glaciers. This can be a especially challenging task in three dimensions (3-D) with the current numerical models. As already numerically investigated by Payne and Dongelmans (1997), three dimensional modelling is a necessity if one plans to investigate formation and evolution of ice streams and surges.

Unfortunately, high resolution three dimensional modelling of the coupled thermo-mechanical solver with existing Stokes flow models is currently reserved for supercomputers and often require the assistance of computer scientists. It is a well known fact that the Stokes solver with non linear rheology is computationally most challenging part of the problem. This is mostly because the current algorithms require the assembly (and inversion) of large sparse matrices to solve the linear problem. The solution of the linear problem can be obtained by using the so called direct solvers in 1-D and 2-D and iterative in 3-D. The memory requirements associated with the matrix assembly (and inversion) grow linearly in 1-D, quadratically in 2-D and cubically in 3-D, therefore high resolution modelling can quickly saturate the available computer memory and any meaningful numerical resolution is not easily achievable with a personal computer. Additionally, algorithms based around matrix assembly are intrinsically serial and often require non regular (random) memory access. Random memory access can be up to two orders of magnitude slower then the regular one (Omlin, 2017). Furthermore, significant reduction in parallel efficiency can be expected. Additionally, advantages of the direct solver, i.e. like the indifference to a high viscosity ratios, vanishes in 3-D when a iterative linear solver is used.

Today, most commonly used computational units are parallel devices based around multi core (CPUs) and many core architectures (GPUs, MIC). Accordingly, these devices are most suited for parallel based algorithms. In addition, current hardware is limited by memory access/transfer speed and not the floating point performance. Hence, faster computation speed often does not bring any significant reduction in wall time. This is especially true for the memory bounded algorithms. Development of the new numerical models suited to the current hardware, combined with an exponential development of the computer graphic cards in the last decade, is a path which can bring most performance increase in a smallest amount of time.

## 1.4 Research questions

We have identified the following challenges that we will try to tackle in this thesis:

1. How to efficiently numerically solve thermo-mechanically coupled flow in 3-D by taking advantage of the modern hardware?
2. How to sufficiently numerically resolve all the non linearities governing the ice flow? In particular, determining which spatial and temporal numerical resolution is sufficient?
3. Do we need additional heat sources to heat the ice to the melting temperature at the base? How significant heat source is the strain heating?
4. Can the heterogeneity in ice flow velocities be explained only by a creep instability mechanism?

We plan to tackle this challenges by developing a thermo-mechanically coupled Stokes solver that efficiently utilize the modern computer graphic card accelerators or graphical processing units (GPUs).

The GPUs are massively parallel devices originally developed to transfer the computations regarding the computer visualization from the central processing unit (CPU) and therefore relaxing at least some computational load from the more serial task oriented CPU. A GPU is hence optimized for calculating the color of a pixel independently from each other; in which case latency can be masked by high throughput, i.e., compute as many threads as possible in a reasonable time. The GPUs programming model is based around a well-known parallel principle called Single Instruction Multiple Data (SIMD), where each single instruction is executed on multiple data. Therefore a block of instructions can be executed by thousands of different threads in parallel fashion, each thread calculating a single grid point. The GPUs are, in consequence, perfectly suited for stencil based numerical methods like the finite difference method (FDM). Additionally with the usage of staggered regular grid stencil operation, i.e. derivative calculation, requires only neighbouring values, therefore memory access is minimal, local and regular. This can result in significant performance increases since all the performant properties of modern hardware are taken in consideration while developing an algorithm. Furthermore, we plan to use an iterative matrix free pseudo-transient (PT) continuation method (Kelley and Keyes, 1998; Yang and Mittal, 2014) to minimise the resulting system residuals thus avoiding the drawbacks like the need for a matrix assembly, set-up and inversion. Additional benefits from our approach reside in the ease of numerically coupling mechanical and energy/temperature solvers and the fact that the obtained solution is implicit, in a sense that both velocity and temperature are determined simultaneously. Accordingly, we expect to gain significant performance increase that will enable us to make use of the high numerical resolution, both spatial and temporal, on a consumer desktops with NVIDIA graphic cards.

The crucial step while developing a numerical model is the verification of obtained numerical solutions. The goal is to obtain at least some knowledge on how well the numerical model approximate the mathematical model used to describe a physical process one wishes to study.

This can ideally be achieved by comparing the obtained numerical results with analytical solutions when available. By constructing the so called manufactured analytical solution or by benchmarking the numerical model results with the solutions of other existing numerical models in a variety of different, carefully thought scenarios. Unfortunately, every approach has a significant drawback. Analytical solutions are almost impossible to obtain for such complex three dimensional physics. Hence, analytical solutions are often obtainable only for the very specific cases and are not representative of the full system behaviour. Manufactured analytical solutions can verify that the algorithm is implemented correctly, i.e. reduce the probability of implementation errors to a minimum, but unfortunately uses non physical source terms and therefore can not give as any information about the actual physical model we want to simulate (Brown, 2011). Even though both presented methods can provide us with some kind of measurement error (i.e. discretization error), there is a significant difference between the two, given that the error obtained by measuring against analytical solution inform us how well our numerical model approximate the true physical process described by a given mathematical model, therefore capturing both spatial scales and time scales for the processes to operate. The third option for verifying the numerical implementation are the community model benchmarks. They often include the numerical solutions of different continuum assumptions and they are therefore not numerically solving the same mathematical model. This makes it almost impossible to create a meaningful measurement of the numerical errors even between the models of the same continuum assumptions. Nevertheless if a problem of sufficient complexity is addressed, model benchmark can at least point to, or reveal new, complications with participating models (Bueler, 2008).

In this thesis we plan to investigate the numerical and computational behaviour of our a new numerical model for ice sheets and glaciers by benchmarking it against a variety of analytical solutions and by comparison with solutions obtained by more commonly used models. We start in Chapter 2 by presenting an iterative pseudo transient (PT) method used to numerically solve the thermo mechanically coupled mathematical model describing the ice flow. In this chapter we further present the algorithm implementation on modern computer graphic cards and take advantage of its intrinsic parallelism. We also show significant performance gain, up to two orders of magnitude, while using the GPU implementation compared to a vectorised CPU version. Hence, avoiding the limitations imposed by some more often used methods. We find that high spatial and temporal numerical resolution is needed to capture the highly non linear ice flow. In Chapter 3, using the developed model, we have investigated the influence of different physical processes on the coupled flow, i.e. additional stress gradients, advection and diffusion. We have shown that additional stress gradients can have a first order effect on the solution. We have further shown two different regimes on which strain heating can operate. Additionally importance of advection in stabilizing the flow was shown. Finally, we present our conclusions and future work directions in Chapter 4.

## Bibliography

- Aschwanden, A., Bueler, E., Khroulev, C., Blatter, H., 2012. An enthalpy formulation for glaciers and ice sheets. *Journal of Glaciology* 58(209), 441–457.
- Bamber, J. L., Vaughan, D. G., Joughin, I., 2000. Widespread Complex Flow in the Interior of the Antarctic Ice Sheet. *Annals of Glaciology* 287, 1248–1250.
- Baral, D., Hutter, K., Greve, R., 2001. Asymptotic theories of large-scale motion, temperature, and moisture distribution in land-based polythermal ice sheets: A critical review and new developments. *Applied Mechanics Reviews* 54, 215–256.
- Bassis, J., 2010. Hamilton-type principles applied to ice-sheet dynamics: new approximations for large-scale ice sheet flow. *Journal of Glaciology* (56)97, 497–513.
- Blatter, H., 1995. Velocity and stress fields in grounded glaciers: a simple algorithm for including deviatoric stress gradients. *Journal of Glaciology* 5(138), 333–344.
- Bons, P. D., Kleiner, T., Llorens, M., Prior, D. J., Sachau, T., Weikusat, I., Jansen, D., 2018. Greenland Ice Sheet: Higher nonlinearity of ice flow significantly reduces estimated basal motion. *Geophysical Research Letters* 45, 6542–6548.
- Brinkerhoff, D. J., Johnson, J. V., 2013. Data assimilation and prognostic whole ice sheet modelling with the variationally derived, higher order, open source, and fully parallel ice sheet model VarGlaS. *The Cryosphere* 7, 1161–1184.
- Brinkerhoff, D. J., Johnson, J. V., 2015. Dynamics of thermally induced ice streams simulated with a higher-order flow model. *Journal of Geophysical Research: Earth Surface* 120, 1743–1770.
- Brown, J. A. K., 2011. Computational methods for ice flow simulation. Ph.D thesis, ETH Zürich.
- Bueler, E., 2008. Lessons from the short history of ice sheet model intercomparison. *The Cryosphere Discussions* 2, 399–412.
- Bueler, E., Brown, J., 2009. Shallow shelf approximation as a "sliding law" in a thermomechanically coupled ice sheet model. *Journal of Geophysical research* 114, F03008.
- Bueler, E., Brown, J., Lingle, C., 2007. Exact solutions to the thermomechanically coupled shallow-ice approximation: effective tools for verification. *Journal of Glaciology* 53(182), 499–516.

- Burg, J.-P., Gerya, T. V., 2005. The role of viscous heating in Barrovian metamorphism of collisional orogens: thermomechanical models and application to the Lepontine Dome in the Central Alps. *Journal of Metamorphic Geology* 23, 75–95.
- Chandler, D. M., Hubbard, A. L., Hubbard, B. P., Nienow, P. W., 2006. A Monte Carlo error analysis for basal sliding velocity calculations. *Journal of Geophysical Research* 111, F04005.
- Choi, E., Tan, E., Lavier, L. L., Calo, V. M., 2013. DynEarthSol2D: An efficient unstructured finite element method to study long-term tectonic deformation. *Journal of Geophysical Research: Solid Earth* 118(5), 2429–2444.
- Clarke, G. K. C., 2005. Subglacial processes. *Annual Review of Earth and Planetary Sciences* 33, 247–276.
- Clarke, G. K. C., Nitsan, U., Paterson, W. S. B., 1977. Strain heating and creep instability in glaciers and ice sheets. *Reviews of geophysics and space physics* 15 (2), 235–247.
- Cohen, D., Iverson, N. R., Hooyer, T. S., Fischer, U. H., Jackson, M., Moore, P. L., 2005. Debris-bed friction of hard-bedded glaciers. *Journal of Geophysical Research* 110, F02007.
- Cook, S., 2012. *CUDA Programming*. Morgan Kaufmann, Elsevier.
- Costa, A., Macedonio, G., 2003. Viscous heating in fluids with temperature-dependent viscosity: implications for magma flows. *Nonlinear Processes in Geophysics* 10, 545–555.
- Cundall, P., Coetzee, M., Hart, R., Varona, P., 1993. *FLAC users manual*. Itasca Consulting Group, 23–26.
- Dold, J., 1985. Analysis of the early stage of thermal runaway. *The Quarterly Journal of Mechanics and Applied Mathematics* 38(3), 361–387.
- Dupaigne, L., 2011. *Stable solutions of elliptic partial differential equations*. Vol. 1. Chapman and Hall, CRC.
- Duretz, T., Räss, L., Podladchikov, Y., Schmalholz, S., 2019. Resolving thermomechanical coupling in two and three dimensions: spontaneous strain localization owing to shear heating. *Geophysical Journal International* 216, 365–379.
- Egholm, D., M.F., K., Clark, C., Lesemann, J., 2011. Modeling the flow of glaciers in steep terrains: The integrated second-order shallow ice approximation (iSOSIA). *Journal of Geophysical Research: Earth Surface* 116, F02012.
- Fowler, A., 1980. The existence of multiple steady states in the flow of large ice masses. *Journal of Glaciology* 25 (91), 183–184.

- Fowler, A., 1986. Sub-temperate basal sliding. *Journal of Glaciology* 32(110), 3–5.
- Fowler, A., 2013. Correspondence: Thermal convection in ice sheets. *Journal of Glaciology* 59(213), 190–192.
- Fowler, A., Toja, R., Vazquez, C., 2010. Temperature-dependent shear flow and the absence of thermal runaway in valley glaciers. *Proceedings of Royal Society A* 466 (2114), 363–382.
- Fowler, A. C., Johnson, C., 1996. Ice-sheet surging and ice-stream formation. *Annals of Glaciology* 23, 68–73.
- Fowler, A. C., Larson, D., 1980a. The uniqueness of steady state flows of glaciers and ice sheets. *Geophysical Journal International* 63 (1), 333–345.
- Fowler, A. C., Larson, D., 1980b. Thermal stability properties of a model of glacier flow. *Geophysical Journal International* 63 (1), 347–359.
- Frank-Kamenetzky, D. A., 1939. Calculation of thermal explosion limits. *Acta physicochimica U.R.S.S* 10, 365–370.
- Frankel, S. P., 1950. Convergence rates of iterative treatments of partial differential equations. *Mathematical Tables and Other Aids to Computation* 4(30), 65–75.
- Fujita, H., 1969. On the nonlinear equations  $\Delta u + e^u = 0$  and  $\frac{\partial v}{\partial t} = \Delta v + e^v$ . *Bulletin of the American Mathematical Society* 75, 132–135.
- Gagliardini, O., Zwinger, T., 2008. The ISMIP-HOM benchmark experiments performed using the finite-element code Elmer. *The Cryosphere* 2, 67–76.
- Gagliardini, O., Zwinger, T., Gillet-Chaulet, F., Durand, G., Favier, L., de Fleurian, B., Greve, R., Malinen, M., Martín, C., Råback, P., Ruokolainen, J., Sacchetti, M., Schäfer, M., Seddik, H., Thies, J., 2013. Capabilities and performance of Elmer/Ice, a new-generation ice sheet model. *Geoscientific Model Development* 6, 1299–1318.
- Garofalo, F., 1963. An empirical relation defining the stress dependence of minimum creep rate in metals. *Transactions of the Metallurgical Society of AIME* 227, 351–356.
- Gerya, T., 2009. *Introduction to Numerical Geodynamic Modelling*. Cambridge University Press, Cambridge, United Kingdom.
- Gerya, T. V., Yuen, D. A., 2003. Characteristics-based marker-in-cell method with conservative finite-differences schemes for modeling geological flows with strongly variable transport properties. *Physics of the Earth and Planetary Interiors* 140(4), 293–318.

- Gilbert, A., Gagliardini, O., Vincent, C., Wagnon, P., 2014. A 3-D thermal regime model suitable for cold accumulation zones of polythermal mountain glaciers. *Journal of Geophysical Research:Earth Surface* 119, 8761893.
- Glen, J., 1955. The creep of polycrystalline ice. *Proceedings of the Royal Society of London A* 228, 519–538.
- Glen, J. W., 1952. The flow law of ice from measurements in glacier tunnels, laboratory experiments and the Jungfraufirn borehole experiment. *Journal of Glaciology* 2, 111–114.
- Goldberg, D., 2011. A variationally-derived, depth-integrated approximation to the Blatter Pattyn balance. *Journal of Glaciology* 57(201), 157–170.
- Gong, Y., Zwinger, T., Åström, J., Altena, B., Schellenberger, T., Gladstone, R., Moore, J. C., 2018. Simulating the roles of crevasse routing of surface water and basal friction on the surge evolution of Basin 3, Austfonna ice cap. *The Cryosphere* 12, 1563–1577.
- Grigoryan, S., Krass, M., Shumskiy, P., 1976. Mathematical model of a three dimensional non-isothermal glacier. *Journal of Glaciology* 7(77), 401–417.
- Gruntfest, I. J., 1963. Thermal feedback in liquid flow: Plane shear at constant stress. *Transactions of The Society of Rheology* 7, 195–207.
- Harlow, F. H., Welch, E., 1965. Numerical calculation of time-dependent viscous flow of fluid with free surface. *Physics of Fluids* 8(12), 2182–2189.
- Haseloff, M., Schoof, C., Gagliardini, O., 2018. The role of subtemperate slip in thermally driven ice stream margin migration. *The Cryosphere* 12, 2545–2568.
- Hewitt, I. J., Schoof, C., 2017. Models for polythermal ice sheets and glaciers. *The Cryosphere* 11, 541–551.
- Hindmarsh, R. C. A., 2004. Thermoviscous stability of ice-sheet flows. *Journal of fluid mechanics* 502, 17–40.
- Hindmarsh, R. C. A., 2006. Stress gradient damping of thermoviscous ice flow instabilities. *Journal of Geophysical Research:Earth Surface* 111, B12409.
- Hindmarsh, R. C. A., 2009. Consistent generation of ice-streams via thermo-viscous instabilities modulated by membrane stresses. *Geophysical research letters* 36, L06502.
- Hughes, T., 2009. Thermal convection and the origin of ice streams. *Journal of Glaciology* 55(191), 524–536.
- Hughes, T., 2012. Correspondence. Are ice-stream tributaries the surface expression of thermal convection rolls in the Antarctic ice sheet? *Journal of Glaciology* 58(210), 811–814.

- Hutter, K., 1983. Theoretical glaciology: material science of ice and the mechanics of glaciers and ice sheets. Vol. 1. Springer.
- Huybrechts, P., Payne, T., 1996. The EISMINT benchmarks for testing ice-sheet models. *Annals of Glaciology* 23, 1–12.
- Isaac, T., Stadler, G., Ghattas, O., 2015. Solution of Nonlinear Stokes Equations Discretized by High-order Finite Elements on Nonconforming and Anisotropic Meshes, with Application to Ice Sheet Dynamics. *SIAM Journal on Scientific Computing*, B804–B833.
- Jarosch, A., 2008. Icetools: a full Stokes finite element model for glaciers. *Computers and Geosciences* 34, 1005–1014.
- Johns, L. E., Narayanan, R., 1997. Frictional heating in plane Couette flow. *Proceedings of Royal Society A* 453 (1963), 1653–1670.
- Joughin, I., Smith, B., Howat, I., Scambos, T., Moon, T., 2010. Greenland flow variability from ice-sheet-wide velocity mapping. *Journal of Glaciology* 56, 416–430.
- Jouvet, G., Picasso, M., Rappaz, J., Blatter, H., 2008. A new algorithm to simulate the dynamics of a glacier: theory and applications. *Journal of Glaciology* 54, 801–811.
- Kelley, C. T., Keyes, D. E., 1998. Convergence Analysis of Pseudo-Transient Continuation. *SIAM Journal on Numerical Analysis* 35(2), 508–523.
- Kelley, C. T., Liao, L.-Z., 2013. Explicit pseudo-transient continuation. *Pacific Journal of Optimization* 9(1), 77–91.
- Kleiner, T., Rückamp, M., Bondzio, J. H., Humbert, A., 2015. Enthalpy benchmark experiments for numerical ice sheet models. *The Cryosphere* 9, 217–228.
- Krabbendam, M., 2016. Sliding of temperate basal ice on a rough, hard bed: creep mechanisms, pressure melting, and implications for ice streaming. *The Cryosphere* 10, 1915–1932.
- Kyrke-Smith, T. M., Katz, R. F., Fowler, A. C., 2015. Subglacial hydrology as a control on emergence, scale, and spacing of ice streams. *Journal of Geophysical Research:Earth Surface* 120, 1501–1514.
- Landau, L. D., Lifshitz, E. M., 1963. *Fluid Mechanics*. Vol. 1. Pergamon Press.
- Larour, E., Seroussi, H., Morlighem, M., Rignot, E., 2012. Continental scale, high order, high spatial resolution, ice sheet modeling using the Ice Sheet System Model (ISSM). *Journal of Geophysical research* 117, 1–20.

- Leng, W., Ju, L., Gunzburger, M., Price, S., 2014. A Parallel Computational Model for Three-Dimensional, Thermo-Mechanical Stokes Flow Simulations of Glaciers and Ice Sheets. *Computer Physics Communications* 16(4), 1056–1080.
- Leng, W., Ju, L., Gunzburger, M., Ringler, T., 2012. A parallel high- order accurate finite element nonlinear Stokes ice sheet model and benchmark experiments. *Journal of Geophysical research* 117, F01001.
- Lliboutry, L. A., 1987. *Very Slow Flows of Solids: Basics of Modeling in Geodynamics and Glaciology*. Vol. 7. Springer Netherlands.
- MacAyeal, D. R., 1992. The basal stress distribution of Ice Stream E, Antarctica, inferred by control methods. *Journal of Geophysical Research: Earth Surface* 97, 595–603.
- Moore, P., Iverson, N., Cohen, D., 2009. Ice flow across a warm-based/cold-based transition at a glacier margin. *Annals of Glaciology* 50 (52), 1–8.
- Morland, L., 1984. Thermomechanical balances of ice sheet flows. *Geophysical and Astrophysical Fluid Dynamics* 29, 237–266.
- Nye, J. F., 1953. The flow law of ice from measurements in glacier tunnels, laboratory experiments and the Jungfraufirn borehole experiment. *Proceedings of Royal Society A* 219, 477–489.
- Ogawa, M., Schubert, G., Zebib, A., 1991. Numerical simulations of three-dimensional thermal convection in a fluid with strongly temperature dependent viscosity. *Journal of Fluid Mechanics* 233, 299–328.
- Omlin, S., 2017. Development of massively parallel near peak performance solvers for three-dimensional geodynamic modelling. Ph.D thesis, University of Lausanne.
- Patankar, S., 1980. *Numerical Heat Transfer and Fluid Flow*, Comput. Methods Mech. Thermal Sci. Ser. CRC Press, Boca Raton, Fla.
- Paterson, W., 1994. *The physics of glaciers*. Third edition. Elsevier.
- Pattyn, F., 2003. A new three-dimensional higher-order thermomechanical ice sheet model: basic sensitivity, ice stream development and ice flow across subglacial lakes. *Journal of Geophysical Research* 108(B8), 2382.
- Pattyn, F., Perichon, L., Aschwanden, A., Breuer, B., de Smedt, B., Gagliardini, O., Gudmundsson, G. H., Hindmarsh, R. C. A., Hubbard, A., Johnson, J. V., Kleiner, T., Konovalov, Y., Martin, C., Payne, A. J., Pollard, D., Price, S., Rückamp, M., Saito, F., Soucek, O., Sugiyama, S., , Zwinger, T., 2008. Benchmark experiments for higher-order and full-Stokes ice sheet models (ISMIP- HOM). *The Cryosphere* 2, 95–108.

- Payne, A., Dongelmans, P., 1997. Self-organization in the thermomechanical flow of ice sheets. *Journal of Geophysical research* 102(B6), 219–233.
- Payne, T., Baldwin, D., 2000. Analysis of ice-flow instabilities identified in the EISMINT intercomparison exercise. *Annals of Glaciology* 30, 204–210.
- Payne, T., Huybrechts, P., Abe-Ouchi, A., Calov, R., Fastook, J., Greve, R., Marshall, S., Marsiat, I., Ritz, C., Tarasov, L., Thomassen, M., 2000. Results from the EISMINT model intercomparison: the effects of thermomechanical coupling. *Journal of Glaciology* 46(153), 227–238.
- Perego, M., Gunzburger, M., Burkardt, J., 2012. Parallel finite element implementation for higher order ice-sheet models. *Journal of Glaciology* 58(207), 76–88.
- Poliakov, A. N. B., Cundall, P. A., Podladchikov, Y. Y., Lyakhovsky, V. A., 1993. An explicit inertial method for the simulation of viscoelastic flow: An evaluation of elastic effects on diapiric flow in two- and three-layers models. *Flow and Creep in the Solar Systems: Observations, Modeling and Theory*, 175–195.
- Pollard, D., DeConto, R. M., 2012. Description of a hybrid ice sheet-shelf model, and application to Antarctica. *Geoscientific Model Development* 5, 1273–1295.
- Räss, L., Simon, N., Podladchikov, Y., 2018. Spontaneous formation of fluid escape pipes from subsurface reservoirs. *Scientific Reports* 8 (11116).
- Robin, G. d. Q., 1955. Ice movement and temperature distribution in glaciers and ice sheets. *Journal of Glaciology* 2 (18), 523–532.
- Saito, F., Abe-Ouchi, A., Blatter, H., 2006. European Ice Sheet Modelling Initiative (EISMINT) model intercomparison experiments with first-order mechanics. *Journal of Geophysical Research* 111, F02012.
- Schäfer, M., Gillet-Chaulet, F., Gladstone, R., Pettersson, R., Pohjola, V., Strozzi, T., Zwinger, T., 2014. Assessment of heat sources on the control of fast flow of Vestfonna ice cap, Svalbard. *The Cryosphere* 8, 1951–1973.
- Schoof, C., 2005. The effect of cavitation on glacier sliding. *Proceedings of Royal Society A* 461, 609–627.
- Schoof, C., Hewitt, I. J., 2016. A model for polythermal ice incorporating gravity-driven moisture transport. *Journal of fluid mechanics* 797, 504–535.
- Schoof, C., Hindmarsh, R., 2010. Thin film flows with wall slip: an asymptotic analysis of higher order glacier flow models. *The Quarterly Journal of Mechanics and Applied Mathematics* 63(1), 73–114.

- Schubert, G., Yuen, D., 1982. Initiation of ice ages by creep instability and surging of the East Antarctic ice sheet. *Nature* 296 (5853), 127–130.
- Shapiro, D. R., Joughin, I., Poinar, K., Morlighem, M., Gillet-Chaulet, F., 2016. Basal resistance for three of the largest Greenland outlet glaciers. *Journal of Geophysical Research: Earth Surface* 121, 168–180.
- Shin, D., Strikwerda, J. C., 1997. Inf-Sup conditions for finite-difference approximations of the Stokes equations. *Journal of the Australian Mathematical Society. Series B. Applied Mathematics* 39(01), 121–134.
- Solomon, S., Qin, D., Manning, M., Chen, Z., Marquis, M., Averyt, K., Tignor, M., Miller, H., 2007. The physical science basis p.235–337, IPCC report AR4 . New York and Cambridge: Cambridge University Press.
- Stearns, L. A., Van der Veen, C. J., 2018. Friction at the bed does not control fast glacier flow. *Science* 361(6399), 273–277.
- Steinemann, S., 1958. Experimentelle Untersuchungen zur Plastizität von Eis. *Beiträge zur Geologie der Schweiz. Hydrologie* 10.
- Suckale, J., Platt, J., Perol, T., Rice, J., 2014. Deformation-induced melting in the margins of the West Antarctic ice streams. *Journal of Geophysical Research:Earth Surface* 119, 1004–1025.
- Tezaur, I. K., Perego, M., Salinger, A. G., Tuminaro, R. S., Price, S. F., 2015. Albany/FELIX: a parallel, scalable and robust, finite element, first-order Stokes approximation ice sheet solver built for advanced analysis. *Geoscientific Model Development* 8, 1197–1220.
- Turcotte, D., Schubert, G., 2014. *Geodynamics 3rd Edition. Vol. 1.* Cambridge University Press.
- Van der Veen, C., Oerlemans, J., 1984. Global thermodynamics of a polar ice sheet. *Tellus* 36A, 228–235.
- Wong, W. A., Jonas, J. J., 1968. Aluminum extrusion as a thermally activated process. *Transactions of the Metallurgical Society of AIME* 242, 2271–2280.
- Yang, X. I., Mittal, R., 2014. Acceleration of the Jacobi iterative method by factors exceeding 100 using scheduled relaxation. *Journal of Computational Physics* 274, 695–708.
- Yuen, D., Saari, M., Schubert, G., 1986. Explosive growth of shear heating instabilities in the down-slope creep of ice sheets. *Journal of Glaciology* 32 (112), 314–320.

- Yuen, D., Schubert, G., 1977. Asthenospheric shear flow: thermally stable or unstable. *Geophysical research letters* 4 (11), 503–506.
- Yuen, D., Schubert, G., 1979a. On the stability of frictionally heated shear flows in the asthenosphere. *Geophysical Journal International* 57 (1), 189–207.
- Yuen, D., Schubert, G., 1979b. The role of shear heating in the dynamics of large ice masses. *Journal of Glaciology* 4 (90), 195–212.
- Zhang, T., Ju, L., Leng, W., Price, S., Gunzburger, M., 2015. Thermomechanically coupled modelling for land-terminating glaciers: a comparison of two-dimensional, first-order and three-dimensional, full-Stokes approaches. *Journal of Glaciology* 61(228), 702–711.
- Zoet, L. K., Iverson, N. R., 2016. Rate-weakening drag during glacier sliding. *Journal of Geophysical Research: Earth Surface* 121, 1206–1217.
- Zwinger, T., Greve, R., Gagliardini, O., Shiraiwa, T., Lyly, M., 2007. A full Stokes-flow thermo-mechanical model for firn and ice applied to the Gorshkov crater glacier, Kamchatka. *Annals of Glaciology* 45, 29–37.

## CHAPTER 2

---

### Modelling the coupled thermo-mechanical ice flow using the implicit pseudo-transient method on the computer graphics cards

---

**Aleksandar Licul<sup>1,3</sup>, Ludovic Räss<sup>2,3</sup>, Yury Y. Podladchikov<sup>2,3</sup> and Frédéric Herman<sup>1,3</sup>**

<sup>1</sup>Faculté des géosciences et de l'environnement, Institut des dynamiques de la surface terrestre, University of Lausanne, Lausanne, Switzerland.

<sup>2</sup>Faculté des géosciences et de l'environnement, Institut des Sciences de la Terre, University of Lausanne, Lausanne, Switzerland.

<sup>3</sup>Swiss Geocomputing Centre, University of Lausanne, Lausanne, Switzerland.

## Abstract

Under certain conditions thermo-mechanical coupling could be the first order physics governing the flow of ice below melting temperature. Temperature can affect the rheology of ice, and through that the ice velocity. Numerous studies have investigated this coupling using analytical and numerical approaches. Here we develop a model based on the pseudo-transient method with the implicit coupling between ice viscosity and temperature. The pseudo-transient (PT) method is based on the finite difference discretization and a pseudo-time integration, and therefore results in a matrix free form. This results in a simple and a highly parallelizable algorithm that enables high spatial numerical resolution in one, two and three dimensions. The developed algorithms make use of the intrinsic parallelism of the computer graphic cards (GPU), which enable us to accelerate the developed algorithms. We first test the computationally most intensive part, i.e. the Stokes solver, in a set of experiments and compare its performance in both two and three-dimensional simulations with a code widely used in glaciology, the finite element code Elmer/Ice, using simple test case scenarios. The simulation results show that the PT method can deliver results in a good agreement with the Elmer/Ice Stokes solver. Second, we show that up to a two order of magnitude increase in computational performance can be reached when the code is translated from MATLAB to CUDA C (cf Nvidia). Third, a time evolution simulation of the coupled thermo-mechanical model is presented. We find that: 1) high spatial numerical resolution is needed to properly capture the highly non-linear thermo-mechanical coupling; 2) numerical coupling method has only minor effects on the result; 3) high temporal numerical resolution is at least equally important as the high spatial numerical resolution. The codes examples based on PT method in both MATLAB and CUDA C programming language are provided.

## 2.1 Introduction

The publication of the fourth IPCC report (Solomon et al., 2007) revealed that ice sheet flow models did not provide an accurate description of polar ice sheet discharge (e.g., Gagliardini et al., 2013; Pattyn et al., 2008) due to their inability to model slow and fast ice flow simultaneously (Bueler and Brown, 2009; Gagliardini et al., 2013). This was attributed to the fact that, at the time, most ice flow models were based on a simplified asymptotic approximations of the non-linear Stokes equations. Since then, the primary focus of ice flow modelling community has been on the mechanics of the ice flow either through development of more computationally tractable shallow ice models (Bassis, 2010; Bueler and Brown, 2009; Egholm et al., 2011; Goldberg, 2011; Perego et al., 2012; Pollard and DeConto, 2012; Schoof and Hindmarsh, 2010; Tezaur et al., 2015) or through the development of full Stokes flow models (Brinkerhoff and Johnson, 2013; Gagliardini and Zwinger, 2008; Gagliardini et al., 2013; Isaac et al., 2015; Jarosch, 2008; Jouvét et al., 2008; Larour et al., 2012; Leng et al., 2014, 2012). In that context, the physics of ice flow is best described by a mathematical model for incompressible, homogeneous non-linearly viscous fluid with a strong temperature dependence of viscosity (Hutter, 1983; Morland, 1984; Robin, 1955). It is therefore crucial that a fully coupled thermo-mechanical system of equations is solved simultaneously and mass, momentum and energy are conserved at every point in space and time. This requires both high spatial and temporal resolutions. However, thermo-mechanically coupled transient Stokes models are scarce and verification of the numerical solution is difficult since analytical solutions are lacking. Meanwhile model benchmarks often concentrated on verifying the mechanical model only, i.e. EISMINT (Huybrechts and Payne, 1996) and ISMIP (Pattyn et al., 2008) benchmark experiments, and there is only one model inter-comparison investigating the physical thermo-mechanical coupling, i.e. EISMINT 2 (Payne et al., 2000). Unfortunately, the experiments in EISMINT 2 are usually performed using a coupled thermo-mechanical shallow approximation model (Brinkerhoff and Johnson, 2015; Bueler et al., 2007; Hindmarsh, 2006, 2009; Payne and Baldwin, 2000; Saito et al., 2006), i.e. shallow ice model or a first order model, and often produce numerical solutions that do not converge under grid refinement, therefore making any comparison difficult.

Even though thermo mechanically coupled Stokes models exist (Gilbert et al., 2014; Gong et al., 2018; Leng et al., 2014; Schäfer et al., 2014; Zhang et al., 2015; Zwinger et al., 2007), there is no investigation into the numerical aspects of the implemented model, i.e. the influence of the numerical resolution, numerical coupling method and numerical time integration method used, with exception of Duretz et al. (2019). This motivated us to investigate the behaviour of a fully coupled thermo-mechanical 2D and 3D Stokes model with a primary goal to distinguish between the effects of physics and numerics. To achieve this, we have developed a numerical model based on the pseudo-transient (PT) method (Cundall et al., 1993; Frankel, 1950; Kelley and Keyes, 1998; Kelley and Liao, 2013; Poliakov et al., 1993). This iterative

method combined with the finite difference discretization of the system of equations results in matrix free form and it is suitable for modern parallel hardware like the computer graphic cards (Duretz et al., 2019; Omlin, 2017; Räss et al., 2018).

We start by giving an overview of the mathematical model describing the ice dynamics, where we also describe the developed method and its numerical implementation. We continue by giving an overview of graphics processing units (GPUs) and explain our GPU implementation of the model. We then describe the model configuration and experiments used to verify our numerical adaptation of the model, followed by the results and performance measurements. Finally, we discuss pros and cons of the method and give our concluding remarks.

## 2.2 Model

### 2.2.1 Mathematical model

The mathematical model describing the flow of an incompressible non linear viscous fluid with temperature dependent rheology under the external force is given by the following set of conservation laws (Equations 2.1-2.3 ) and rheology (Equation 2.4). Ice is usually considered to be an incompressible fluid, so the equation for conservation of mass, or the continuity equation, reduces to the following form:

$$\frac{\partial v_i}{\partial x_i} = 0 \quad (2.1)$$

where  $v_i$  are velocity components in  $x_i$  spatial direction.

Newton's second and third laws state that linear momentum is conserved if the sum of all forces acting on an object is equal to zero. Since dimensional scaling shows that ice is not accelerating or decelerating, all body forces are balanced due to external force (gravity) and the equations for conservation of linear momentum can be written as:

$$\frac{\partial \tau_{ij}}{\partial x_j} - \frac{\partial P}{\partial x_i} + F_i = 0 \quad (2.2)$$

where  $F_i$  is the external force defined as  $F_i = \rho g \sin \alpha (1, 0, -\cot \alpha)$ . Ice density is denoted by  $\rho$ ,  $g$  is the gravitational acceleration and  $\alpha$  is the characteristic bed slope.  $P$  is the isotropic pressure and  $\tau_{ij}$  is the deviatoric stress tensor. The deviatoric stress tensor  $\tau_{ij}$  is obtained by decomposing the Cauchy stress tensor  $\sigma_{ij}$  in terms of deviatoric stress  $\tau_{ij}$  and the isotropic pressure  $P$ .

The governing equation for the conservation of heat in the case of incompressible fluid with no melt is given by:

$$\rho c \left( \frac{\partial T}{\partial t} + v_i \frac{\partial T}{\partial x_i} \right) = \frac{\partial}{\partial x_i} \left( k \frac{\partial T}{\partial x_i} \right) + \tau_{ij} \dot{\epsilon}_{ij} \quad (2.3)$$

where  $T$  represents the temperature deviation from the initial temperature  $T_0$ , usually chosen at the ice surface,  $c$  is the specific heat capacity,  $k$  is the thermal conductivity and  $\dot{\epsilon}_{ij}$  is the strain rate tensor. The term  $\tau_{ij}\dot{\epsilon}_{ij}$  represent the strain heating, a viscous heating source term. Thermal conductivity can be either constant or temperature dependent. Note that here we are not accounting for the phase change, and hence we do not impose the constraint on the temperature by the pressure melting point.

The rheology of ice is best described by Glen's flow law (Glen, 1952; Nye, 1953)

$$\dot{\epsilon}_{ij} = \frac{1}{2} \left( \frac{\partial v_i}{\partial x_j} + \frac{\partial v_j}{\partial x_i} \right) = a_0 \tau_{II}^{n-1} e^{-\frac{Q}{R(T+T_0)}} \tau_{ij} \quad (2.4)$$

where  $a_0$  is the pre-exponential factor,  $R$  is the universal gas constant,  $Q$  is the activation energy,  $n$  is the stress exponent and  $\tau_{II}$  is the second invariant of the stress tensor defined by  $\tau_{II} = \sqrt{\frac{1}{2}(\tau_{xx}^2 + \tau_{yy}^2 + \tau_{zz}^2 + 2(\tau_{xy}^2 + \tau_{yz}^2 + \tau_{xz}^2))}$ . For modelling ice, it is generally assumed that the Glen flow law exponent  $n$  equals 3.

Our physical domain of interest involves top, bottom and lateral boundaries. At the ice top surface  $\Gamma_t(t)$ , we impose the upper surface boundary condition  $\sigma_{ij}n_j = -P_{atm}n_j$  where  $n_j$  denotes the normal unit vector at the ice surface boundary, and  $P_{atm}$  the atmospheric pressure. Because atmospheric pressure is negligible relative to pressure within ice column, we can also use a standard stress free simplification of the upper surface boundary condition  $\sigma_{ij}n_j = 0$ .

On the bottom bedrock surface we can impose two different boundary conditions. For the parts of ice-bedrock interface  $\Gamma_0(t)$  where ice is frozen to the ground, we impose zero velocity  $v_i = 0$  boundary condition, which includes both the no sliding condition and the impermeability condition. On the parts of ice-bedrock interface  $\Gamma_s(t)$  where ice is at its the melting point, we impose a Rayleigh friction boundary condition or the so-called linear sliding law given by:

$$v_i n_i = 0 \quad n_i \sigma_{ij} t_j = -\beta^2 v_j t_j \quad (2.5)$$

where parameter  $\beta^2$  denotes a given sliding coefficient,  $n_i$  denotes the normal unit vector at the ice bottom surface, and  $t_j$  denotes any unit vector tangential to the bottom surface. On the side or lateral boundaries, we impose either Dirichlet boundary conditions if the velocities are known, or periodic boundary conditions.

For numerical purposes, it is often preferable to use dimensionless variables. Here, we use two different set of scales, depending on whether we solve the mechanic parts of the model or thermo-mechanically coupled system of equations. In the former, we use the scales often used across the glaciology literature (Baral et al., 2001; Hutter, 1983), while in the latter the importance of diffusion length scale is recognized.

In the case of mechanics only the following independent scales are used to non-dimensionalize the equations

$$L_{sc} = H \quad , \quad \tau_{sc} = \rho g L_{sc} \sin \alpha \quad , \quad v_{sc} = 2^n A_0 L_{sc} \tau_{sc}^n \quad (2.6)$$

where  $H$  is the glacier thickness or the maximum vertical domain size,  $A_0$  is the isothermal deformation rate factor and  $\alpha$  is the mean bed slope.

In the form of the non-dimensionalized variables we can then rewrite the governing equations as follows:

$$\frac{\partial v'_i}{\partial x'_i} = 0 \quad (2.7)$$

$$\frac{\partial \tau'_{ij}}{\partial x'_j} - \frac{\partial P'}{\partial x'_i} + F'_i = 0 \quad (2.8)$$

$$\dot{\epsilon}'_{ij} = \frac{1}{2} \left( \frac{\partial v'_i}{\partial x'_j} + \frac{\partial v'_j}{\partial x'_i} \right) = 2^{-n} \tau_{II}^{n-1} \tau'_{ij} \quad (2.9)$$

where  $F'_i$  is now defined as  $F'_i = (1, 0, -\cot \alpha)$ .

The model parameters are the stress exponent  $n$ , the mean bed slope  $\alpha$  and domain size in each horizontal direction, i.e.  $L'_x$  and  $L'_y$ .  $L'_z$  is always arbitrarily chosen equal to 1.

In the case of the thermo-mechanically coupled set of equations, the four independent scales are used to non-dimensionalize the thermo-mechanically coupled equations: temperature, stress, time and length. The characteristic scales are chosen such that the coefficients in front of the diffusion and strain heating terms in the temperature evolution equation (Equation 2.3) reduce to 1.

$$\bar{T} = \frac{nRT_0^2}{Q} \quad , \quad \bar{\tau} = \rho c_p \bar{T} \quad , \quad \bar{t} = 2^{-n} a_0^{-1} \bar{\tau}^{-n} e^{\frac{Q}{RT_0}} \quad , \quad \bar{L} = \sqrt{\frac{k}{\rho c_p} \bar{t}} \quad (2.10)$$

Additionally, we can derive their dependent combinations such as the velocity scale given by  $\bar{v} = \frac{\bar{L}}{\bar{t}}$ . We obtain the dimensionless primed-variables by normation with the characteristic scale for the variable given in Equation 2.10.

In the form of the non-dimensionalized variables, we can then rewrite the governing equations as follows:

$$\frac{\partial v'_i}{\partial x'_i} = 0 \quad (2.11)$$

$$\frac{\partial \tau'_{ij}}{\partial x'_j} - \frac{\partial P'}{\partial x'_i} + F'_i = 0 \quad (2.12)$$

$$\frac{\partial T'}{\partial t'} + v'_i \frac{\partial T'}{\partial x'_i} = \frac{\partial^2 T'}{\partial x'^2_i} + \tau'_{ij} \dot{\epsilon}'_{ij} \quad (2.13)$$

$$\dot{\epsilon}'_{ij} = \frac{1}{2} \left( \frac{\partial v'_i}{\partial x'_j} + \frac{\partial v'_j}{\partial x'_i} \right) = 2^{-n} \tau_{II}^{n-1} \exp \left( \frac{nT'}{1 + \frac{T'}{T'_0}} \right) \tau'_{ij} \quad (2.14)$$

where  $F'_i$  is now defined as  $F'_i = \bar{F}(1, 0, -\cot \alpha)$  and  $\bar{F} = \frac{\rho g \sin \alpha \bar{L}}{\bar{\tau}}$ .

The model parameters are the non-dimensional initial temperature  $T'_0$ , stress exponent  $n$ , non-dimensional force  $\bar{F}$ , the mean bed slope  $\alpha$ , non-dimensional domain height  $L'_z$  and horizontal domain size  $L'_x$  and  $L'_y$ .

Furthermore, we analyse a special mathematical case, in 1-D, and in which case all horizontal derivatives vanish ( $\frac{\partial}{\partial x'} = \frac{\partial}{\partial y'} = 0$ ). The only non-vanishing stress component  $\tau_{xz}$  and pressure  $P$  are determined by analytical integration and are constant in time for a fixed domain. To derive the equations, we use the fact that stresses vanish at the surface and the boundary condition on the velocity, where we set the basal velocity (both horizontal and vertical component) to 0, which leads to

$$\frac{\partial T'(z, t)}{\partial t'} = \frac{\partial^2 T'(z, t)}{\partial z'^2} + 2^{(1-n)} (\bar{F} L'_z)^{(n+1)} \left(1 - \frac{z'}{L'_z}\right)^{(n+1)} \exp \left( \frac{nT'(z, t)}{1 + \frac{T'(z, t)}{T'_0}} \right) \quad (2.15)$$

$$v'_x(z, t) = 2^{(1-n)} (\bar{F} L'_z)^n \int_0^z \left(1 - \frac{z'}{L'_z}\right)^n \exp \left( \frac{nT'(z, t)}{1 + \frac{T'(z, t)}{T'_0}} \right) dz \quad (2.16)$$

where  $L'_z$  is the non-dimensional height of the domain (ice thickness).

Note that the velocity and strain heating terms (Equations 2.15 and 2.16) are now a function of temperature only, and hence, depth and time. Therefore, to obtain a solution of the coupled system one first needs to determine the temperature evolution profile, while the velocity can then be obtained diagnostically by a simple numerical integration. This decoupling of the strain heating term from the velocity dependence enable us to obtain a reference numerical solution of a 1D coupled thermo-mechanical model by solving numerically just the temperature evolution equation.

## 2.2.2 Numerical implementation

The coupled thermo-mechanical Stokes equations (Equations 2.11-2.14) are discretized using the Finite Difference Method (FDM) on a staggered Cartesian grid. Depending on the experiment both regular and irregular grid spacing is used. Among many numerical methods currently used to solve partial differential equations, the finite difference method (FDM) is most commonly used and has been successfully applied in solving the same set of equations in many geophysical problems, i.e geodynamics community (Gerya, 2009; Harlow and Welch, 1965; Ogawa et al., 1991). The staggering of the grid provides that the method is second

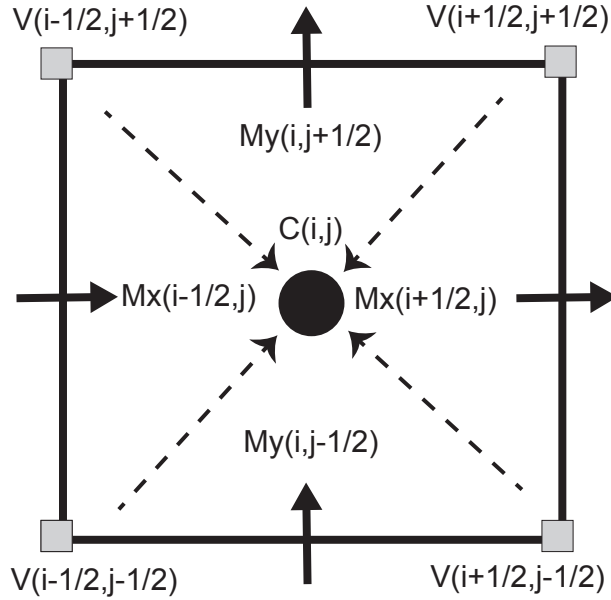


**Figure 2.1:** 2D staggered grid positioning:  $C$  represents variables located at cell center,  $V$  depicts variables located at cell vertices and  $M_x$  and  $M_y$  represents variables located at cell mid-faces in  $x$  or  $y$  direction.

order conservative (Gerya and Yuen, 2003; Patankar, 1980) and free of the oscillatory pressure modes (Shin and Strikwerda, 1997). Furthermore, the finite difference discretization of the thermo-mechanically coupled Stokes equations on a staggered grid produce simple, yet highly compact stencils. This can easily lead to easily parallelizable algorithms that are well suited for modern highly parallel architectures like computer graphics cards (Omlin, 2017). Since our main motivation is to develop a 3-D solver capable of resolving the highly non linear physics at the high spatial and temporal resolution efficiently utilize the modern hardware is crucial.

On the staggered grid different physical variables are located on the different geometrical positions. For example, pressure nodes and normal components of the strain rate tensor nodes are located at the cell centres. Velocity components are located at the cell mid-faces, while shear components are located at the cell vertices (Gerya and Yuen, 2003). Figure 2.1 illustrates staggering of the variables in two dimensions. For the viscous fluid, rheology is given by a power law in the form of the Glen's flow law and therefore viscosity is a function of the second invariant of the strain rate tensor (Equation 2.4). Values of the shear and normal strain rate components are hence evaluated on the same grid position. This is done by averaging the shear strain rate components to interpolate the values to the wanted position. The same interpolation by averaging is needed to obtain the shear stress components which are located on the cell vertices, but in that case averaging is done on the viscosity field.

The advection term in the temperature equation is discretized using the first order upwind scheme while the physical time integration is done using the implicit backward Euler numerical scheme.

Our numerical approach for solving the above system of the coupled non-linear partial differential equations is based on a classical pseudo-transient (PT) continuation method or the relaxation method (Cundall et al., 1993; Frankel, 1950; Kelley and Keyes, 1998; Kelley and Liao, 2013; Poliakov et al., 1993). This is an iterative and a matrix-free method. The basis behind the method is the introduction of numerical time derivative  $\tau$  (or the pseudo time) into the actual physical equations one wishes to solve.

The modified equations (Equations 2.11-2.13) are then corresponding to the following:

$$\begin{aligned}\frac{dP}{d\tau_p} &= \frac{\partial v_i}{\partial x_i} \\ \frac{dv_i}{d\tau_v} &= \frac{\partial \tau_{ij}}{\partial x_j} - \frac{\partial P}{\partial x_i} + F_i \\ \frac{dT}{d\tau_T} &= -\frac{\partial T}{\partial t} - v_i \frac{\partial T}{\partial x_i} + \frac{\partial^2 T}{\partial x_i^2} + \tau_{ij} \dot{\epsilon}_{ij}\end{aligned}\tag{2.17}$$

where we drop the primes for clarity. The right hand side of the equations is then substituted by the force  $f_v$ , pressure  $f_p$  and temperature  $f_T$  residuals. These residuals quantify the magnitude of the imbalance of the corresponding equations. Hence, they represent the discretized equation of the previous iteration level with the current solution vector.

$$\begin{aligned}\frac{dP}{d\tau_p} &= f_p \\ \frac{dv_i}{d\tau_v} &= f_v \\ \frac{dT}{d\tau_T} &= f_T\end{aligned}\tag{2.18}$$

The spatial derivatives are then discretized on a staggered grid as described previously, while the pseudo temporal integration is performed as follows:

$$x^{k+1} = x^k + \Delta\tau_x f_x\tag{2.19}$$

where  $x$  represents either temperature, pressure or a specific velocity component,  $k$  is the iteration number and  $\Delta\tau_x$  is the numerical time-step. The variable specific definition of each numerical time-step will be provided further down in this section.

The algorithm iterates until pressure, force and temperature residuals vanish, meaning that steady state (in pseudo time) is reached and the implicit numerical solution of the original form of the physical equations is obtained. It is also important to emphasize here that this

procedure leads to the two-way numerical coupling between temperature and mechanics, and enables us to, upon convergence, recover an implicit solution of the non-linear partial differential equations (PDEs), since both the coupling terms and rheology are treated implicitly. For example, physical viscosity  $\eta_k$  is a function of temperature and the velocity field (via the the second invariant of the strain rate tensor); during the iterative process the physical viscosity is always evaluated at the current time step and thus the non linear coupling terms is treated implicitly.

In every iteration  $k$ , we update the effective viscosity  $\eta_{eff}^k$  in the logarithmic space by taking a fraction  $r_\eta$  of the actual physical viscosity  $\eta_k$  and a fraction  $(1 - r_\eta)$  of the effective viscosity calculated in the previous iteration  $\eta_{eff}^{k-1}$ .

$$\eta_{eff}^k = \exp(r_\eta \ln[\eta_k] + (1 - r_\eta) \ln[\eta_{eff}^{k-1}]) \quad (2.20)$$

The ratio  $r_\eta$  is a viscosity relaxation factor and its value is set between 0 and 1. This relaxation of the non-linearity is a continuation method since the effective viscosity iteratively approaches the physical and non linear viscosity values within the pseudo-transient iterations. A similar non-linear viscosity relaxation approach was successfully implemented in the ice sheet model development by Tezaur et al. (2015).

During the iterative procedure the material is made slightly compressible, and thereby criterion of incompressibility is relaxed. To balance the divergence free formulation of strain rates, we introduce a parameter  $\eta_b$ . This is the numerical equivalent of the bulk viscosity and is introduced during the normal stress component evaluation, where it is multiplied with the pressure residual  $f_p$ . Normal stress is hence given by  $\tau_{ii} = 2\eta_b(\dot{\epsilon}_{ii} + \eta_b f_p)$ . Once the method converges, pressure residual  $f_p$  vanishes and the incompressible form of the normal stress is recovered.

The numerical time steps needed for the pseudo temporal integration are chosen according to the following rules and may vary at each grid point since  $\eta_{eff}^k$  is evaluated at the specific grid point:

$$\begin{aligned} \Delta\tau_{v_i} &= r_{v_i} \frac{\min(\Delta x, \Delta y, \Delta z)^2}{2.1 n_{dim} \eta_{eff}^k (1 + \eta_b)} \\ \Delta\tau_p &= r_p \frac{2.1 n_{dim} \eta_{eff}^k (1 + \eta_b)}{\max(n_x, n_y, n_z)} \\ \Delta\tau_T &= \frac{1}{\frac{2 n_{dim}}{\min(\Delta x, \Delta y, \Delta z)^2} + \frac{1}{\Delta t}} \end{aligned} \quad (2.21)$$

where  $r_{v_i}$  and  $r_p$  are relaxation parameters,  $n_{dim}$  is the number of dimensions,  $\Delta x$ ,  $\Delta y$  and  $\Delta z$  are grid spacing,  $n_x$ ,  $n_y$  and  $n_z$  are the number of numerical grid points.  $\Delta t$  is the actual physical time step used for advancing the temperature in time. It can be noticed that  $\Delta\tau_{v_i}$  and  $\Delta\tau_T$  are modified explicit Courant-Friedrich-Lewy (CFL) diffusive time steps. The  $\Delta\tau_p$

is chosen such to balance the viscosity term introduced in  $\Delta\tau_{v_i}$  and therefore reduce the sensitivity of the iterative method on the value of physical viscosity.

Next, we define the velocity, pressure and temperature increments as:

$$\begin{aligned}\Delta v_i^k &= \Delta\tau_{v_i} f_v^k + \left(1 - \frac{\nu}{n_i}\right) \Delta v_i^{k-1} \\ \Delta P^k &= \Delta\tau_p f_p^k \\ \Delta T^k &= \Delta\tau_T f_T^k\end{aligned}\tag{2.22}$$

where we apply damping on the velocity increments with a goal of significantly reducing the number of iterations needed for the method to converge. The similar strategy in damping of the velocity increments was already successfully applied by Choi et al. (2013) and Yang and Mittal (2014). The optimal value of the introduced parameter  $\nu$  is found to be in a range between 1 and 10, and it is usually problem dependent. This approach was successfully implemented in recent PT developments by Räss et al. (2018) and Duretz et al. (2019).

The velocity, pressure and temperature fields are then updated at each iteration using the following rules:

$$\begin{aligned}v_i^k &= v_i^{k-1} + \Delta v_i^k \\ P^k &= P^{k-1} + \Delta P^k \\ T^k &= T^{k-1} + \Delta T^k\end{aligned}\tag{2.23}$$

The iteration procedure is repeated until an exit criterion  $\max[\text{abs}(f^{k+1} - f^k)] < \text{tol}_{nl}$  is reached where  $\text{tol}_{nl}$  is chosen threshold value.

We implemented the PT method in MATLAB and CUDA C programming languages. Computations in CUDA C can be performed in both double and single floating point precision. If not emphasized differently, the computations in CUDA C are performed in double floating point precision. The implementation in the CUDA C is explained in the next section. The codes examples based on PT method in both MATLAB and CUDA C programming language are available for download from Bitbucket at <https://bitbucket.org/alicul/tmc/>.

## 2.3 Implementation of the method on computer graphic cards

Our GPU algorithm development effort is motivated by the aim to resolve the coupled thermo-mechanical system of equations (Equations 2.11-2.14) with high spatial and temporal accuracy in three dimensions. To achieve this we have exploited the low level intrinsic parallelism of a shared memory device, i.e. the computer graphic card. Recent trends in the computing industry show a shift from single core to many core architectures as an effective way of increasing computational performance. This trend is common with both central processing

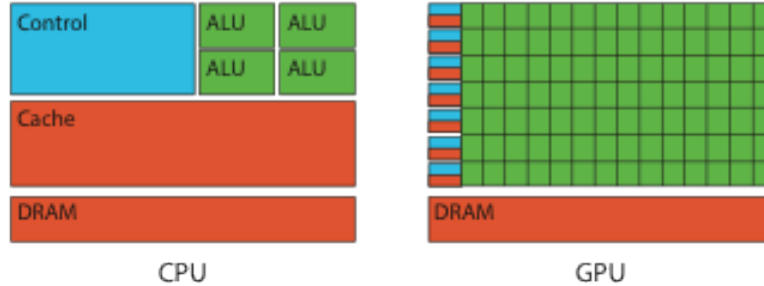


**Figure 2.2:** Chip schematic for both the central processing unit (CPU) and graphical processing unit (GPU) architecture: GPU architecture consist of thousands arithmetic and logical units (ALU). On the CPU most of the on-chip space is devoted to controlling units and cache memory, while the number of ALUs is significantly reduced

units (CPU) and graphic processing units (GPU) hardware architectures (Cook, 2012). A GPU is a massively parallel device originally optimized for calculating the color of a pixel independently from each other; in which case latency can be masked by high throughput, i.e. compute as many jobs as possible in a reasonable time. A schematic representation (Figure 2.2) highlights the conceptual discrepancy between GPU and CPU; on the GPU chip, the majority of the area is devoted to the arithmetic units while on the CPU a large area of the chip hosts scheduling and control microsystems.

The programming model behind the GPUs is based around well-known parallel principle called Single Instruction Multiple Data (SIMD), where each single instruction is executed on each different data. The same block of instructions is executed by each thread. Massive parallelism of the GPU, and with that very high performance, is achieved by executing thousands of threads at the same time, which can effectively hide the latency. In numerical techniques such as the finite-difference method one computes values on a grid of mesh points by approximating spatial derivatives by differences between two (or more) adjacent neighbouring grid points. This results in minimal, local and regular memory access. Additionally, this so-called stencil operation is identical for each grid point throughout the entire computational domain. Combined with matrix free discretization of the equations and iterative updates the FD stencil evaluation is well suited for the SIMD programming philosophy behind the GPUs. The key here is that one thread is calculating one grid point in each kernel. Since, on the device, one core can simultaneously execute several threads, the set of operations are executed on the entire computational domain almost concurrently. In order to mask the latency and achieve high performance the optimal thread occupancy and thus numerical resolution must be high.

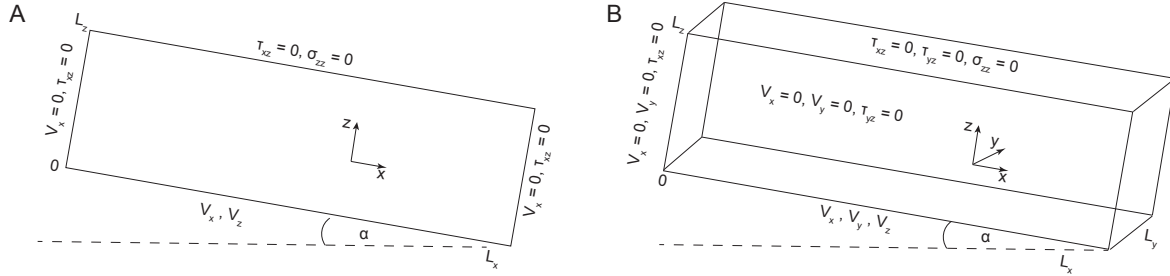


**Figure 2.3:** Schematic illustrating the set-up for the numerical experiments: A) two-dimensional model B) three-dimensional model. Both surface and the bed are flat and inclined for a constant slope angle  $\alpha$ . The model coordinate axes are shown and the applied boundary conditions are also presented.

Some general disadvantages of using GPUs are therefore the time one needs to invest into development of the new algorithm, and the need that this algorithm is suited to the GPU massively parallel architecture. Algorithm development also needs to strongly take into the account GPU threads and memory hierarchy and limit the transfer of data from and to the GPU device. On the other hand, GPU's are compact, highly available, relatively programmable devices which offer high performance (theoretical memory peak bandwidth and gigaflops performance) and good price to performance ratio. To summarize, GPUs offer a successful alternative to conventional CPUs and thanks to their massively parallel architecture philosophy with thousands of cores and threads the performance gap between them today can be more then two orders of magnitude (Omlin, 2017).

## 2.4 Model configuration

In order to verify the numerical implementation of the developed PT model, we consider three numerical experiments based on a inclined box featuring a mean slope angle  $\alpha$ . We perform these numerical experiments on both two- and three-dimensional computational domains (Figure 2.3A 2.3B, respectively). The extent of the computational domain is given by  $\Omega_{2D} = [0 \ L_x] \times [0 \ L_z]$  and  $\Omega_{3D} = [0 \ L_x] \times [0 \ L_y] \times [0 \ L_z]$  for two and three-dimensional domain, respectively. The difference between the 2D and the 3D configuration lies in the boundary conditions imposed at the base and at the lateral sides. At the surface, the zero stress  $\sigma_{ij}n_j = 0$  boundary condition is prescribed in all experiments.

The aim of Experiment 1 and 2 is to first verify the implementation of the mechanical part of the solver, i.e. the Stokes solver, which is the most computationally expensive part (Equations 2.7-2.9). For these experiments, the model can therefore be considered isothermal. We compare the numerical solutions we obtain to the solutions delivered by the finite element Stokes

solver Elmer/Ice (Gagliardini et al., 2013), which has been tested thoroughly (Gagliardini and Zwinger, 2008; Pattyn et al., 2008). Experiment 3 is thermo-mechanically coupled.

The model parameters are the stress exponent  $n$ , the mean bed slope  $\alpha$  and two horizontal distances  $L_x$  and  $L_y$  in their respective dimensions  $(x, y)$  and are given in Table 2.1.

**Table 2.1:** Non-dimensional model parameters and the dimensional values for comparison

Experiment	$L_x$	$L_y$	$\alpha$	$n$	$\beta_0$	$L_x^D$	$L_y^D$	$L_z^D$
Exp.1 2D	10	-	10	3	-	2 km	/	200 m
Exp.1 3D	10	4	10	3	-	2 km	800 m	200 m
Exp.2 2D	10	-	0.1	3	0.1942	10 km	/	1 km
Exp.2 3D	10	10	0.1	3	0.1942	10 km	10 km	1 km

impose a no-slip or zero-velocity condition for all directions

In the Experiment 1, at the base, we impose a no-slip or zero-velocity condition in all directions. We set the free slip boundary conditions at the lateral boundaries. Experiment 2 differs from the first one with regards to both the implemented periodic boundary conditions on the lateral sides, and the basal prescribed linear sliding law (Equation 2.5). The 3D and 2D sliding coefficients are given as follows:

$$\begin{aligned}\beta^2(x, y) &= \beta_0 \left( 1 + \sin \frac{2\pi x}{L_x} \sin \frac{2\pi y}{L_y} \right) \\ \beta^2(x) &= \beta_0 \left( 1 + \sin \frac{2\pi x}{L_x} \right)\end{aligned}\tag{2.24}$$

where  $\beta_0$  is a chosen non-dimensional constant. Therefore, the model configuration of Experiment 2 corresponds to the ISMIP benchmark (Pattyn et al., 2008) experiment C in the 3D or experiment D in the 2D case. The differences can arise depending on the prescribed values of the parameters  $\alpha$ ,  $L_x$ ,  $L_y$  and  $\beta_0$ . This experiment is exactly the same as ISMIP experiments C and D at  $L = 10$  km (Pattyn et al., 2008), but in our case we use non-dimensional variables. In contrast to Experiments 1 and 2, for Experiment 3 the configuration and the boundary conditions are identical to the Experiment 1, while the additional boundary conditions are given on the temperature and fluxes. The deviation of the surface temperature  $T_0$  is kept equal to 0 at the surface. At the bottom we set the vertical flux  $q_z$  to 0, while on the lateral sides both fluxes  $q_x$  and  $q_z$  are set to 0 as well. Additionally, Experiment 3 comprises also the 1D model. The model parameters used in the Experiment 3 can be found in Table 2.2.

**Table 2.2:** Experiment 3: Non-dimensional model parameters and the dimensional values for comparison

Experiment	$L_x$	$L_y$	$L_z$	$\alpha$	$n$	$\bar{F}$	$T_0$	$L_x^D$	$L_y^D$	$L_z^D$	$T_0^D$
1D	-	-	$3 \times 10^5$	10	3	$2.8 \times 10^{-8}$	9.15	/	/	300 m	-10 °C
2D	$10L_z$	-	$3 \times 10^5$	10	3	$2.8 \times 10^{-8}$	9.15	3 km	/	300 m	-10 °C
3D	$10L_z$	$4L_z$	$3 \times 10^5$	10	3	$2.8 \times 10^{-8}$	9.15	3km	1.2 km	300 m	-10 °C

## 2.5 Results and performance

### 2.5.1 Experiments results

#### Experiments 1 and 2: Stokes solver

In this section, we report and compare our numerical solutions obtained by the PT method (CUDA C implementation) to the reference Elmer/Ice model. All the values are reported in their dimensionless form, while the horizontal axes are always scaled with their aspect ratio.

In Figure 2.4, the results of the two-dimensional Experiment 1 simulation are reported. Since this is a two-dimensional experiment, we report both horizontal  $V_x$  and vertical velocity  $V_z$  components at the top surface. Since at the left and right boundary horizontal velocity is set to zero, the maximum value obtained by the ice flow is located in the middle of the slab. Contrary to the horizontal velocity, the boundary condition on the vertical velocity reduces to a free slip boundary condition ( $\partial V_z / \partial x = 0$ ). On the left side, the ice is pushed down (compression), and therefore the values of the vertical velocity are negative, while on the right side the ice is being pulled up (extension), and values of the vertical velocity are positive. The results obtained with our PT algorithm are in good agreement with the numerical solutions produced by Elmer/Ice. The numerical resolution of the Elmer/Ice model is  $1001 \times 275$  ( $8.25 \times 10^5$  DoF's) grid points in x and z directions, while we employed  $2047 \times 511$  ( $31.38 \times 10^5$  DoF's) grid points for the PT method. The DoF represent the number of degrees of freedom (DoF), i.e. 3 variables in 2D ( $V_x, V_z, P$ ) and 4 variables in 3D ( $V_x, V_y, V_z, P$ ) multiplied by the number of grid points involved.

In Figure 2.5, the results of the three-dimensional Experiment 1 simulation are reported. We report the horizontal  $V_x, V_y$  and vertical velocity  $V_z$  components at the top surface in the upper panel, while a comparison with the reference solution from Elmer/Ice at  $y \approx L_y/4$  is made in the lower panel. Again, there is a good agreement between the models. In the case of the PT method, the numerical resolution used was  $319 \times 159 \times 119$  ( $\approx 24.14 \times 10^6$  DOF's) grid points in x, y and z directions. The numerical resolution used in Elmer/Ice was set to  $61 \times 61 \times 21$  ( $\approx 3.1 \times 10^5$  DOF's).

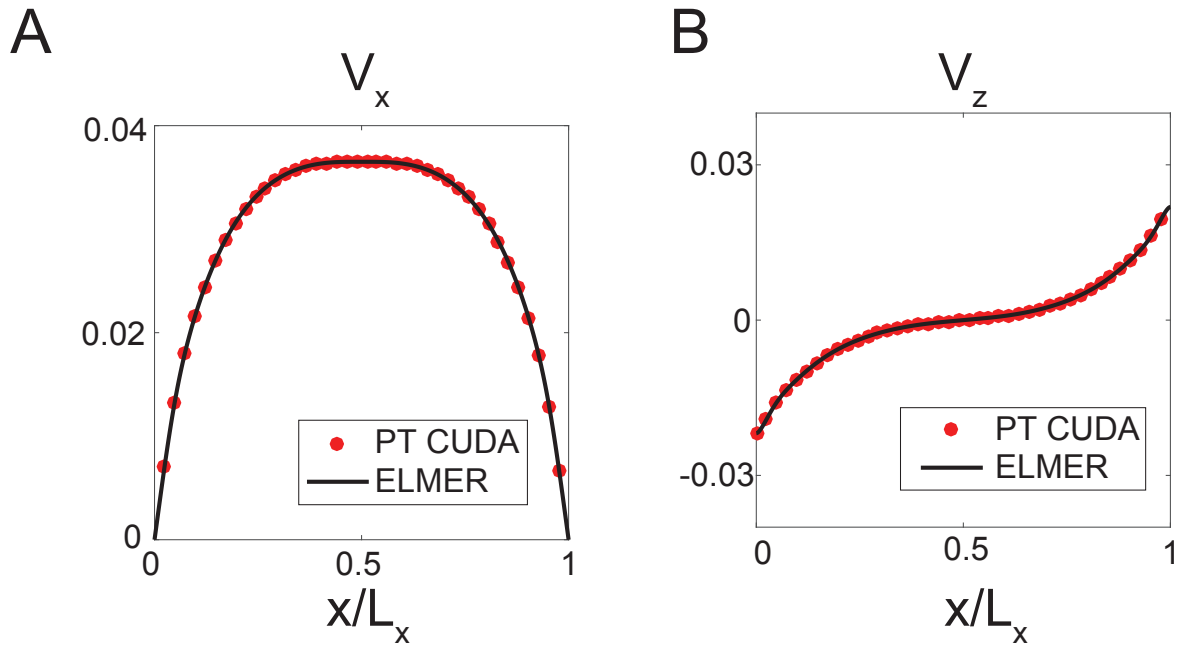


**Figure 2.4:** Non-dimensional simulation results for the 2D set-up of Experiment 1: A) horizontal surface velocity B) vertical surface velocity across the slab. The results of both PT CUDA model and Elmer/Ice model are reported and compared. The horizontal distance  $x$  is scaled with the reported aspect ratio  $L_x$ , while the non-dimensional values of velocities are reported. For comparison the maximum horizontal velocity ( $\approx 0.0365$ ) would correspond to  $\approx 174 \frac{\text{m}}{\text{yr}}$ . The horizontal distance is 2 km, while the ice thickness is 200 m. The box is inclined for  $10^\circ$ .

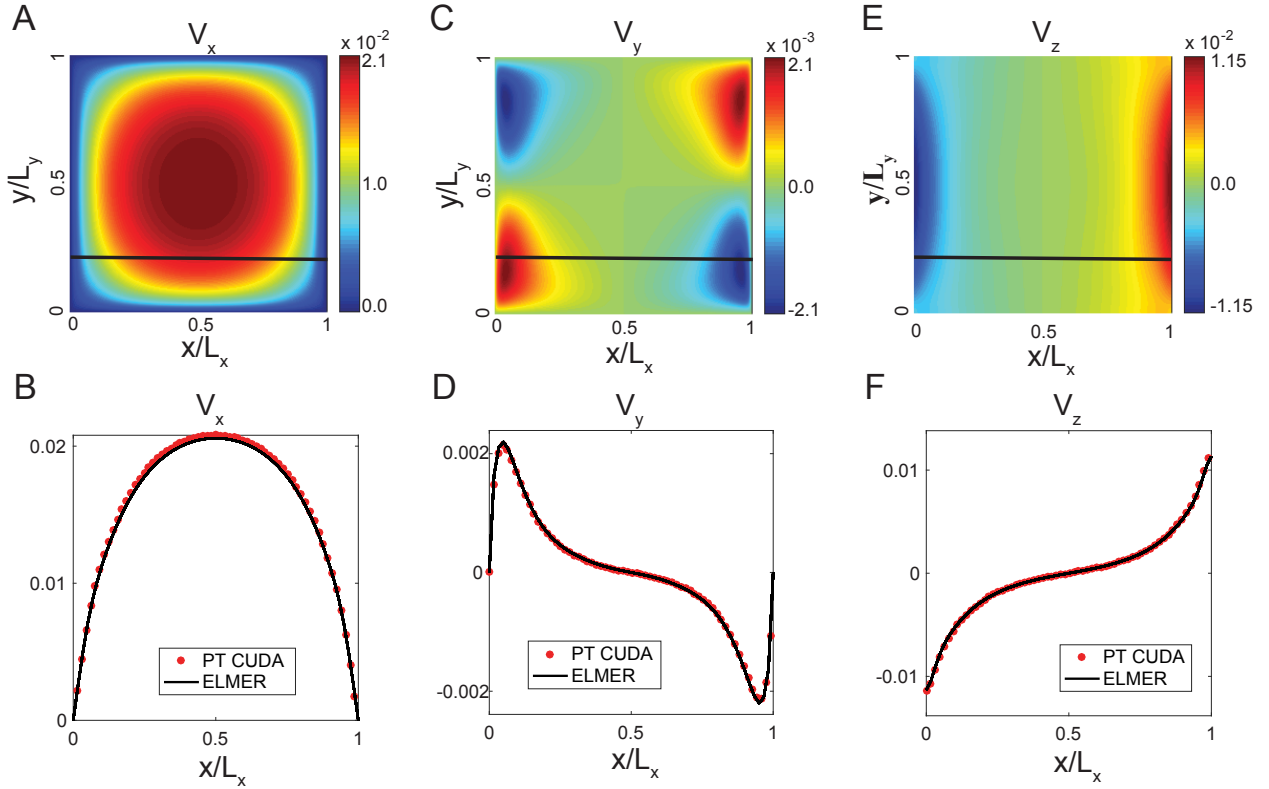


**Figure 2.5:** Non-dimensional simulation results for the 3D set-up of Experiment 1: in the upper panel from left to right (A, C and E) surface velocity components ( $V_x$ ,  $V_y$  and  $V_z$ ) are shown. The black solid line depicts the position where  $y = \frac{L_y}{4}$ . In the bottom panel from left to right (B, D and F), the surface velocity components ( $V_x$ ,  $V_y$  and  $V_z$ ) at  $y = \frac{L_y}{4}$  are reported and compared with Elmer/Ice model. Horizontal distances  $x$  and  $y$  are scaled with the reported aspect ratio  $L_x$  and  $L_y$  respectively, while all the values of the velocity are given in their non-dimensional form. For comparison the maximum horizontal velocity ( $\approx 0.022$ ) would correspond to  $\approx 105 \frac{\text{m}}{\text{yr}}$ . The horizontal distance is 2 km in x-direction, 800 m in y-direction, while the ice thickness is 200 m. The box is inclined for  $10^\circ$ .

Experiment 2 considers the case where ice is sliding at the base. This experiment is exactly the same as ISMIP experiments C and D at  $L = 10$  km, but in our case we use non-dimensional variables. The periodic boundary conditions are prescribed at the lateral boundaries. In Figure 2.6, the results of the two-dimensional Experiment 2 simulation are reported. Elmer/Ice solution was obtained with the numerical resolution of  $241 \times 120$  ( $\approx 8.7 \times 10^4$  DOF's), while the PT method used the numerical resolution of  $511 \times 127$  grid points ( $1.95 \approx 10^5$  DOF's). Both velocity components ( $V_x$  and  $V_z$ ) at the surface of the slab are shown and compared between the models. Again, excellent agreement between the models is obtained.

In Figure 2.7, the PT method simulation results for the surface velocity components ( $V_x$ ,  $V_y$  and  $V_z$ ) are shown in the upper panel, while in the lower panel surface velocity components at  $y \approx L_y/4$  are presented and compared. In this simulation the Elmer/Ice model used the numerical resolution of  $61 \times 61 \times 21$  ( $\approx 3.12 \times 10^5$  DOF's), while the solution obtained with the PT method used the numerical resolution of  $63 \times 63 \times 31$  ( $\approx 1.23 \times 10^5$  DOF's). Good agreement between the numerical implementations is seen, even though some differences between the solutions can be seen in horizontal velocity component  $V_y$ . We explain this differences with the fact that the grid does not coincide with the  $y = \frac{L_y}{4}$  and its dependent on the numerical resolution. Additionally, since the flow is driven by the basal boundary condition velocity component  $V_y$  is more then two orders smaller then the velocity component  $V_x$ , therefore the differences are more pronounced.

As already stated, the differences between Experiments 1 and 2 can be found in the applied boundary conditions. Periodic boundary conditions are applied on the lateral side, while linear sliding law is applied at the base. This results in order of magnitude higher values in the convergence rate and therefore higher time to the solution. A closer investigation reveals that this is due to the periodic boundary conditions, since the viscosity ratio is similar in both experiments and additional non-linearities due to slip do not introduce new significant non-linearities.

### **Numerical time integration and thermo-mechanical coupling: Benchmarking of our implementation**

Here we report the numerical solutions obtained by the three developed algorithms based on the PT method. They are implemented in either MATLAB or CUDA C programming languages; the 3D model, addressing the full set of equations in  $x, y$  and  $z$  coordinates, the 2D model in which there is no variation in  $y$  direction, thus delivering a numerical solution only in  $x$  and  $z$  coordinates; the 1D model in which there is no variation in neither  $x$  nor  $y$  direction.

The 1D model is a special mathematical case, in which we can employ analytical integration to derive a physically semi-decoupled set of PDEs (Equation 2.15 and 2.16). From a

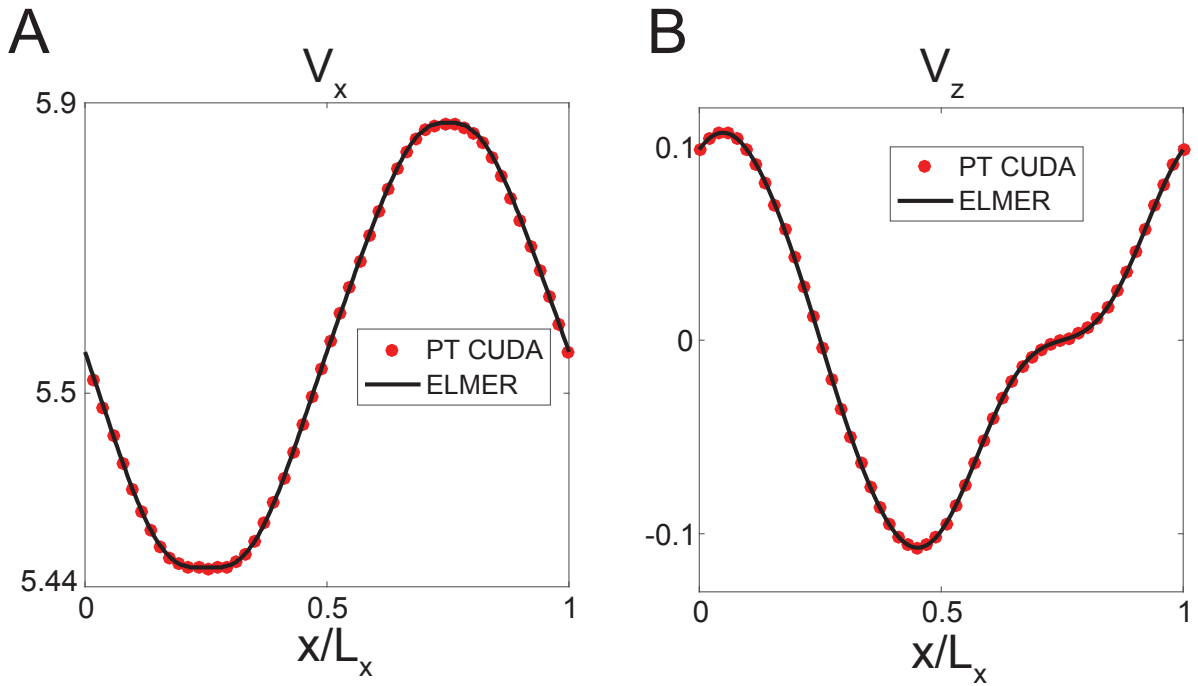


**Figure 2.6:** Non-dimensional simulation results for the 2D set-up of Experiment 2: A) horizontal surface velocity B) vertical surface velocity across the slab. The results of both PT CUDA model and Elmer/Ice model are reported and compared. The horizontal distance  $x$  is scaled with the reported aspect ratio  $L_x$ , while the non-dimensional values of velocities are reported. For comparison the maximum horizontal velocity ( $\approx 5.58$ ) would correspond to  $\approx 16.9 \frac{\text{m}}{\text{yr}}$ . The horizontal distance is 10 km, while the ice thickness is 1 km. The box is inclined for  $0.1^\circ$ .

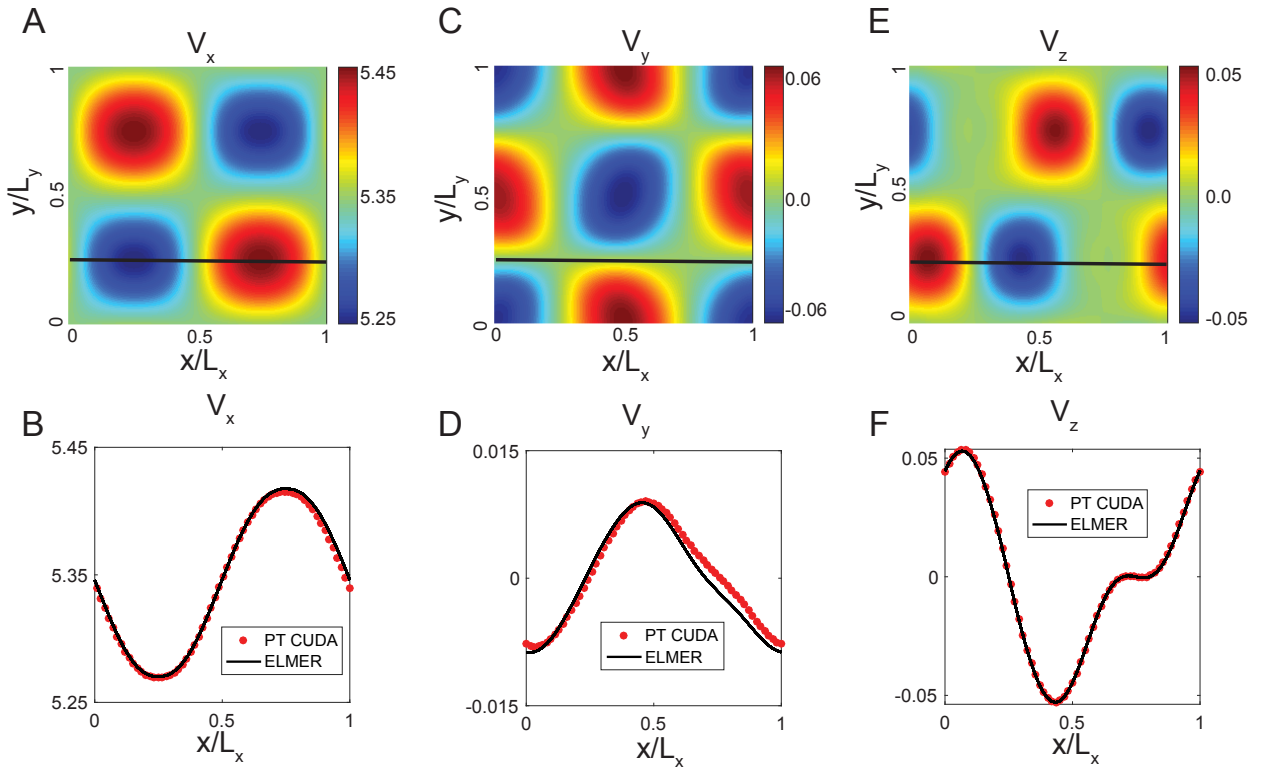


**Figure 2.7:** Non-dimensional simulation results for the 3D set-up of Experiment 2: in the upper panel from left to right (A, C and E) surface velocity components ( $V_x$ ,  $V_y$  and  $V_z$ ) are shown. The black solid line depicts the position where  $y = \frac{L_y}{4}$ . In the bottom panel from left to right (B, D and F), the surface velocity components ( $V_x$ ,  $V_y$  and  $V_z$ ) at  $y = \frac{L_y}{4}$  are reported and compared with Elmer/Ice model. The horizontal distances  $x$  and  $y$  are scaled with the reported aspect ratio  $L_x$  and  $L_y$  respectively, while all the values of the velocity are given in their non-dimensional form. For comparison the maximum horizontal velocity ( $\approx 5.42$ ) would correspond to  $\approx 16.4 \frac{\text{m}}{\text{yr}}$ . The horizontal distance is 10 km in x-direction, 10 km in y-direction, while the ice thickness is 1 km. The box is inclined for  $0.1^\circ$ .

computational point of view, one can numerically solve this PDE with a high spatial and temporal resolution and therefore minimize the influence of numerical errors. To establish a 1D reference solution for both the temperature and velocity profile, we have numerically solved Equation 2.15 on regular grid, varying numerical time steps until we have determined a reference solution. The influence of different time integration methods was also investigated. As a reference solution, we taken the run with 4000 grid points and a time step of  $5 \times 10^5$  in dimensionless value. The numerical time integration is performed using a backward Euler implicit method. The total simulation time was  $2.9 \times 10^8$  and therefore 580 numerical time steps were performed. The 1D algorithm was implemented using the MATLAB programming language. Using the dimensional value, the numerical time step used would correspond to around 4.3 days, while the total simulation time corresponds to approximately 6.7 years. All the values are reported in their dimensionless form using the scales given in the Equation 2.10, while the horizontal axes are scaled with the non-dimensional ice thickness  $L_z$  in all the figures.

The PT solver was then run with exactly the same physical parameters as the reference model, for varying numerical resolutions. In Figure 2.8, we show the reference solution and compare it at three different spatial numerical resolutions and three different physical times. The grey area in Figure 2.8 highlights when melting temperature is passed. The vertical numerical resolution  $n_z$  used was 31, 95 and 201 grid points. The numerical solutions were compared at non-dimensional times  $1 \times 10^8$ ,  $2 \times 10^8$  and  $2.9 \times 10^8$ . (Using the dimensional values this would correspond to 2.3, 4.6 and 6.7 years). One can notice that at relatively short times, while the coupling is still minor, solutions at all numerical resolutions agree with each other and with the reference solution. As soon as the coupling becomes stronger, the solutions obtained with a lower numerical resolution start to deviate from the reference model, while the solution obtained at high spatial resolution with PT model is still satisfactory. Note that after 6.7 years, the model would reach melting temperature and is not realistic.

Next, the influence of the numerical coupling method and numerical time integration in physical time is studied. Hence, three different numerical models were compared. The first model is the coupled PT method, described in the numerical section, where the viscosity and therefore the strain heating term is implicitly determined at the current time step. The numerical time integration in physical time is performed using the backward Euler implicit method. The second model differs from the first one in a sense that the mechanical and thermal model are numerically decoupled. Physically, the viscosity, and hence the strain heating term, are still coupled and are a function of temperature. For this case, in the mechanical model viscosity and strain heating terms are a function of temperature obtained at the previous time step. The strain heating term can therefore, during a single time step, be considered as a constant source term in the temperature evolution equation. Again, for the second model numerical time integration in physical time is performed using the backward Euler implicit method. The

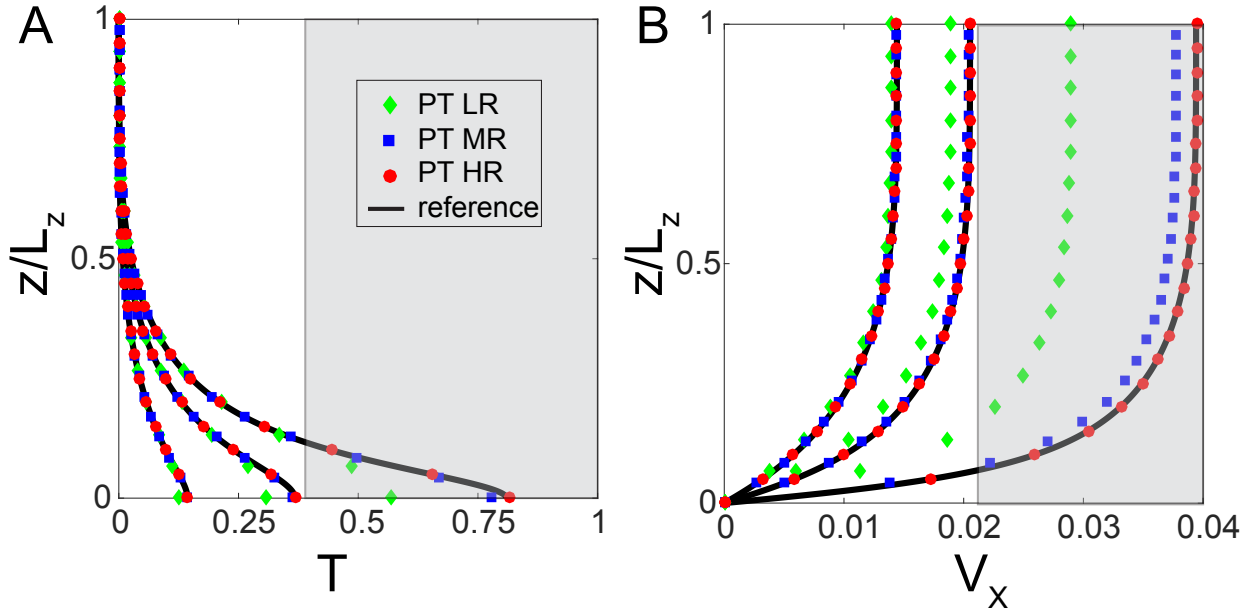


**Figure 2.8:** Non-dimensional simulation results for the A) temperature deviation  $T$  B) horizontal velocity component  $V_x$ . The results of the PT model at three different numerical resolutions are reported and compared with a reference model results. Vertical resolutions used are  $LR = 31$ ,  $MR = 95$  and  $HR = 201$  grid points. The results are compared at non-dimensional times  $1 \times 10^8$ ,  $2 \times 10^8$  and  $2.9 \times 10^8$ . Using the dimensional values this would correspond to 2.3, 4.6 and 6.7 years. The vertical distance  $z$  is scaled with the ice thickness  $L_z$ , while the non-dimensional values of temperature deviation and velocities are reported on x axis. Shaded area corresponds to the part of the solution which is above the melting temperature and it is therefore unphysical. The melting temperature in non dimensional units approximately corresponds to 0.35. This configuration would correspond to a 300 m thick slab inclined for the  $10^\circ$  angle with a surface temperature of  $-10^\circ\text{C}$ . Maximum initial velocity for the isothermal slab would correspond to approximately  $486 \frac{\text{m}}{\text{yr}}$ , while the maximum velocity just before the melting point is reached correspond to  $830 \frac{\text{m}}{\text{yr}}$ . The flow law constant  $a_0$  used corresponds to  $8.75 \times 10^{-13} \text{Pa}^{-3} \text{s}^{-1}$

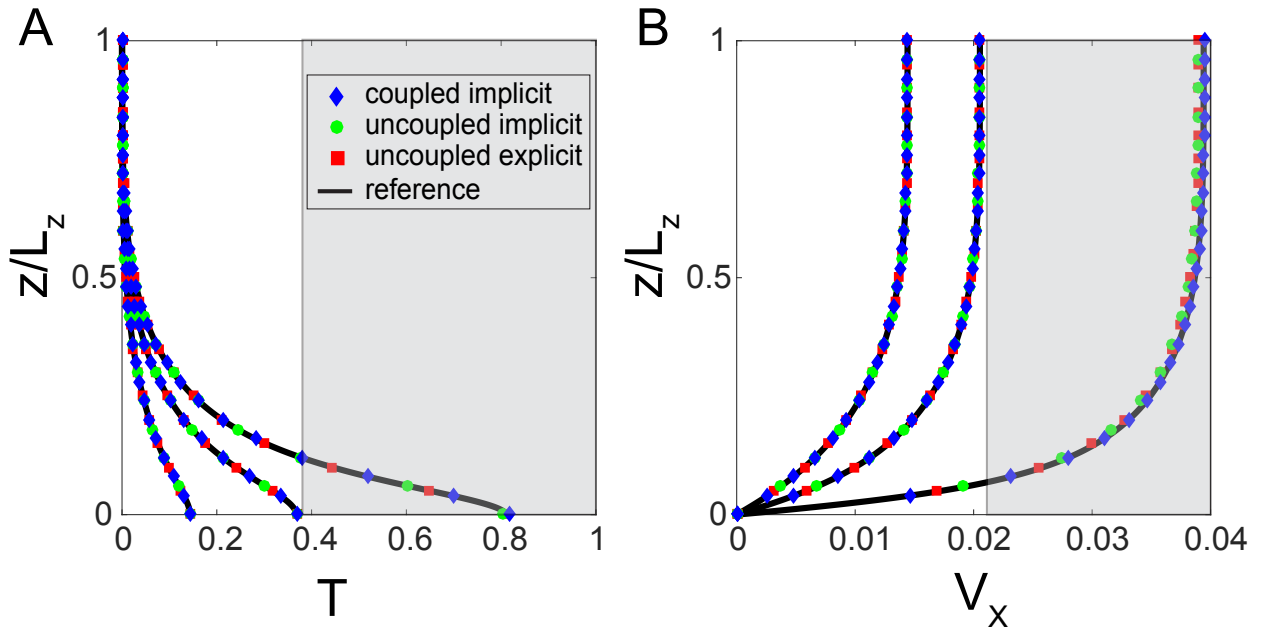


**Figure 2.9:** Non-dimensional simulation results for the A) temperature deviation  $T$  B) horizontal velocity component  $V_x$ . The results of both coupled and uncoupled model with different numerical time integration methods at three different times are reported and compared with a reference model results. The results are compared at non-dimensional times  $1 \times 10^8$ ,  $2 \times 10^8$  and  $2.9 \times 10^8$ . Using the dimensional values this would correspond to 2.3, 4.6 and 6.7 years. The vertical distance  $z$  is scaled with the ice thickness  $L_z$ , while the non-dimensional values of temperature deviation and velocities are reported on x axis. Shaded area corresponds to the part of the solution which is above the melting temperature and it is therefore unphysical. The melting temperature approximately corresponds to 0.35 of temperature deviation. This configuration would correspond to a 300 m thick slab inclined for the  $10^\circ$  angle with a surface temperature of  $-10^\circ\text{C}$ . Maximum initial velocity for the isothermal slab would correspond to approximately  $486 \frac{\text{m}}{\text{yr}}$ , while the maximum velocity just before the melting point is reached correspond to  $830 \frac{\text{m}}{\text{yr}}$ . The flow law constant  $a_0$  used corresponds to  $8.75 \times 10^{-13} Pa^{-3} s^{-1}$

third model differs from the second one such that a numerical time integration in physical time is performed using the forward Euler explicit method. Therefore, in this case we investigate the influence of the numerical coupling and the numerical time integration method on the numerical solution. For both explicit and implicit numerical time integration the same time step is used  $5 \times 10^5$  in dimensionless value. The total simulation time was  $2.9 \times 10^8$  and therefore 580 numerical time steps were performed. The vertical numerical resolution with 201 grid points is used for all models. We make sure that the chosen time step for explicit integration of diffusion equation is below the stability condition or the Courant–Friedrichs–Lewy condition (CFL) for the explicit scheme given by  $\frac{\Delta z^2}{2.1}$ , where  $\Delta z$  represent the grid spacing in vertical direction. In Figure 2.9, we show the numerical solutions of the fully coupled method with backward Euler (implicit) time integration and two uncoupled methods with either backward (implicit) or forward (explicit) Euler time integration. These results are also compared with the reference model solution. Interestingly, a good agreement between all methods is achieved, suggesting that if high enough spatial and temporal resolution are chosen all methods can capture the coupled flow correctly. For larger times, when a physical coupling is stronger, both the uncoupled models give a slightly smaller values then for the coupled model for both the temperature and velocity.

Next, we have additionally verified that developed 2D and 3D algorithms can also reproduce the same results if appropriate boundary conditions are implemented. For example, in both 2D and 3D models periodic boundary conditions are implemented on the lateral side, similar to the Experiment 2 case. In this case, all the variable variations in  $x$  or  $y$  coordinate vanish ( $\frac{\partial}{\partial x}$  and  $\frac{\partial}{\partial y}$ ) and therefore both models reduces to the 1D problem. In the 3D model run, we used the numerical resolution of  $127 \times 127 \times 127$  grid points in  $x$ ,  $y$  and  $z$  direction, while in the case of a 2D model the numerical resolution of  $127 \times 127$  grid points in  $x$  and  $z$  directions was used.

In Figures 2.10 and 2.11, we show the non-dimensional numerical simulations results for the temperature  $T$  and horizontal velocity  $V_x$  for both the three and two-dimensional cases at three different physical times. The numerical solutions were compared at times  $0.7 \times 10^8$ ,  $1.4 \times 10^8$  and  $1.9 \times 10^8$ . Using the dimensional values this would correspond to 1.6, 3.2 and 4.4 years. All units are non-dimensional. As expected from a 1D model solution, temperature varies only as a function of time and depth with the highest value obtained close to the base and at the later times. Similarly, the velocity profile is equivalent to the 1D model solution and the largest velocity value is found at the surface. For the 2D and 3D model we report only the horizontal velocity component  $V_x$ , since  $V_y$  and  $V_z$  are negligible. Hence, spatial variation can only be seen in the vertical direction.

In Figure 2.12, we show a comparison of all PT method based models and a reference solution. Good agreement between all models is achieved at initial times, while temperature values are still low, and the coupling is not so pronounced. At later times, closer to the thermal runaway

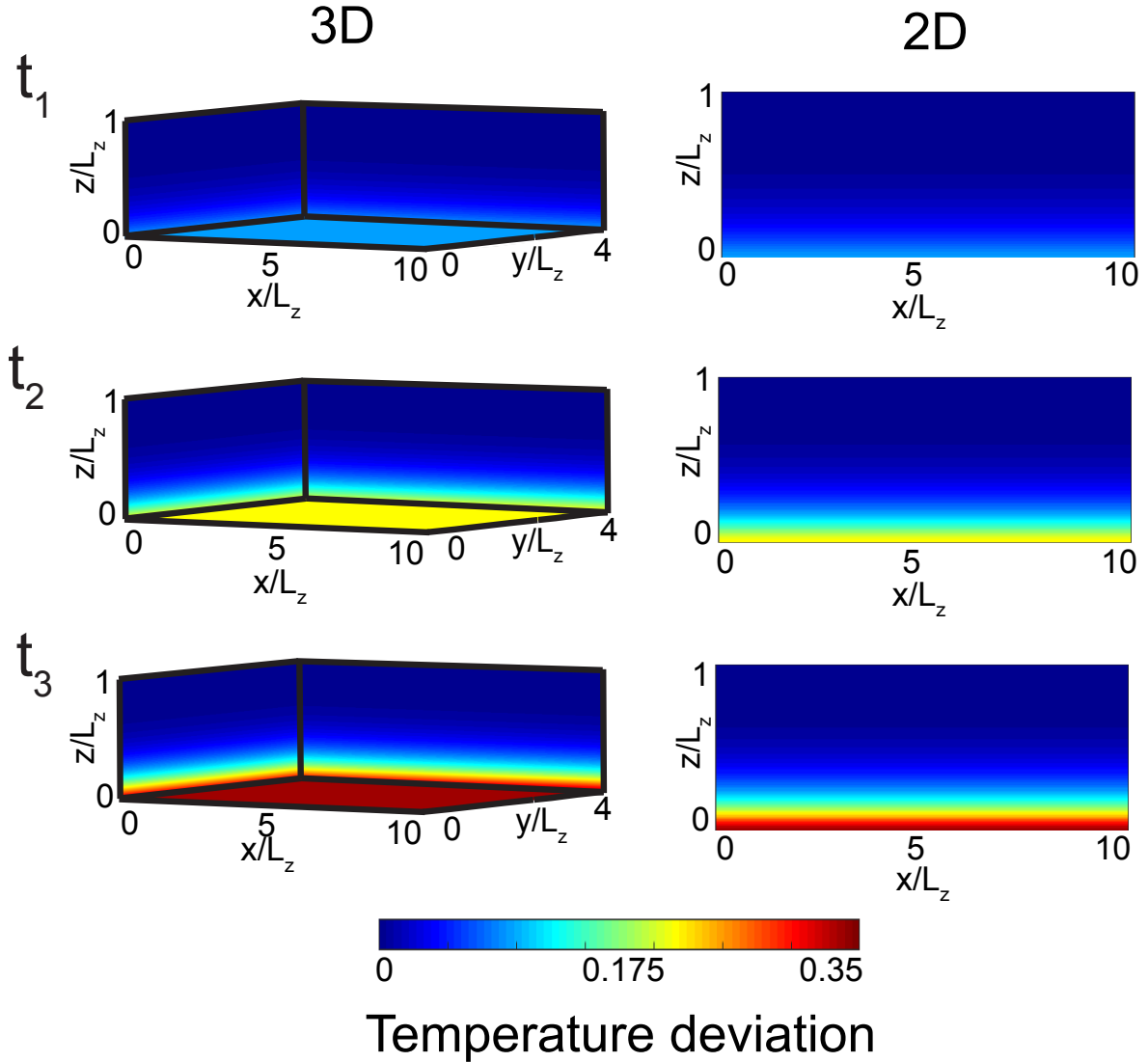


**Figure 2.10:** Non-dimensional simulation results at three different time stages for both 2D and 3D model implementations are presented. In the left column the spatial distribution of the temperature deviation from the initial temperature  $T$  is shown for a 3D model, while in the right column the same is shown for a 2D model implementation. For readability, the length scales are rescaled with  $L_z$ . The numerical solutions were compared at times  $0.7 \times 10^8$ ,  $1.4 \times 10^8$  and  $1.9 \times 10^8$ . Using the dimensional values this would correspond to 1.6, 3.2 and 4.4 years. This configuration would correspond to a 300 m thick slab inclined for the  $10^\circ$  angle with a initial surface temperature of  $-10^\circ\text{C}$ . Maximum initial velocity for the isothermal slab would correspond to approximately  $486 \frac{\text{m}}{\text{yr}}$ , while the maximum velocity just before the melting point is reached correspond to  $830 \frac{\text{m}}{\text{yr}}$ .

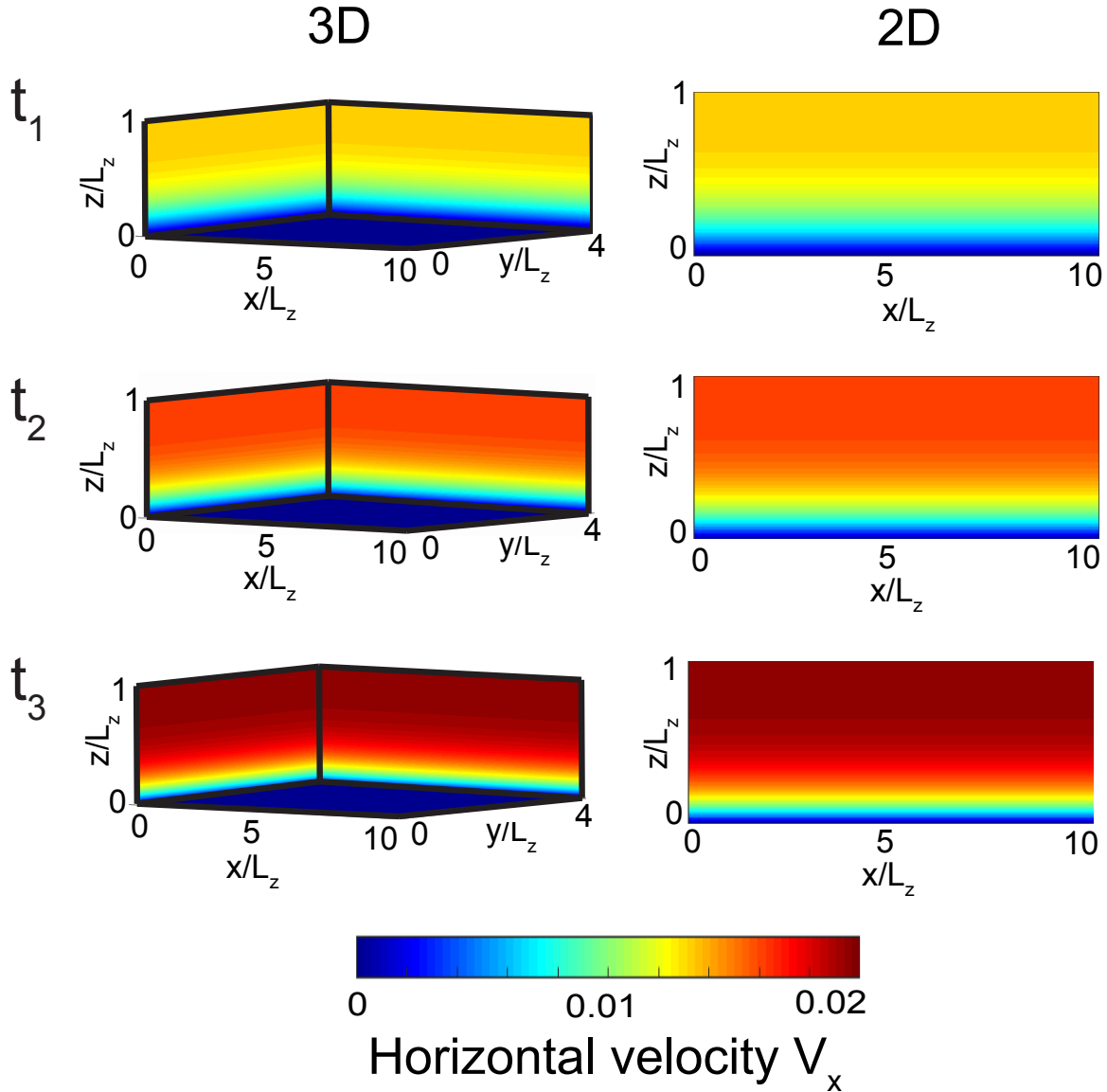


**Figure 2.11:** Non-dimensional simulation results at three different time stages for both 2D and 3D model implementations are presented. In the left column the spatial distribution of the horizontal velocity component  $V_x$  is shown for a 3D model, while in the right column the same is shown for a 2D model implementation. For readability, the length scales are rescaled with  $L_z$ . The numerical solutions were compared at times  $0.7 \times 10^8$ ,  $1.4 \times 10^8$  and  $1.9 \times 10^8$ . Using the dimensional values this would correspond to 1.6, 3.2 and 4.4 years. This configuration would correspond to a 300 m thick slab inclined for the  $10^\circ$  angle with a initial surface temperature of  $-10^\circ\text{C}$ . Maximum initial velocity for the isothermal slab would correspond to approximately  $486 \frac{\text{m}}{\text{yr}}$ , while the maximum velocity just before the melting point is reached correspond to  $830 \frac{\text{m}}{\text{yr}}$ .

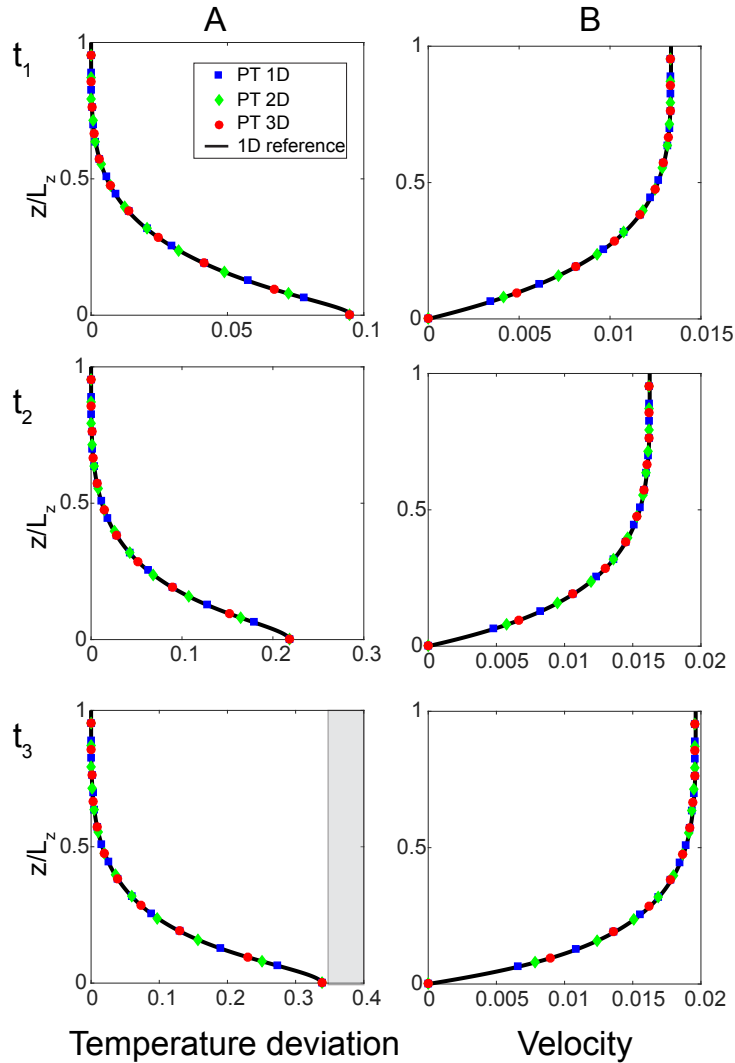


**Figure 2.12:** Non-dimensional simulation results for the A) temperature deviation  $T$  B) horizontal velocity component  $V_x$ . Results of three PT models implementations (1D, 2D and 3D model) at three different times are reported and compared with a reference model results. Vertical resolutions used are 31, 95 and 201 grid points. The results are compared at non-dimensional times  $0.7 \times 10^8$ ,  $1.4 \times 10^8$  and  $1.9 \times 10^8$ . Using the dimensional values this would correspond to 1.6, 3.2 and 4.4 years. The results of a 2D model are taken at location  $x = \frac{L_x}{2}$ , while the results of a 3D model were taken at location  $x = \frac{L_x}{2}$  and  $y = \frac{L_y}{2}$ . The vertical distance  $z$  is scaled with the ice thickness  $L_z$ , while the non-dimensional values of temperature and velocities are reported on x axis. Shaded area corresponds to the part of the solution which is above the melting temperature and it is therefore unphysical. The melting temperature approximately corresponds to 0.35 of temperature deviation. This configuration would correspond to a 300 m thick slab inclined for the  $10^\circ$  angle with a surface temperature of  $-10^\circ\text{C}$ . Maximum initial velocity for the isothermal slab would correspond to approximately  $486 \frac{\text{m}}{\text{yr}}$ , while the maximum velocity just before the melting point is reached correspond to  $830 \frac{\text{m}}{\text{yr}}$ .

(Clarke et al., 1977), slight deviations of all lower resolution models (127 grid points) can be noticed, which suggest that a higher spatial resolutions is needed to properly capture the behaviour close to the thermal runaway. This is additionally corroborated with the previous results, where a higher vertical resolution of 201 grid points prove sufficient to model the coupled flow even at the larger times. The lower vertical resolution of only 127 grid points is chosen because of the 3D model, to achieve reasonable computation times. Therefore, it is established that at high enough numerical resolution all algorithms can successfully resolve the coupled thermo-mechanical ice flow.

### Experiments 3: Thermo-mechanical coupling

Now we report the numerical solutions obtained by the 2D and 3D PT algorithms. The obtained solutions are compared to the 1D solutions to investigate the spatial variations in temperature and velocity for the prescribed boundary conditions. All the values are reported in their dimensionless form, while the horizontal axes are always scaled with their aspect ratio. In the 3D model run, we used the numerical resolution of  $511 \times 255 \times 127$  grid points, while in the case of a 2D model the numerical resolution of  $511 \times 127$  grid points was used. The numerical time step used was  $5 \times 10^5$  in dimensionless value. The total simulation non-dimensional time was  $2.9 \times 10^8$  and 580 numerical time steps were performed. The results were compared at non-dimensional times  $1 \times 10^8$ ,  $2 \times 10^8$  and  $2.5 \times 10^8$ . Using the dimensional values this would correspond to 2.3, 4.6 and 5.8 years.

In Figures 2.13 and 2.14, the results of both two and three-dimensional Experiment 1 simulations are reported for temperature  $T$  and velocity component  $V_x$ . Contrary to the previous experiment, all three velocity components are now variable in space and time. At all times, both temperature and velocity reach their highest value at the middle of the box set-up at locations  $x = \frac{L_x}{2}$  and  $y = \frac{L_y}{2}$  in 3D and at  $x = \frac{L_x}{2}$  in 2D. The highest values of temperature are always located at the bottom, while the highest value of velocity is now just below the surface. This can be seen at all times. Interestingly, a significant temperature rise is also located close to the stagnant lateral boundaries. This can be assigned to a now spatially variable strain heating term. Additionally, spatial variability of the temperature in all directions confirms the need for high spatial numerical resolution not only in the vertical direction, but also in the horizontal directions.

In Figure 2.15, we compare the 1D model, obtained by the PT method and reference solution, with the solutions obtained with the 2D PT model and the 3D PT model for both the temperature  $T$  and horizontal velocity component  $V_x$  at three different times. The numerical solutions at  $x = \frac{L_x}{2}$  location is taken for the 2D model, while the numerical solution at location  $x = \frac{L_x}{2}$  and  $y = \frac{L_y}{2}$  is taken in the 3D case. Since the initial time, the temperature deviation is 0 throughout the slab for all models, the only differences between the models

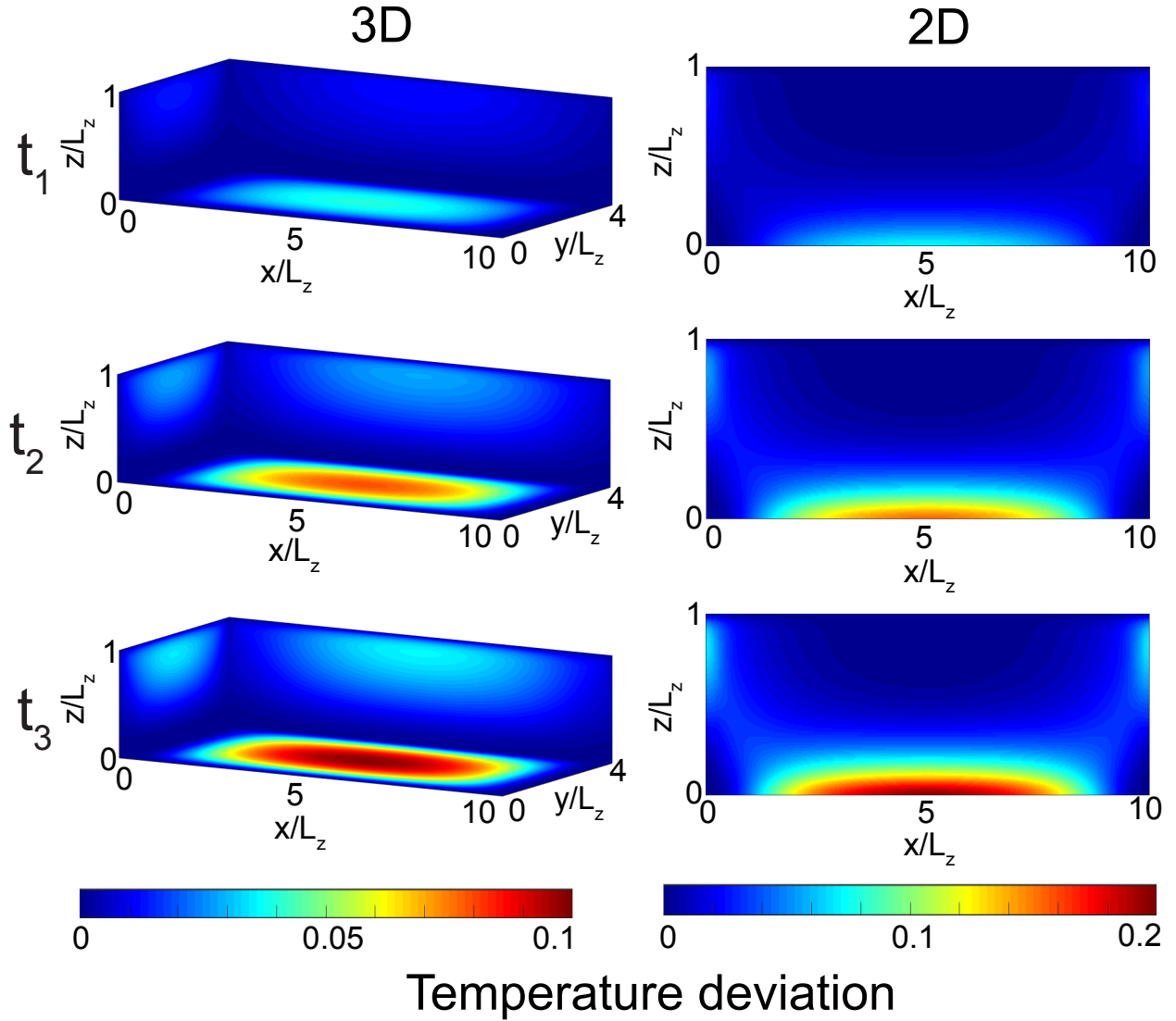


**Figure 2.13:** Non-dimensional simulation results for the Experiment 3 at three different time stages for both 2D and 3D model implementations are presented. In the left column the spatial distribution of the temperature deviation from the initial temperature  $T$  is shown for a 3D model, while in the right column the same is shown for a 2D model implementation. For readability, the length scales are rescaled with  $L_z$ . The results are compared at non-dimensional times  $1 \times 10^8$ ,  $2 \times 10^8$  and  $2.5 \times 10^8$ . Using the dimensional values this would correspond to 2.3, 4.6 and 5.8 year. The melting temperature approximately corresponds to 0.35 of temperature deviation. This configuration would correspond to a 300 m thick slab inclined for the  $10^\circ$  angle with a surface temperature of  $-10^\circ\text{C}$

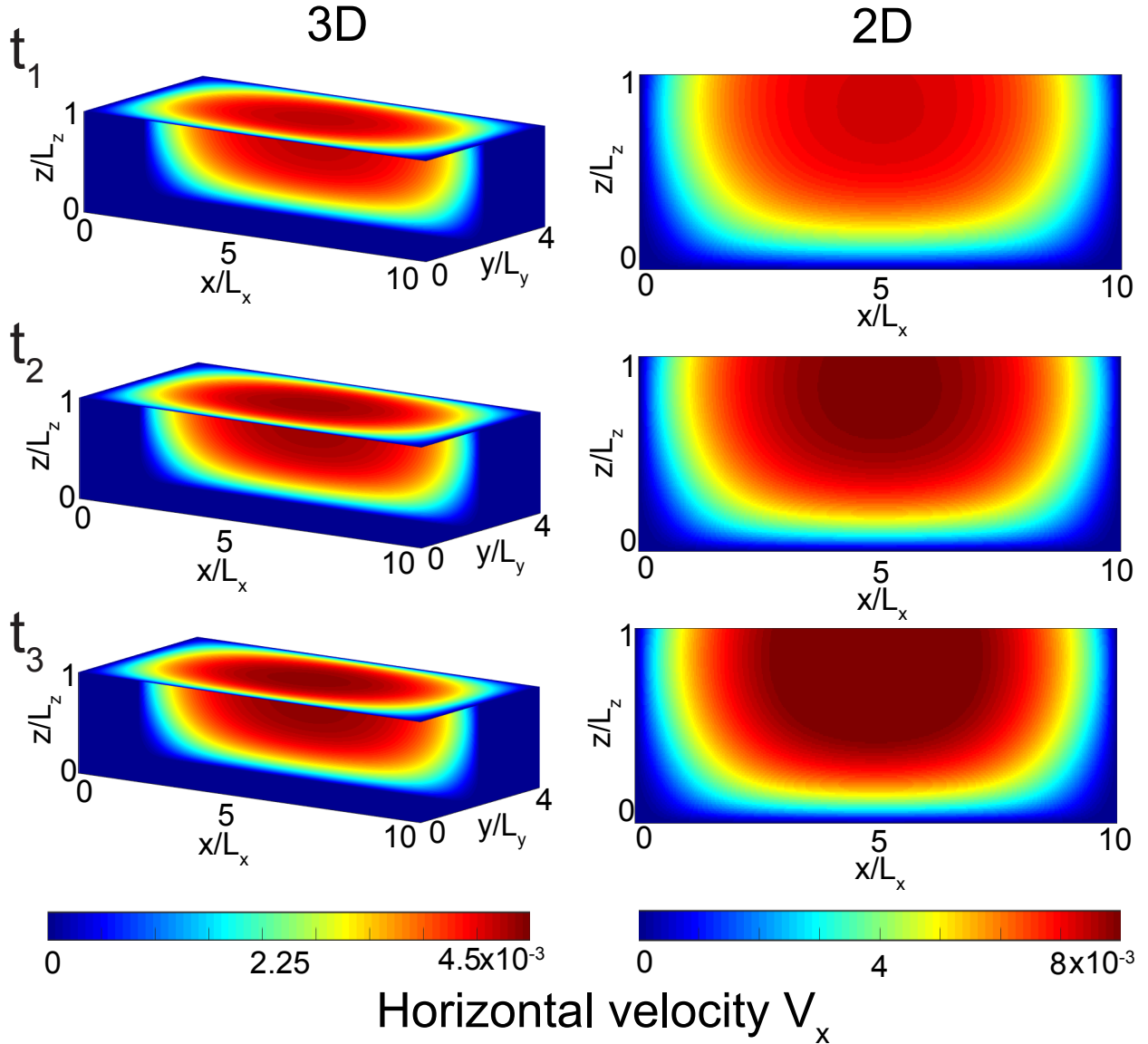


**Figure 2.14:** Non-dimensional simulation results for the Experiment 3 at three different time stages for both 2D and 3D model implementations are presented. In the left column the spatial distribution of the horizontal velocity component  $V_x$  is shown for a 3D model, while in the right column the same is shown for a 2D model implementation. For readability, the length scales are rescaled with  $L_z$ . The results are compared at non-dimensional times  $1 \times 10^8$ ,  $2 \times 10^8$  and  $2.5 \times 10^8$ . Using the dimensional values this would correspond to 2.3, 4.6 and 5.8 years.

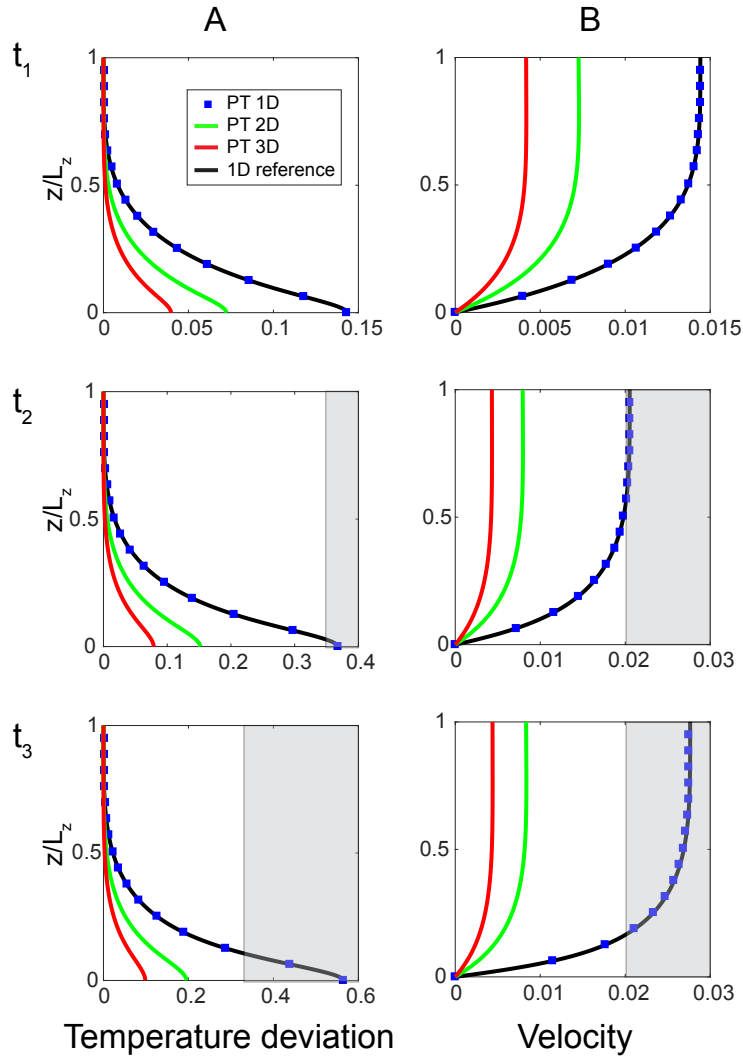


**Figure 2.15:** Non-dimensional simulation results for the Experiment 3: for the A) temperature deviation  $T$  B) horizontal velocity component  $V_x$ . Results of three PT models implementations (1D, 2D and 3D model) with a periodic boundary conditions at the lateral sides at three different times are reported and compared with a reference model results. The results are compared at non-dimensional times  $1 \times 10^8$ ,  $2 \times 10^8$  and  $2.5 \times 10^8$ . Using the dimensional values this would correspond to 2.3, 4.6 and 5.8 year. Results of a 2D model are taken at location  $x = \frac{L_x}{2}$ , while the results of a 3D model were taken at location  $x = \frac{L_x}{2}$  and  $y = \frac{L_y}{2}$ . Vertical distance  $z$  is scaled with the ice thickness  $L_z$ , while the non-dimensional values of temperature and velocities are reported on x axis. Shaded area corresponds to the part of the solution which is above the melting temperature and it is therefore unphysical. The melting temperature approximately corresponds to 0.35 of temperature deviation. This configuration would correspond to a 300 m thick slab inclined for the  $10^\circ$  angle with a surface temperature of  $-10^\circ\text{C}$ . The non-dimensional velocity of 0.02 corresponds to approximately  $830 \frac{\text{m}}{\text{yr}}$ .

at initial time arise because of different stress distribution. For example, additional stress tensor components in 2D and 3D, for aspect ratio used, can be as large as the shear stress tensor component, therefore, velocity is reduced in the 2D and 3D dimension models. This also gives rise to the differences in the strain heating term, and hence the source term in the temperature evolution equation. Additionally, in the 1D case the shear stress tensor component is a function only of depth and therefore a constant in time. This is not the case in the 2D and 3D cases, where all stress tensor components are a function of both the spatial position and time. This is further corroborated by the results in Figure 2.15, where both the temperature and therefore the velocity are highest for the 1D model and significantly reduced for the 2D and 3D models. This additionally confirms the need for the high resolution 3D coupled models.

### 2.5.2 Computational performance

Now that we have verified our method, we wish to assess the computational performance of the algorithm. We use two different metrics to assess the PT algorithm performance; the effective memory throughput ( $MTP_{eff}$ ) and the wall time. We first compare the effective memory throughput of the vectorised MATLAB CPU implementation and CUDA C GPU implementation. We employ double (DP) floating point precision for the CUDA C for fair comparison. Next, we utilize the wall-time metric to compare the performance of our various implementation (MATLAB, CUDA C) and compare those with the time-to-solution of the Elmer/Ice solver. Comparison with Elmer/Ice is not the objective here. Results obtained with Elmer/Ice are therefore used just for reference. We use two different methods to solve the linear system in Elmer/Ice: the direct method and the iterative method, for the 2D experiments and the 3D experiments, respectively. The direct method utilized the UMFPACK routines to solve the linear system, while the bi-conjugate gradient stabilized method (BICGstab) method with ILU0 preconditioning was utilized to solve the linear system in 3D experiments. We employ the Experiment 1 configuration for all the performance measurements. An Intel i7 4960HQ 2.6 GHz (Haswell architecture) 4-cores CPU with Turbo Boost up to 3.8 GHz is used for all model runs involving the CPU. For simplicity, in all experiments a single core of the CPU was utilized, hence no parallelization techniques were employed in the CPU algorithms. Hence, our reference MATLAB or Elmer/Ice single core CPU implementation is not representative of the CPU hardware capabilities.

The PT solver relies on evaluating a finite difference stencil; each cell of the computational domain needs thus to access neighbouring values in order to approximate derivatives. These memory access operations are the performance bottleneck of the algorithm, making it memory bounded. The performance of the algorithm therefore depend crucially on the speed of the

memory transfers and not the rate of the floating point operations. This reflects today’s hardware specifications displaying a significantly important flops-to-bytes ratio.

As shown by Omlin (2017), a relevant metric to assess the performance of the memory bounded algorithms is therefore the effective memory throughput ( $MTP_{eff}$ ) (Equation 2.25). The  $MTP_{eff}$  determines how efficiently data is transferred between the main memory and the computation processor and is inversely proportional to the execution time.

$$MTP_{eff} = \frac{(N_x \cdot N_y \cdot N_z) \cdot n_t \cdot N_{IO} \cdot N_{prec}}{10^9 \cdot t_{nt}} \quad \left[ \frac{\text{GB}}{\text{s}} \right] \quad (2.25)$$

where  $(N_x \cdot N_y \cdot N_z)$  is the total number of grid cells,  $n_t$  is the total number of numerical iterations performed,  $N_{prec}$  is the computational floating point precision (*single* 4 bytes or *double* 8 bytes),  $t_{nt}$  is the total wall time in seconds needed to compute the required number of iterations and the  $N_{IO}$  is the number of memory accesses performed.  $N_{IO}$  represents the minimum of memory operations (read-and-write or read only) required to solve a given physics problem. In our case, if we solve only the mechanical problem, the number of degrees of freedom (DOFs) we need to solve and therefore also update in every iteration is 3 ( $V_x, V_z$  and  $P$ ) in the 2D case, and 4 ( $V_x, V_y, V_z$  and  $P$ ) in the 3D case. The updates therefore require the minimum of 6 (8) read or write operations in 2D (3D). The additional read-and write is needed to resolve the non-linear viscosity. Therefore,  $N_{IO}$  is equal to 10 in 2D case and to 12 in 3D case.

We report the  $MTP_{eff}$  values obtained for the PT algorithm for both the vectorised MATLAB CPU and CUDA C GPU implementation in double precision (Figure 2.16 A). We additionally assess the GPU performance for two separate cases using the single floating point precision. The results we obtain should be compared to the peak  $MTP_{peak}$  values for the specific hardware used. The  $MTP_{peak}$  reports the memory transfer rate obtained by performing just memory copy operations without any computations; this value reflects the hardware performance limit. Measured  $MTP_{peak}$  value for the Intel i7 4960HQ CPU is 20 GB/s, while for the TITAN X GPU the value is 260 GB/s. The MATLAB CPU implementation utilizing a single core of the CPU saturated at about 0.7 GB/s, while the CUDA C implementation reached 16 GB/s. Hence, the MATLAB single core CPU implementation reaches 3.5% of the (CPU) hardware peak value, while the GPU CUDA C versions runs around 6.15% using the double precision arithmetics and 11% using the single precision arithmetics. From the GPU  $MTP_{eff}$  value it is seen that further performance gains can be obtained by optimising the GPU code using more on the fly calculations or more efficient kernel arrangement.

We report the wall-time to the solution obtained with PT CUDA C solver, with both 2D and 3D configurations, in Figure 2.16 B. In more detail, PT CUDA C enables us to solve  $\approx 24 \times 10^6$  DOF’s in around 15 minutes. This wall time further reduces if a single precision floating point arithmetic is used on the TITAN X (Maxwell) GPU, where only 3 minutes

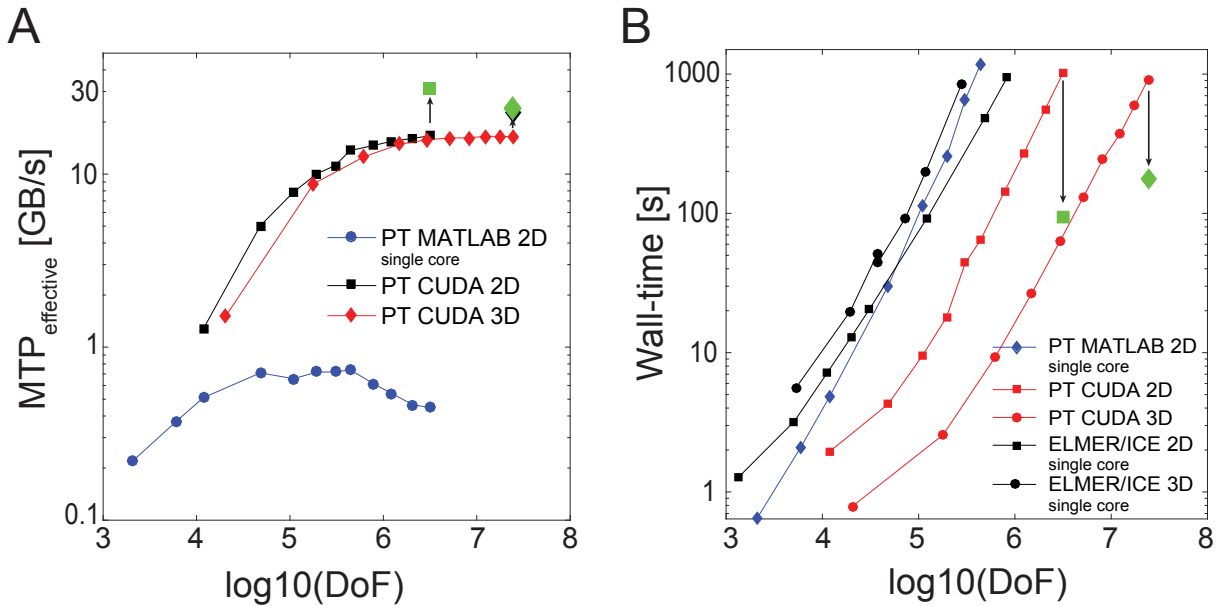


**Figure 2.16:** Performance evaluation of the PT mechanical solver in terms of: A) effective memory throughput  $MTP_{\text{effective}}$  in  $\frac{GB}{s}$ ; B) Wall time (in seconds) to converge the Stokes solver to  $\text{eps} = 1e - 8$ . The DoF represent the number of degrees of freedom, i.e. 3 variables in 2D ( $V_x, V_z, P$ ) and 4 variables in 3D ( $V_x, V_y, V_z, P$ ) multiplied by the number of grid points used. We report the results obtained using 2D PT CPU single core vectorised implementation in MATLAB, the PT CUDA C (2D and 3D) GPU implementation and Elmer/Ice FEM single CPU core model run with a direct solver in 2D and iterative in 3D. The CPU codes were running on the Intel i7 4960HQ CPU processor with 8 GB RAM, while the GPU codes were running on Nvidia Titan X (Maxwell) GPU with 12 GB on board RAM. All the computations were performed in double precision floating point arithmetic's, except the two runs represented in the figure with the green square (2D) and diamond (3D), which are performed using the single precision arithmetic's. The PT MATLAB CPU and Elmer/Ice single core CPU runs are only shown as a reference and are not to be used for performance comparison.

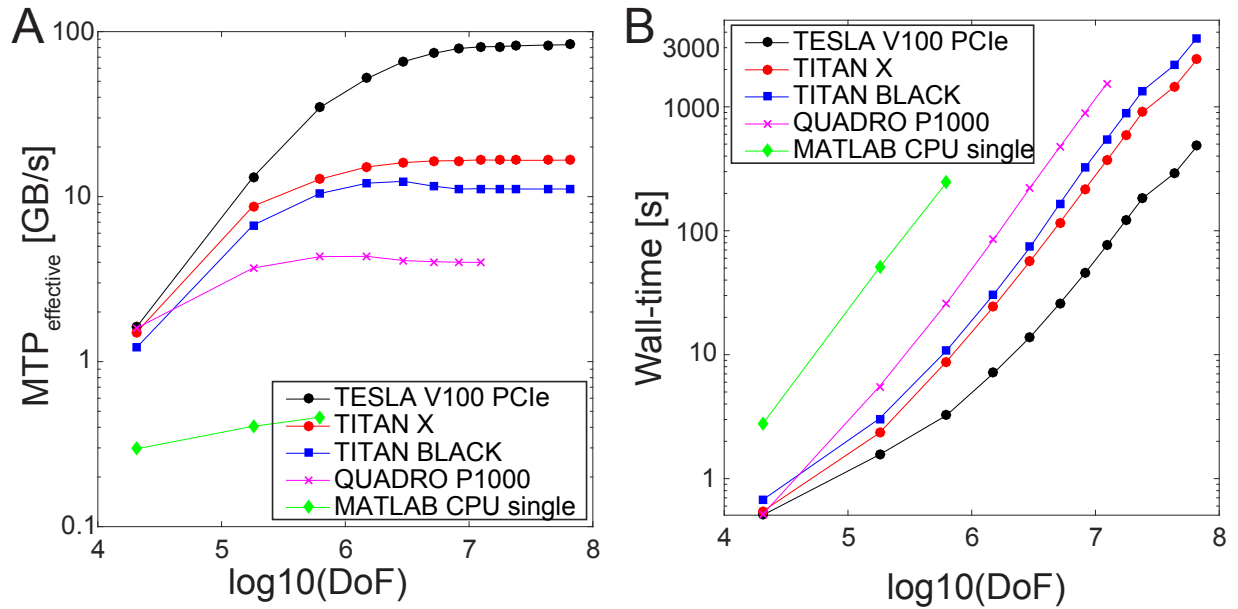


**Figure 2.17:** Performance evaluation of the PT mechanical solver in terms of: A) effective memory throughput  $MTP_{\text{effective}}$  in  $\frac{\text{GB}}{\text{s}}$ ; B) Wall time (in seconds) to converge the Stokes solver to  $\text{eps} = 1e - 8$ . The DoF represent the number of degrees of freedom, 4 variables in 3D ( $V_x, V_y, V_z, P$ ) multiplied by the number of grid points used. We report the results obtained using PT single CPU core vectorised implementation in MATLAB and the PT CUDA C GPU implementation while running on different GPU chip. The CPU codes were running on the Intel i7 4960HQ CPU processor with 8 GB RAM, while the GPU codes were running on Nvidia Titan Black (Kelvin) GPU with 6 GB on board RAM, Nvidia Titan X (Maxwell) GPU with 12 GB on board RAM, Nvidia Quadro P1000 (Pascal) GPU with 4 GB on board RAM and Nvidia Tesla GV100 (Volta) GPU with 16 GB on board RAM. All the computations were performed in double precision floating point arithmetic's. The PT MATLAB single core CPU runs are only shown as a reference and are not to be used for performance comparison.

are needed to obtain the solution for the same amount of DOF's. In further investigation, it would be interesting to compare the results of the CPU algorithms obtained by utilizing all cores with an algorithm using the GPU card of the same price and energy consumption range like the CPU.

We further report the performance results obtained using the PT GPU CUDA C implementation, using four different graphical processing units(Figure 2.17). We produced the data-points using only 3D PT codes. All the calculations are performed using double precision floating point arithmetics. We compared the  $MTP_{eff}$  and wall time while varying the numerical resolution used ( $DoF$ ). We use GPUs from various price range and chip generation. Using both the entry level GPU like QUADRO P1000 (Pascal), high end gaming cards TITAN Black (Kepler) or TITAN X (Maxwell) and HPC GPU accelerators like Tesla V100 (Volta). MATLAB implementation peaks at 0.46  $GB/s$ , QUADRO P1000 (Pascal) peaks at 4.3  $GB/s$ , TITAN Black (Kepler) reaches 12.4  $GB/s$ , TITAN X (Maxwell) reaches 16.7  $GB/s$  while the Tesla V100 (Volta) peaks at 83.2  $GB/s$ . This performance differences can be seen in terms of a wall time where numerical resolution of  $511 \times 255 \times 127$  grid points ( $66 \times 10^6$   $DoFs$ ) can be solved in around 1 hour on the TITAN BLACK GPU, 40 minutes on the TITAN X GPU while just 8 minutes is needed on the TESLA V100 GPU. Also, it is worth mentioning that around 4.5 GB of memory is used for solving a mechanical Stokes model at this resolution. For example, this is more than the amount available on the QUADRO P1000 (4 GB). Additionally, the results show that using the more advanced GPU solutions like the HPC GPU accelerators Tesla V100 (Volta) offers us a significant - order of magnitude higher - performance increase compared to an entry level GPU solution, like the QUADRO P1000.

## 2.6 Discussion

Numerically resolving the first order physics governing the ice flow is imperative to properly model the complex behaviour of ice sheets and glaciers. Current studies reveal that thermo-mechanically coupled models do not converge below the grid refinement; it is thus questionable how well numerical models approximates the mathematical ones. Unfortunately, only a few studies investigate the numerical aspects of the thermo-mechanically coupled Stokes solvers (Duretz et al., 2019). Few others (Zhang et al., 2015) are usually done with a very low spatial (vertical) resolution, and do not address the influence of the numerical coupling method and numerical time integration methods at all. The reasons are mainly the computational limitation for numerical modelling of high resolution 3D non-linear ice flow.

To address these issues, we have developed a new numerical model based on an iterative pseudo transient (PT) finite difference method. This results in a simple, highly parallelizable matrix free algorithm well suited to make use of the intrinsic parallelism of the modern

hardware accelerators, such as GPUs. These properties of the PT method, combined with the modern graphic cards enable us to use the developed algorithms with a high spatial numerical resolution in all three dimensions while still retaining reasonable computation times. This was shown with extensive performance tests by investigating time to solution and the efficiency of exploiting the current hardware capabilities. To verify that the solver gives accurate and coherent results a set of experiments was performed and an excellent agreement with a widely used glacier flow model Elmer/Ice is obtained.

One additional advantage of the PT transient method is its simple implementation and readable codes and hence the potential to also use it for educational purposes.

The efficiency of the PT method is limited by the viscosity contrast across the domain and the implemented boundary conditions. This is mostly seen in the Experiment 2, where the periodic boundary conditions are implemented and the number of iterations needed for the model to converge, and therefore the time to solution, significantly increases.

The influence of two numerical integration methods, forward (explicit) and backward (implicit) Euler method were studied and the influence of the numerical time step on the solution was established. To determine the influence of the numerical time step, we have first chosen a one-dimensional coupled thermo-mechanical experiment in which the coupling is strong. Since the model does not account for a phase change, i.e. melting, and we do not impose the constrain given by the pressure melting temperature the model solution will result in a thermal runaway and the solution will diverge. We run the 1D model to the time  $2.9 \times 10^8$  just before the thermal runaway starts to occur. Therefore the value of the numerical time step needs to be chosen sufficiently small to resolve the physical process. By using the explicit numerical time integration scheme time step is limited by the stability restriction (CFL condition) associated with the numerical method. This restriction limits the time step value and if a high enough numerical resolution is used the time step can easily reduce to the value needed to resolve the physical process. At low numerical resolutions this stability condition (CFL condition) is not a good enough choice for the physical process in question. More specifically, while the non-dimensional time needed to rise the temperature in our example was around  $2 \times 10^8$ , low resolution (less than 20 grid points) stability (CFL) condition results in values higher than this time and hence it does not resolve the physical process sufficiently. On the other side, usage of the implicit scheme for the time integration (both coupled or uncoupled) should guarantee numerical stability and allows one to chose the time step for advancing in time. Since the physical coupling is highly non-linear (exponential term) there is no guarantee for convergence of any solver when using too large numerical time step not relevant to the physical process in question and not capable of resolving the actual physics. Therefore, even in the cases when we used the implicit scheme, the value of the numerical time step is reduced to the values close to the explicit stability condition. One can also envision that usage of more advance numerical time integration methods, i.e. Crank-Nicolson can improve the numerical

stability, but the numerical time step will still have to be small enough to resolve the process. Criterion needed to determine the sufficient time step for resolving the physical process will be investigated in further detail in the next chapter of this thesis.

Next, two different methods of numerical thermo-mechanical coupling were investigated and compared. It was shown that at high enough spatial and temporal resolution the differences between the coupling method are relatively small, but nevertheless uncoupled model always produce the numerical solution with less localization than a coupled one. On the other hand, numerical coupling method can turn out to be an important factor when temperature advection is included in the model and the additional physical coupling needs to be taken into account. One can speculate that adding temperature advection into the model again indicate the need for a high spatial resolution or will show a need for some better, flux conservative, scheme than upwind.

To summarize, the presented PT method combined with the modern accelerators like the high end gaming GPU's enable us to run transient high resolution three-dimensional thermo-mechanically coupled simulations on a desktop computer. Hence, enabling us to investigate the influence of different coupling methods and tackle the problem of non-convergent solutions under the grid refinement.

## 2.7 Conclusions

In this study, we developed an iterative model (PT model) well suited to exploit the capabilities and advantages of the modern hardware, like the computer graphic card. The pseudo-transient (PT) model is an iterative, matrix-free method based on the finite difference discretisation. The algorithm implementation results in simple and readable codes, with great potential for using in educational purposes. The developed algorithm is ported to CUDA C programming language to benefit from the parallel capabilities of the GPU. This enabled us to use the high spatial and temporal resolution in three dimensions and to investigate the thermo-mechanical coupling and resolve the first order physics governing the ice flow.

We first benchmarked the mechanical component of the developed model against a community standard model Elmer/Ice in a set of experiments specifically designed to test the various components of the solver. For example, we first determined that the mechanical solver gives accurate and coherent results for a variety of different set-ups and boundary conditions, all while providing reasonable and competitive computation times. We later investigated two different methods of numerical thermo-mechanical coupling and also investigated the influence of two numerical integration methods, explicit and implicit. We showed that the numerical time step needs to be chosen with care, no matter the implemented numerical time integration scheme and that sufficiently high temporal resolution needs to be used to resolve

the physical process in question. On the other hand, even though the differences between the numerically uncoupled and coupled model are small, uncoupled model always produce the numerical solution with less localization than a coupled one. Additionally, numerical coupling can show to be important when temperature advection is studied.

We have also established that a relatively high spatial numerical resolution is needed to properly resolve all the non-linearities of the coupled ice flow. For example, vertical resolution of more than 100 grid points on a regular grid is needed, contrary to the previous studies using only 5 – 20 grid points in the vertical direction. Additionally, we have also shown that the horizontal spatial variation can influence the ice flow and hence high spatial numerical resolution in all direction is needed to properly resolve the physics of the ice flow. Further we have shown that, compared to lower order approximations, additional stress component can significantly slow down the process of thermal runaway.

Our results provides a new insight into the importance of different numerical implementations of thermo-mechanical coupling and shows the significance of the high spatial resolution, both horizontal and vertical, in numerically resolving the highly non-linear coupled physics.

## Bibliography

- Aschwanden, A., Bueler, E., Khroulev, C., Blatter, H., 2012. An enthalpy formulation for glaciers and ice sheets. *Journal of Glaciology* 58(209), 441–457.
- Bamber, J. L., Vaughan, D. G., Joughin, I., 2000. Widespread Complex Flow in the Interior of the Antarctic Ice Sheet. *Annals of Glaciology* 287, 1248–1250.
- Baral, D., Hutter, K., Greve, R., 2001. Asymptotic theories of large-scale motion, temperature, and moisture distribution in land-based polythermal ice sheets: A critical review and new developments. *Applied Mechanics Reviews* 54, 215–256.
- Bassis, J., 2010. Hamilton-type principles applied to ice-sheet dynamics: new approximations for large-scale ice sheet flow. *Journal of Glaciology* (56)97, 497–513.
- Blatter, H., 1995. Velocity and stress fields in grounded glaciers: a simple algorithm for including deviatoric stress gradients. *Journal of Glaciology* 5(138), 333–344.
- Bons, P. D., Kleiner, T., Llorens, M., Prior, D. J., Sachau, T., Weikusat, I., Jansen, D., 2018. Greenland Ice Sheet: Higher nonlinearity of ice flow significantly reduces estimated basal motion. *Geophysical Research Letters* 45, 6542–6548.
- Brinkerhoff, D. J., Johnson, J. V., 2013. Data assimilation and prognostic whole ice sheet modelling with the variationally derived, higher order, open source, and fully parallel ice sheet model VarGlaS. *The Cryosphere* 7, 1161–1184.

- Brinkerhoff, D. J., Johnson, J. V., 2015. Dynamics of thermally induced ice streams simulated with a higher-order flow model. *Journal of Geophysical Research: Earth Surface* 120, 1743–1770.
- Brown, J. A. K., 2011. Computational methods for ice flow simulation. Ph.D thesis, ETH Zürich.
- Bueler, E., 2008. Lessons from the short history of ice sheet model intercomparison. *The Cryosphere Discussions* 2, 399–412.
- Bueler, E., Brown, J., 2009. Shallow shelf approximation as a "sliding law" in a thermomechanically coupled ice sheet model. *Journal of Geophysical research* 114, F03008.
- Bueler, E., Brown, J., Lingle, C., 2007. Exact solutions to the thermomechanically coupled shallow-ice approximation: effective tools for verification. *Journal of Glaciology* 53(182), 499–516.
- Burg, J.-P., Gerya, T. V., 2005. The role of viscous heating in Barrovian metamorphism of collisional orogens: thermomechanical models and application to the Lepontine Dome in the Central Alps. *Journal of Metamorphic Geology* 23, 75–95.
- Chandler, D. M., Hubbard, A. L., Hubbard, B. P., Nienow, P. W., 2006. A Monte Carlo error analysis for basal sliding velocity calculations. *Journal of Geophysical Research* 111, F04005.
- Choi, E., Tan, E., Lavier, L. L., Calo, V. M., 2013. DynEarthSol2D: An efficient unstructured finite element method to study long-term tectonic deformation. *Journal of Geophysical Research: Solid Earth* 118(5), 2429–2444.
- Clarke, G. K. C., 2005. Subglacial processes. *Annual Review of Earth and Planetary Sciences* 33, 247–276.
- Clarke, G. K. C., Nitsan, U., Paterson, W. S. B., 1977. Strain heating and creep instability in glaciers and ice sheets. *Reviews of geophysics and space physics* 15 (2), 235–247.
- Cohen, D., Iverson, N. R., Hooyer, T. S., Fischer, U. H., Jackson, M., Moore, P. L., 2005. Debris-bed friction of hard-bedded glaciers. *Journal of Geophysical Research* 110, F02007.
- Cook, S., 2012. *CUDA Programming*. Morgan Kaufmann, Elsevier.
- Costa, A., Macedonio, G., 2003. Viscous heating in fluids with temperature-dependent viscosity: implications for magma flows. *Nonlinear Processes in Geophysics* 10, 545–555.
- Cundall, P., Coetzee, M., Hart, R., Varona, P., 1993. *FLAC users manual*. Itasca Consulting Group, 23–26.

- Dold, J., 1985. Analysis of the early stage of thermal runaway. *The Quarterly Journal of Mechanics and Applied Mathematics* 38(3), 361–387.
- Dupaigne, L., 2011. *Stable solutions of elliptic partial differential equations*. Vol. 1. Chapman and Hall, CRC.
- Duretz, T., Räss, L., Podladchikov, Y., Schmalholz, S., 2019. Resolving thermomechanical coupling in two and three dimensions: spontaneous strain localization owing to shear heating. *Geophysical Journal International* 216, 365–379.
- Egholm, D., M.F., K., Clark, C., Lesemann, J., 2011. Modeling the flow of glaciers in steep terrains: The integrated second-order shallow ice approximation (iSOSIA). *Journal of Geophysical Research: Earth Surface* 116, F02012.
- Fowler, A., 1980. The existence of multiple steady states in the flow of large ice masses. *Journal of Glaciology* 25 (91), 183–184.
- Fowler, A., 1986. Sub-temperate basal sliding. *Journal of Glaciology* 32(110), 3–5.
- Fowler, A., 2013. Correspondence: Thermal convection in ice sheets. *Journal of Glaciology* 59(213), 190–192.
- Fowler, A., Toja, R., Vazquez, C., 2010. Temperature-dependent shear flow and the absence of thermal runaway in valley glaciers. *Proceedings of Royal Society A* 466 (2114), 363–382.
- Fowler, A. C., Johnson, C., 1996. Ice-sheet surging and ice-stream formation. *Annals of Glaciology* 23, 68–73.
- Fowler, A. C., Larson, D., 1980a. The uniqueness of steady state flows of glaciers and ice sheets. *Geophysical Journal International* 63 (1), 333–345.
- Fowler, A. C., Larson, D., 1980b. Thermal stability properties of a model of glacier flow. *Geophysical Journal International* 63 (1), 347–359.
- Frank-Kamenetzky, D. A., 1939. Calculation of thermal explosion limits. *Acta physicochimica U.R.S.S* 10, 365–370.
- Frankel, S. P., 1950. Convergence rates of iterative treatments of partial differential equations. *Mathematical Tables and Other Aids to Computation* 4(30), 65–75.
- Fujita, H., 1969. On the nonlinear equations  $\Delta u + e^u = 0$  and  $\frac{\partial v}{\partial t} = \Delta v + e^v$ . *Bulletin of the American Mathematical Society* 75, 132–135.
- Gagliardini, O., Zwinger, T., 2008. The ISMIP-HOM benchmark experiments performed using the finite-element code Elmer. *The Cryosphere* 2, 67–76.

- Gagliardini, O., Zwinger, T., Gillet-Chaulet, F., Durand, G., Favier, L., de Fleurian, B., Greve, R., Malinen, M., Martín, C., Råback, P., Ruokolainen, J., Sacchettini, M., Schäfer, M., Seddik, H., Thies, J., 2013. Capabilities and performance of Elmer/Ice, a new-generation ice sheet model. *Geoscientific Model Development* 6, 1299–1318.
- Garofalo, F., 1963. An empirical relation defining the stress dependence of minimum creep rate in metals. *Transactions of the Metallurgical Society of AIME* 227, 351–356.
- Gerya, T., 2009. *Introduction to Numerical Geodynamic Modelling*. Cambridge University Press, Cambridge, United Kingdom.
- Gerya, T. V., Yuen, D. A., 2003. Characteristics-based marker-in-cell method with conservative finite-differences schemes for modeling geological flows with strongly variable transport properties. *Physics of the Earth and Planetary Interiors* 140(4), 293–318.
- Gilbert, A., Gagliardini, O., Vincent, C., Wagnon, P., 2014. A 3-D thermal regime model suitable for cold accumulation zones of polythermal mountain glaciers. *Journal of Geophysical Research:Earth Surface* 119, 8761893.
- Glen, J., 1955. The creep of polycrystalline ice. *Proceedings of the Royal Society of London A* 228, 519–538.
- Glen, J. W., 1952. The flow law of ice from measurements in glacier tunnels, laboratory experiments and the Jungfraufirn borehole experiment. *Journal of Glaciology* 2, 111–114.
- Goldberg, D., 2011. A variationally-derived, depth-integrated approximation to the Blatter Pattyn balance. *Journal of Glaciology* 57(201), 157–170.
- Gong, Y., Zwinger, T., Åström, J., Altena, B., Schellenberger, T., Gladstone, R., Moore, J. C., 2018. Simulating the roles of crevasse routing of surface water and basal friction on the surge evolution of Basin 3, Austfonna ice cap. *The Cryosphere* 12, 1563–1577.
- Grigoryan, S., Krass, M., Shumskiy, P., 1976. Mathematical model of a three dimensional non-isothermal glacier. *Journal of Glaciology* 7(77), 401–417.
- Gruntfest, I. J., 1963. Thermal feedback in liquid flow: Plane shear at constant stress. *Transactions of The Society of Rheology* 7, 195–207.
- Harlow, F. H., Welch, E., 1965. Numerical calculation of time-dependent viscous flow of fluid with free surface. *Physics of Fluids* 8(12), 2182–2189.
- Haseloff, M., Schoof, C., Gagliardini, O., 2018. The role of subtemperate slip in thermally driven ice stream margin migration. *The Cryosphere* 12, 2545–2568.

- Hewitt, I. J., Schoof, C., 2017. Models for polythermal ice sheets and glaciers. *The Cryosphere* 11, 541–551.
- Hindmarsh, R. C. A., 2004. Thermoviscous stability of ice-sheet flows. *Journal of fluid mechanics* 502, 17–40.
- Hindmarsh, R. C. A., 2006. Stress gradient damping of thermoviscous ice flow instabilities. *Journal of Geophysical Research:Earth Surface* 111, B12409.
- Hindmarsh, R. C. A., 2009. Consistent generation of ice-streams via thermo-viscous instabilities modulated by membrane stresses. *Geophysical research letters* 36, L06502.
- Hughes, T., 2009. Thermal convection and the origin of ice streams. *Journal of Glaciology* 55(191), 524–536.
- Hughes, T., 2012. Correspondence. Are ice-stream tributaries the surface expression of thermal convection rolls in the Antarctic ice sheet? *Journal of Glaciology* 58(210), 811–814.
- Hutter, K., 1983. *Theoretical glaciology: material science of ice and the mechanics of glaciers and ice sheets*. Vol. 1. Springer.
- Huybrechts, P., Payne, T., 1996. The EISMINT benchmarks for testing ice-sheet models. *Annals of Glaciology* 23, 1–12.
- Isaac, T., Stadler, G., Ghattas, O., 2015. Solution of Nonlinear Stokes Equations Discretized by High-order Finite Elements on Nonconforming and Anisotropic Meshes, with Application to Ice Sheet Dynamics. *SIAM Journal on Scientific Computing*, B804–B833.
- Jarosch, A., 2008. Icetools: a full Stokes finite element model for glaciers. *Computers and Geosciences* 34, 1005–1014.
- Johns, L. E., Narayanan, R., 1997. Frictional heating in plane Couette flow. *Proceedings of Royal Society A* 453 (1963), 1653–1670.
- Joughin, I., Smith, B., Howat, I., Scambos, T., Moon, T., 2010. Greenland flow variability from ice-sheet-wide velocity mapping. *Journal of Glaciology* 56, 416–430.
- Jouvet, G., Picasso, M., Rappaz, J., Blatter, H., 2008. A new algorithm to simulate the dynamics of a glacier: theory and applications. *Journal of Glaciology* 54, 801–811.
- Kelley, C. T., Keyes, D. E., 1998. Convergence Analysis of Pseudo-Transient Continuation. *SIAM Journal on Numerical Analysis* 35(2), 508–523.
- Kelley, C. T., Liao, L.-Z., 2013. Explicit pseudo-transient continuation. *Pacific Journal of Optimization* 9(1), 77–91.

- Kleiner, T., Rückamp, M., Bondzio, J. H., Humbert, A., 2015. Enthalpy benchmark experiments for numerical ice sheet models. *The Cryosphere* 9, 217–228.
- Krabbendam, M., 2016. Sliding of temperate basal ice on a rough, hard bed: creep mechanisms, pressure melting, and implications for ice streaming. *The Cryosphere* 10, 1915–1932.
- Kyrke-Smith, T. M., Katz, R. F., Fowler, A. C., 2015. Subglacial hydrology as a control on emergence, scale, and spacing of ice streams. *Journal of Geophysical Research:Earth Surface* 120, 1501–1514.
- Landau, L. D., Lifshitz, E. M., 1963. *Fluid Mechanics*. Vol. 1. Pergamon Press.
- Larour, E., Seroussi, H., Morlighem, M., Rignot, E., 2012. Continental scale, high order, high spatial resolution, ice sheet modeling using the Ice Sheet System Model (ISSM). *Journal of Geophysical research* 117, 1–20.
- Leng, W., Ju, L., Gunzburger, M., Price, S., 2014. A Parallel Computational Model for Three-Dimensional, Thermo-Mechanical Stokes Flow Simulations of Glaciers and Ice Sheets. *Computer Physics Communications* 16(4), 1056–1080.
- Leng, W., Ju, L., Gunzburger, M., Ringler, T., 2012. A parallel high-order accurate finite element nonlinear Stokes ice sheet model and benchmark experiments. *Journal of Geophysical research* 117, F01001.
- Lliboutry, L. A., 1987. *Very Slow Flows of Solids: Basics of Modeling in Geodynamics and Glaciology*. Vol. 7. Springer Netherlands.
- MacAyeal, D. R., 1992. The basal stress distribution of Ice Stream E, Antarctica, inferred by control methods. *Journal of Geophysical Research: Earth Surface* 97, 595–603.
- Moore, P., Iverson, N., Cohen, D., 2009. Ice flow across a warm-based/cold-based transition at a glacier margin. *Annals of Glaciology* 50 (52), 1–8.
- Morland, L., 1984. Thermomechanical balances of ice sheet flows. *Geophysical and Astrophysical Fluid Dynamics* 29, 237–266.
- Nye, J. F., 1953. The flow law of ice from measurements in glacier tunnels, laboratory experiments and the Jungfraufirn borehole experiment. *Proceedings of Royal Society A* 219, 477–489.
- Ogawa, M., Schubert, G., Zebib, A., 1991. Numerical simulations of three-dimensional thermal convection in a fluid with strongly temperature dependent viscosity. *Journal of Fluid Mechanics* 233, 299–328.

- Omlin, S., 2017. Development of massively parallel near peak performance solvers for three-dimensional geodynamic modelling. Ph.D thesis, University of Lausanne.
- Patankar, S., 1980. Numerical Heat Transfer and Fluid Flow, Comput. Methods Mech. Thermal Sci. Ser. CRC Press, Boca Raton, Fla.
- Paterson, W., 1994. The physics of glaciers. Third edition. Elsevier.
- Pattyn, F., 2003. A new three-dimensional higher-order thermomechanical ice sheet model: basic sensitivity, ice stream development and ice flow across subglacial lakes. *Journal of Geophysical Research* 108(B8), 2382.
- Pattyn, F., Perichon, L., Aschwanden, A., Breuer, B., de Smedt, B., Gagliardini, O., Gudmundsson, G. H., Hindmarsh, R. C. A., Hubbard, A., Johnson, J. V., Kleiner, T., Konovalov, Y., Martin, C., Payne, A. J., Pollard, D., Price, S., Rückamp, M., Saito, F., Soucek, O., Sugiyama, S., Zwinger, T., 2008. Benchmark experiments for higher-order and full-Stokes ice sheet models (ISMIP- HOM). *The Cryosphere* 2, 95–108.
- Payne, A., Dongelmans, P., 1997. Self-organization in the thermomechanical flow of ice sheets. *Journal of Geophysical research* 102(B6), 219–233.
- Payne, T., Baldwin, D., 2000. Analysis of ice-flow instabilities identified in the EISMINT intercomparison exercise. *Annals of Glaciology* 30, 204–210.
- Payne, T., Huybrechts, P., Abe-Ouchi, A., Calov, R., Fastook, J., Greve, R., Marshall, S., Marsiat, I., Ritz, C., Tarasov, L., Thomassen, M., 2000. Results from the EISMINT model intercomparison: the effects of thermomechanical coupling. *Journal of Glaciology* 46(153), 227–238.
- Perego, M., Gunzburger, M., Burkardt, J., 2012. Parallel finite element implementation for higher order ice-sheet models. *Journal of Glaciology* 58(207), 76–88.
- Poliakov, A. N. B., Cundall, P. A., Podladchikov, Y. Y., Lyakhovsky, V. A., 1993. An explicit inertial method for the simulation of viscoelastic flow: An evaluation of elastic effects on diapiric flow in two- and three-layers models. *Flow and Creep in the Solar Systems: Observations, Modeling and Theory*, 175–195.
- Pollard, D., DeConto, R. M., 2012. Description of a hybrid ice sheet-shelf model, and application to Antarctica. *Geoscientific Model Development* 5, 1273–1295.
- Räss, L., Simon, N., Podladchikov, Y., 2018. Spontaneous formation of fluid escape pipes from subsurface reservoirs. *Scientific Reports* 8 (11116).
- Robin, G. d. Q., 1955. Ice movement and temperature distribution in glaciers and ice sheets. *Journal of Glaciology* 2 (18), 523–532.

- Saito, F., Abe-Ouchi, A., Blatter, H., 2006. European Ice Sheet Modelling Initiative (EIS-MINT) model intercomparison experiments with first-order mechanics. *Journal of Geophysical Research* 111, F02012.
- Schäfer, M., Gillet-Chaulet, F., Gladstone, R., Pettersson, R., Pohjola, V., Strozzi, T., Zwinger, T., 2014. Assessment of heat sources on the control of fast flow of Vestfonna ice cap, Svalbard. *The Cryosphere* 8, 1951–1973.
- Schoof, C., 2005. The effect of cavitation on glacier sliding. *Proceedings of Royal Society A* 461, 609–627.
- Schoof, C., Hewitt, I. J., 2016. A model for polythermal ice incorporating gravity-driven moisture transport. *Journal of fluid mechanics* 797, 504–535.
- Schoof, C., Hindmarsh, R., 2010. Thin film flows with wall slip: an asymptotic analysis of higher order glacier flow models. *The Quarterly Journal of Mechanics and Applied Mathematics* 63(1), 73–114.
- Schubert, G., Yuen, D., 1982. Initiation of ice ages by creep instability and surging of the East Antarctic ice sheet. *Nature* 296 (5853), 127–130.
- Shapiro, D. R., Joughin, I., Poinar, K., Morlighem, M., Gillet-Chaulet, F., 2016. Basal resistance for three of the largest Greenland outlet glaciers. *Journal of Geophysical Research: Earth Surface* 121, 168–180.
- Shin, D., Strikwerda, J. C., 1997. Inf-Sup conditions for finite-difference approximations of the Stokes equations. *Journal of the Australian Mathematical Society. Series B. Applied Mathematics* 39(01), 121–134.
- Solomon, S., Qin, D., Manning, M., Chen, Z., Marquis, M., Averyt, K., Tignor, M., Miller, H., 2007. The physical science basis p.235–337, IPCC report AR4 . New York and Cambridge: Cambridge University Press.
- Stearns, L. A., Van der Veen, C. J., 2018. Friction at the bed does not control fast glacier flow. *Science* 361(6399), 273–277.
- Steinemann, S., 1958. Experimentelle Untersuchungen zur Plastizität von Eis. *Beiträge zur Geologie der Schweiz. Hydrologie* 10.
- Suckale, J., Platt, J., Perol, T., Rice, J., 2014. Deformation-induced melting in the margins of the West Antarctic ice streams. *Journal of Geophysical Research:Earth Surface* 119, 1004–1025.

- Tezaur, I. K., Perego, M., Salinger, A. G., Tuminaro, R. S., Price, S. F., 2015. Albany/FELIX: a parallel, scalable and robust, finite element, first-order Stokes approximation ice sheet solver built for advanced analysis. *Geoscientific Model Development* 8, 1197–1220.
- Turcotte, D., Schubert, G., 2014. *Geodynamics 3rd Edition*. Vol. 1. Cambridge University Press.
- Van der Veen, C., Oerlemans, J., 1984. Global thermodynamics of a polar ice sheet. *Tellus* 36A, 228–235.
- Wong, W. A., Jonas, J. J., 1968. Aluminum extrusion as a thermally activated process. *Transactions of the Metallurgical Society of AIME* 242, 2271–2280.
- Yang, X. I., Mittal, R., 2014. Acceleration of the Jacobi iterative method by factors exceeding 100 using scheduled relaxation. *Journal of Computational Physics* 274, 695–708.
- Yuen, D., Saari, M., Schubert, G., 1986. Explosive growth of shear heating instabilities in the down-slope creep of ice sheets. *Journal of Glaciology* 32 (112), 314–320.
- Yuen, D., Schubert, G., 1977. Asthenospheric shear flow: thermally stable or unstable. *Geophysical research letters* 4 (11), 503–506.
- Yuen, D., Schubert, G., 1979a. On the stability of frictionally heated shear flows in the asthenosphere. *Geophysical Journal International* 57 (1), 189–207.
- Yuen, D., Schubert, G., 1979b. The role of shear heating in the dynamics of large ice masses. *Journal of Glaciology* 4 (90), 195–212.
- Zhang, T., Ju, L., Leng, W., Price, S., Gunzburger, M., 2015. Thermomechanically coupled modelling for land-terminating glaciers: a comparison of two-dimensional, first-order and three-dimensional, full-Stokes approaches. *Journal of Glaciology* 61(228), 702–711.
- Zoet, L. K., Iverson, N. R., 2016. Rate-weakening drag during glacier sliding. *Journal of Geophysical Research: Earth Surface* 121, 1206–1217.
- Zwinger, T., Greve, R., Gagliardini, O., Shiraiwa, T., Lyly, M., 2007. A full Stokes-flow thermo-mechanical model for firn and ice applied to the Gorshkov crater glacier, Kamchatka. *Annals of Glaciology* 45, 29–37.



## CHAPTER 3

---

### The effect of strain heating on the ice flow

---

**Aleksandar Licul<sup>1,3</sup>, Frédéric Herman<sup>1,3</sup>, and Yury Y. Podladchikov<sup>2,3</sup>**

<sup>1</sup>Faculté des géosciences et de l'environnement, Institut des dynamiques de la surface terrestre, University of Lausanne, Lausanne, Switzerland.

<sup>2</sup>Faculté des géosciences et de l'environnement, Institut des Sciences de la Terre, University of Lausanne, Lausanne, Switzerland.

<sup>3</sup>Swiss Geocomputing Centre, University of Lausanne, Lausanne, Switzerland.

## Abstract

It is often speculated that thermo-mechanical coupling is responsible for glacier and ice sheet surging, the generation and shut down of ice streams and the local transition from no sliding to sliding. The processes controlling these phenomena are still heavily debated. Usually, studies investigating the importance of strain heating are concentrated on one dimensional steady state thermo-mechanical models which, under given assumptions, can be susceptible to the analytical solutions. Here, we have numerically investigated the time evolution of a two dimensional thermo-mechanically coupled model. The results were compared to the solution of a one dimensional model. The importance of advection, horizontal diffusion and additional stress gradients is shown. Additional stress gradients have the first order effects on the solution, while advection plays an important role only in the later stages of the temperature evolution. This was shown with the extended 1D model which approximates the effects of the additional stress gradients. The solutions of the extended 1D model differed only slightly from the computationally more expensive 2D model. By performing the parametric analysis (data collapse), two distinct regimes of a thermo-coupled flow were identified: transient and steady state regime. Parameters controlling the temperature and velocity increase are determined and compared with the so-called stability parameter (Brinkman number), a parameter often used to determine the importance of the strain heating. We have determined that the stability parameter is a good predictor for only the steady state solution, but not for the transient regime which is diffusion length scale independent. The importance of the transient regime can also be deduced from the information that reaching the steady state often requires time even up to 100 diffusion time scales, which is unrealistic. Therefore, we suggest that the transient regime should be investigated further.

### 3.1 General introduction: Towards an effective boundary condition

One of the biggest challenges in glaciology is to understand the physical processes that take place at, or very close to, the ice bedrock interface (Zoet and Iverson, 2016). Today, ice surface velocity can be measured at unprecedented resolution using satellite or airborne measurements (Joughin et al., 2010). However, ice velocity measurements at the base of glaciers are scarce and often very localised. This is primarily because of the limited access to the glacier beds (Chandler et al., 2006). Therefore, constraining the ice velocity at the base of the ice sheet or glaciers still remains challenging and basal sliding remains a major source of uncertainty in ice flow modelling (e.g. Cohen et al., 2005; Stearns and Van der Veen, 2018; Zoet and Iverson, 2016). To circumvent this problem, ice flow modellers usually rely on inverse modelling with a goal of obtaining the slip coefficient (or the so-called friction parameter) and hence constraining the current sliding velocity (e.g. Larour et al., 2012; MacAyeal, 1992; Shapero et al., 2016). In the simplest, linear case, the functional form is given as  $\tau_b = \beta^2 V_b$ , where  $\tau_b$  is the stress at the base,  $V_b$  is the velocity at the base and  $\beta$  is the unknown slip coefficient. The inverse modelling approach is very useful for diagnostic ice flow modelling, but unfortunately it is often not appropriate for long-term prognostic simulations or paleo-ice sheet modelling (e.g., Krabbendam, 2016). This is mostly because the slip coefficient does not inform us about the physics of sliding processes or the dependence of this coefficient on various influences like, for example, temperature, water content, debris, basal topography. To reduce this uncertainty a better understanding of basal processes and a physics based mathematical model of basal sliding is needed (Schoof, 2005; Stearns and Van der Veen, 2018; Zoet and Iverson, 2016). The basal thermal regime, the temperate ice layer, the rheology of basal ice, the effects of basal meltwater and friction, water fluxes, surface water influx and basal topography are often identified as key elements required to properly determine the magnitude of basal sliding. Since the problem of determining basal boundary conditions is closely related to determining the thermal field, detailed thermo-mechanical investigations are needed (Brown, 2011).

In the previous chapter, we have shown that obtaining an accurate numerical solution of the thermo-mechanical Stokes equations requires high numerical resolution. This is mostly due to strain heating, which concentrates most of the shearing close to the base. Analytical studies investigating the strain heating are mostly concerned with the steady state solutions (Clarke et al., 1977; Fowler et al., 2010; Yuen and Schubert, 1979b). While strain heating is often accounted for in numerical models, we have shown that the effects of strain heating with a Stokes models are usually not resolved at a sufficient scale. This is mostly due to the use of low spatial resolution and too large time-steps. Resolving grid spacing of a meter scale and less in the large scale three-dimensional coupled Stokes models is challenging and often not feasible due to computational limitations. Therefore, taking into consideration the temperature and

velocity increase due to strain heating would require us to prescribe an effective boundary condition that accounts for the coupled processes at these scales. This motivated us to quantify the temperature and velocity increase due to strain heating. Additionally, we plan to identify at which conditions these increases are significant enough to require a special treatment of the boundary layer. The primary goal here is stating a relationship between basal drag  $\tau_b$  and velocity increase  $\Delta V$  between Stokes model without strain heating and the thermo-mechanically coupled Stokes model. This relationship would represent the third type of the boundary conditions (Robin boundary condition) or the, so called, effective boundary condition. We start by extending the analysis of Clarke et al. (1977) and Yuen and Schubert (1979b), who have set the theoretical basis on the effects of strain heating on ice flow, to transient regime and two dimensions. This is achieved by solving the coupled full stress equations, which enables us to study the effects of stress components and their gradients. Our approach also gives the opportunity to assess the respective role of horizontal and vertical advection on the stability.

In the following, we start by giving an overview of the mathematical model of the thermo-mechanically coupled flow. Further, we describe the model set-up and the experiments. We continue by presenting the results of the numerical experiments and the differences between the models are shown. We then describe our parameter analysis and the determined relations for the temperature and velocity increases due to strain heating, where we also describe the implications of our results to the real ice masses. Finally, we discuss how our results relate to the previous studies of Clarke et al. (1977) and Yuen and Schubert (1979b) and give our concluding remarks.

### **3.2 Literature review on the effects of strain heating on ice flow**

Viscous heating is a heat source resulting from the transformation of mechanical energy to heat (also often called strain heating). As a consequence of conservation laws, viscous heating is a non-removable part of a system (Burg and Gerya, 2005; Landau and Lifshitz, 1963). It is often considered that viscous heating is the main heat source responsible for melting the ice at the base and therefore making the ice temperate at the bottom. However, the questions that remain open are how does viscous heating influence the fluid (ice) flow and how significant is the heat source?

Many studies have speculated that thermo-mechanical coupling can be responsible for some still unresolved and interesting phenomena such as glacier and ice sheet surging (e.g., Clarke et al., 1977; Schubert and Yuen, 1982), the generation and shut down of ice streams (e.g., Brinkerhoff and Johnson, 2015; Hindmarsh, 2009; Suckale et al., 2014), and the local transition

from no sliding to sliding (e.g., Fowler and Larson, 1980a,b; Moore et al., 2009). Therefore, further investigations of the thermo-mechanical coupling are needed.

Robin (1955) was the first to suggest that temperature can have a strong influence on the ice flow and that ice sheet and glacier surging can be explained by the process of creep instability, or the so called thermal runaway. Thermal runaway results from a positive feedback through thermo-mechanical coupling. For a given stress, an increase in temperature leads to an increase in deformation rate, which leads to an increase in viscous/strain heating, which further increases temperature. The possibility of thermal runaway in glaciers and ice sheets was studied by Clarke et al. (1977). They studied a simple slab model of heat transfer with a fixed ice thickness and concluded that heat transfer in the slab is determined by three dimensionless parameters: stability, advection and geothermal parameters. In particular, they assessed the importance of strain heating with the value of the stability parameter. This stability parameter varies slightly by definition and names, i.e. Brinkman (Turcotte and Schubert, 2014), Grunfest (Grunfest, 1963) or Nahme number (Costa and Macedonio, 2003), and it is in most cases defined as a ratio between heat produced by viscous dissipation and a conductive heat flux. Expressed differently, the stability parameter, or the Brinkman number, measures the ability of the fluid to conduct away the frictionally generated heat - the higher its value, the larger the temperature rises (Turcotte and Schubert, 2014). The stability parameter is often considered as a good indicator for determining the importance of strain heating, even though it presumes that the generated heat is dissipated through the whole thickness of the slab.

Clarke et al. (1977) first numerically calculated the solutions for the steady state heat equation with no advection and no heat flux at the base. Interestingly, their model is mathematically very similar problem to the one in addressing thermal explosions (Frank-Kamenetzky, 1939), with differences lying in the definition of exponential term. They determined that there can exist up to three solutions to the problem which they termed "subcritical", "supercritical" and "hot" branches. Below some critical value of the stability parameter, the three branches exist for the same stability parameter. Above the critical value, only the solution on the "hot" branch exist, which is considered by the authors to be the creep instability or thermal runaway. Note, however, that because temperature can rise well above the melting temperature of ice, such a solution may not be found in natural systems.

Clarke et al. (1977) also numerically calculated a critical value for the stability parameter and they have determined that this value is strongly dependent on the advection and geothermal parameters, and that it can vary by up to 5 orders of magnitude. The authors have estimated the critical values over the range of parameters corresponding to natural ice masses, and concluded that creep instability can easily arise in the accumulation and ablation zones of a glacier or an ice sheet. By extending their analysis further, they also calculated the time scale (i.e., inverse growth rate) needed for the creep instability to develop, with perturbation

analysis using the linearised time-dependent heat equation. The growth rate they obtained by linear analysis showed that the time for the instability to grow is much larger than the residence time of ice in the ablation zone and of the usual surge periods. Therefore, they concluded that creep instability is most likely to occur in the accumulation zone and that creep instability is an unlikely surge mechanism for glaciers. However, they do not exclude the possibility that surges of ice sheets are triggered by creep instabilities.

The second study investigating the role of strain heating was proposed by Yuen and Schubert (1979b). In their analysis, the authors considered the same set-up as Clarke et al. (1977), i.e. a slab on a inclined slope, but used ice surface velocity instead of ice thickness as the main prescribed variable. In the case of Clarke et al. (1977), the ice thickness is known and kept fixed in time. Therefore, the strain heating term can be analytically determined from the momentum balance and rheology. Mechanics can be decoupled from the energy solver, and rheology and the strain heating term depends exponentially on temperature. Therefore, velocity is only computed diagnostically. In the case of Yuen and Schubert (1979b), the a priori known variable is the ice surface velocity, which leads to a coupled non-linear system of equations for temperature and velocity that needs to be solved iteratively, with a goal of determining the unknown ice thickness. Expressed differently, the main difference between the models can be found in how the surface boundary condition in the mechanical solver is implemented. Is it a Neumann boundary condition (BC), or a zero strain rate boundary condition for an a priori given ice thickness, or a Dirichlet BC for an a priori given constant velocity?

As in the case of Clarke et al. (1977), Yuen and Schubert (1979b) obtained multivalued solutions for both temperature and velocity as a function of ice thickness, leading to either subcritical or supercritical branches. Interestingly, both authors found that for certain parameters, solutions on both branches give the basal temperature below the melting temperature for realistic values of ice thickness and surface velocity. They have further linearised both temperature and momentum equations in both one and two dimensions and investigated the stability of their steady state solutions where they found no unstable mode. The linear stability of steady state solutions was then investigated in more details in the studies by Yuen and Schubert (1977) for asthenospheric shear flows by Johns and Narayanan (1997). The main conclusion is that stability depends on the choice of the boundary condition. Stability of steady state solutions on both branches is obtained in the case of a Dirichlet boundary condition, which is the case they considered in the glaciology aspect, but in the case of a Neumann boundary condition, the solutions on supercritical branch are often unstable - at least in one dimensional stability analysis where the perturbation shear stress is fixed, like in the case of Clarke et al. (1977). This physically destabilizing mechanism is explained in more detail in Burg and Gerya (2005), while the differences between one dimensional and multidimensional linear stability can be nicely seen in Yuen and Schubert (1979a), as well as Hindmarsh (2004)

and Hindmarsh (2006); where the stabilising influence of varying the perturbation stress is investigated. Unfortunately, this led to conclusions that thermo-mechanically coupled shallow ice models are ill-posed and are not to be used.

Continuing their analysis, Yuen and Schubert (1979b) stated that even though linear stability analysis shows that both steady state solutions are stable to small perturbations, the destabilizing effect of finite amplitude perturbations should be investigated further. While Schubert and Yuen (1982) investigated the possibility that ice ages are initiated by creep instability (thermal runaway) and surging of the East Antarctic ice sheet, Yuen et al. (1986) studied the explosive growth of creep instability in ice sheets. Altogether, these studies led to the conclusions that linear stability analysis of the growth time is insufficient, and that full non-linear thermo-mechanical coupling should be considered.

In his short note, Fowler (1980) questioned the applicability of the results obtained by Clarke et al. (1977) and Yuen and Schubert (1979b). This was done on the basis that neither ice thickness nor the surface velocity are known a priori, since they result from the ice dynamics, and that ice flux, which depends on the accumulation, should rather be taken as a prescribed variable. As further stated by the author, prescribing the ice flux rather than ice thickness can have a stabilizing effect on the solution since this is equivalent to letting the top surface evolve. Therefore, this may result in the solutions being single-valued. This was further shown by Fowler and Larson (1980a,b) using a two dimensional plane flow and taking the accumulation into the consideration while neglecting advection in the ice. Their results show that the obtained steady state is unique and also linearly stable. Therefore, an important take home message is that including the free surface has a stabilizing effect on the solution.

More recently, Fowler et al. (2010) revived the discussion by reducing the heat equation to a balance between viscous heating and diffusion and assuming that most of the shear happens in a layer near the base. This approximation reduced the parabolic non linear heat equation to an elliptic one which is susceptible to a well known analytical solution (Turcotte and Schubert, 2014). For the chosen boundary conditions, the integration constants were approximated (otherwise they could be determined only numerically) and the solution for the steady state temperature in a slab with no advection was obtained. This approximate solution is then coupled with the surface evolution equation and three separate cases representing glacier flow were numerically considered: cold, temperate and polythermal. The following conclusions were made:

- thermal runaway cannot occur because at the point when it should occur the change of boundary conditions from cold to temperate never allows it, a conclusion similar to the one already obtained by Clarke et al. (1977).
- temperature variations have very little effect on the overall motion of the glacier.

- geothermal heat flux is insufficient to raise the basal temperature to the melting point.
- the importance of an additional heat source (that the authors assign to the latent heat by buried surface meltwater and rainwater).
- that without an extensive heat source concentrated in a basal layer, glaciers would remain cold (and they speculated that in continental cold climates, like that in Antarctica, there would be no melting at the base at all).

Unfortunately, this approximation implies that diffusion has infinite time to dissipate the heat over the whole slab thickness. The actual time to dissipate the heat is limited, by the change of thickness, therefore the generated heat can only dissipate to a limited distance during this time. This distance up to where the heat dissipates is an unknown, and it is the actual thickness of the shear zone, which should be searched as a solution of the problem. Second, this kind of approximation resets the temperature field from the previous time step, therefore energy is not conserved. This analysis showed that there is a need for a direct numerical simulation of ice flow that consistently conserves the mass, energy and momentum.

Another important aspect of the system stability is the role of advection. Clarke et al. (1977) and Lliboutry (1987) have shown that vertical advection can have both stabilizing and unstabilizing effects, and thus should be considered. This is also seen from scaling and non dimensionalization (Baral et al., 2001; Hutter, 1983; Morland, 1984) where both advection terms are shown to have first order effects on the temperature field. Similarly, Van der Veen and Oerlemans (1984) developed a simple global scale model based on conservation of mass, energy and momentum to investigate the feedbacks of thermodynamics on the ice mass discharge and found that ice flow feedbacks with meltwater production may give rise to two different flow regimes, slow and fast.

### 3.3 Model

#### 3.3.1 Mathematical model

The mathematical model describing the flow of an incompressible non linear viscous fluid with temperature dependent rheology under the external force is given by the following set of conservation laws (Equations 3.1-3.3 ) and rheology (Equation 3.4). Mass conservation for the incompressible flow:

$$\frac{\partial v_i}{\partial x_i} = 0 \quad (3.1)$$

where  $v_i$  are velocity components in  $x_i$  spatial direction. Conservation of momentum is given by:

$$\frac{\partial \tau_{ij}}{\partial x_j} - \frac{\partial P}{\partial x_i} + F_i = 0 \quad (3.2)$$

where  $F_i$  is the external force defined as  $F_i = \rho g \sin \alpha (1, 0, -\cot \alpha)$ . Ice density is  $\rho$ ,  $g$  is the gravitational acceleration and  $\alpha$  is the mean bed slope.  $P$  is the pressure and  $\tau_{ij}$  is the deviatoric stress tensor.

The governing equation for the conservation of heat in the case of an incompressible fluid with no melt is given by:

$$\rho c_p \left( \frac{\partial T}{\partial t} + v_i \frac{\partial T}{\partial x_i} \right) = \frac{\partial}{\partial x_i} \left( k \frac{\partial T}{\partial x_i} \right) + \tau_{ij} \dot{\epsilon}_{ij} \quad (3.3)$$

where  $T$  represents the temperature deviation from the initial temperature  $T_0$ , usually chosen at the ice base,  $c_p$  is the specific heat capacity,  $k$  is the thermal conductivity and  $\dot{\epsilon}_{ij}$  is the strain rate tensor. The term  $\tau_{ij} \dot{\epsilon}_{ij}$  represent the strain heating, a viscous heating source term. Thermal conductivity can be either constant or temperature dependent. In this study we consider it as a constant value. In this model, we are not accounting for the phase change and hence we do not impose the constraint on temperature by pressure melting.

The rheology of ice is best described by Glen's flow law (Glen, 1952; Nye, 1953)

$$\dot{\epsilon}_{ij} = \frac{1}{2} \left( \frac{\partial v_i}{\partial x_j} + \frac{\partial v_j}{\partial x_i} \right) = a_0 \tau_{II}^{n-1} e^{-\frac{Q}{R(T+T_0)}} \tau_{ij} \quad (3.4)$$

where  $a_0$  is the pre-exponential factor,  $R$  is the universal gas constant,  $Q$  is the activation energy,  $n$  is the stress exponent and  $\tau_{II}$  is the second invariant of the stress tensor defined by  $\tau_{II} = \sqrt{\frac{1}{2}(\tau_{xx}^2 + \tau_{yy}^2 + \tau_{zz}^2 + 2(\tau_{xy}^2 + \tau_{yz}^2 + \tau_{xz}^2))}$ .

Four independent scales are used to non-dimensionalize the thermo-mechanically coupled equations: temperature, stress, time and length. The characteristic scales are chosen such that the coefficients in-front of the diffusion and strain heating terms in the temperature evolution equation (Equation 3.3) reduce to 1.

$$\bar{T} = \frac{nRT_0^2}{Q} \quad \bar{\tau} = \rho c_p \bar{T} \quad \bar{t} = 2^{-n} a_0^{-1} \bar{\tau}^{-n} e^{\frac{Q}{R\bar{T}_0}} \quad \bar{L} = \sqrt{\frac{k}{\rho c_p} \bar{t}} \quad (3.5)$$

Additionally, we can derive their dependent combinations such as the velocity scale given by  $\bar{v} = \frac{\bar{L}}{\bar{t}}$ . We obtain the dimensionless primed-variables by normation with the characteristic scale for the variable given in Equation 2.10.

In the form of the non-dimensionalized variables we can then rewrite the governing equations as follows:

$$\frac{\partial v'_i}{\partial x'_i} = 0 \quad (3.6)$$

$$\frac{\partial \tau'_{ij}}{\partial x'_j} - \frac{\partial P'}{\partial x'_i} + F'_i = 0 \quad (3.7)$$

$$\frac{\partial T'}{\partial t'} + v'_i \frac{\partial T'}{\partial x'_i} = \frac{\partial^2 T'}{\partial x'^2_i} + \tau'_{ij} \dot{\epsilon}'_{ij} \quad (3.8)$$

$$\dot{\epsilon}'_{ij} = \frac{1}{2} \left( \frac{\partial v'_i}{\partial x'_j} + \frac{\partial v'_j}{\partial x'_i} \right) = 2^{-n} \tau'^{n-1}_{II} e^{\frac{nT'}{1+T'_0}} \tau'_{ij} \quad (3.9)$$

where  $F'_i$  is now defined as  $F'_i = \bar{F}(1, 0, -\cot \alpha)$  and  $\bar{F} = \frac{\rho g \sin \alpha \bar{L}}{\bar{\tau}}$ . The non dimensional viscosity is described as:

$$\eta' = e^{\frac{-T'}{1+T'_0}} \dot{\epsilon}'^{\frac{1-n}{n}}_{II} \quad (3.10)$$

where the second invariant of the strain rate tensor  $\dot{\epsilon}'_{II}$  is defined by

$$\dot{\epsilon}'_{II} = \sqrt{\frac{1}{2}(\dot{\epsilon}'^2_{xx} + \dot{\epsilon}'^2_{yy} + \dot{\epsilon}'^2_{zz} + 2(\dot{\epsilon}'^2_{xy} + \dot{\epsilon}'^2_{yz} + \dot{\epsilon}'^2_{xz}))} \quad (3.11)$$

The model parameters are the non dimensional initial temperature  $T'_0$ , stress exponent  $n$ , non dimensional force  $\bar{F}$ , the mean bed slope  $\alpha$ , aspect ratio  $\epsilon$  and non dimensional domain height  $L'_z$ .

### 3.3.2 Numerical model setup

In order to assess the importance of strain heating on the ice flow we start by looking at the simple two dimensional parallel sided slab setup, as shown in Figure 1, where all boundaries are flat and the slab is inclined for a given angle  $\alpha$ . At the base we prescribe the zero horizontal (no slip) and vertical velocity (no melting or freezing) and zero vertical heat flux. At the top surface a stress free surface is prescribed and temperature deviation from the initial temperature is set to zero, meaning that surface temperature does not change during the run. On the left and right boundaries, horizontal velocity and temperature flux is set to zero, while the shear stress is also set to zero. The temperature deviation is set to zero everywhere inside the slab, meaning that at the start of simulation the slab can be considered isothermal with non dimensional initial temperature  $T'_0$ . The model parameters are given in Table 3.1.

**Table 3.1:** Reference run - non dimensional numbers and the dimensional values for comparison

$n_x$	$n_z$	$L'_z$	$\epsilon$	$L'_x$	$\bar{F}$	$\alpha$	$T'_0$	$n$	$L_x^D$	$L_z^D$	$T_0^D$
399	39	$2 \times 10^5$	10	$\epsilon \times L_z$	$1.4 \times 10^{-8}$	5	9.15	3	2 km	200 m	-10 °C

The aspect ratio  $\epsilon$ , i.e., the slab length divided by the slab thickness, is chosen such that the effects of longitudinal stress play an important role for the flow. Therefore, stabilizing effects of longitudinal stresses can be investigated.

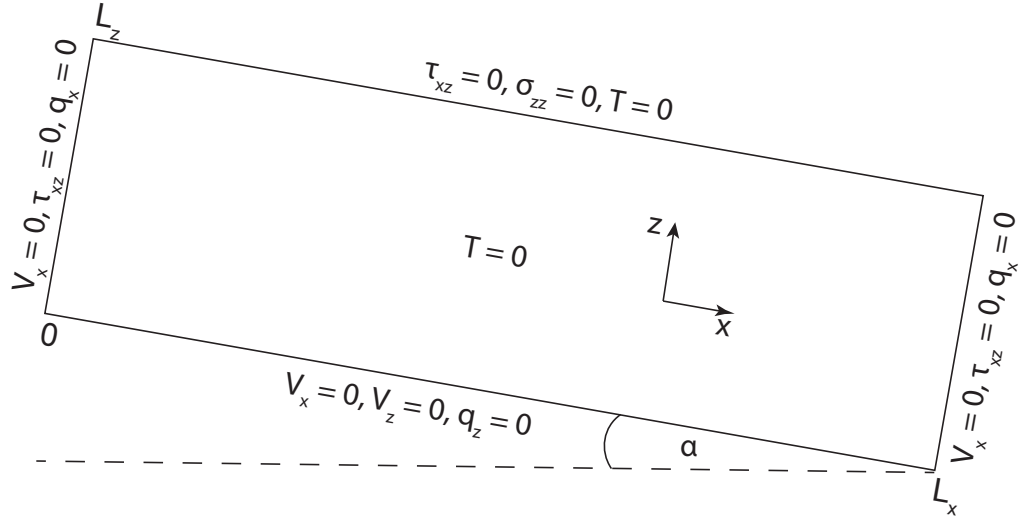


**Figure 3.1:** Schematic illustrating the model set-up. Both the surface and bed are flat and inclined at a constant slope angle  $\alpha$ . The model coordinate axes are shown and the applied boundary conditions are also plotted.

More specifically, the goal of the modelling exercise is to investigate the importance of different physical terms in the full set of mathematical equations. The reference run (model 1) is a fully coupled (i.e., two way) thermo-mechanical two dimensional model. In the second model (model 2) advection (blue color) is omitted from the temperature Equation 3.12, therefore the temperature at all times reflects a balance between diffusion and the strain heating. The third model (model 3) also excludes the horizontal diffusion term (red color).

$$\frac{\partial T'}{\partial t'} + v'_x \frac{\partial T'}{\partial x'} + v'_z \frac{\partial T'}{\partial z} = \frac{\partial^2 T'}{\partial x'^2} + \frac{\partial^2 T'}{\partial z'^2} + H_s'^{2D} \quad (3.12)$$

The strain heating term in two dimensions is given by Equation 3.13 and should preferably be written as a function of both the viscosity and the second strain rate invariant, since both viscosity, a material property, and a second invariant of a strain rate tensor are independent of the orientation of the coordinate system.

$$H_s'^{2D} = \tau'_{xx} \dot{\epsilon}'_{xx} + \tau'_{zz} \dot{\epsilon}'_{zz} + 2\tau'_{xz} \dot{\epsilon}'_{xz} = 4\eta' \dot{\epsilon}'_{II} \quad (3.13)$$

The obtained results are compared with the solutions of a one dimensional model, appropriate to model an infinite channel or a slab, meaning that all horizontal derivatives vanish. The 1D model is therefore equivalent to the models used by Clarke et al. (1977) and Yuen and Schubert (1979). It should be noted that for the chosen parameters, a one dimensional model

can reach steady state on the subcritical branch, but the use of slightly different parameters can result in thermal runaway and the steady state solution is not obtainable any more with a one dimensional model.

$$\frac{\partial T'}{\partial t'} = \frac{\partial^2 T'}{\partial z'^2} + H_s'^{1D} \quad (3.14)$$

Therefore in the case of the one dimensional infinite channel, the conservation of energy reduces to a balance between temperature evolution, vertical diffusion and strain heating term as in Equation 3.14. It should be noted that in a one dimensional case, the strain heating is only due to shear stress and can be explicitly stated as in Equation 3.15.

$$H_s'^{1D} = 2\tau'_{xz}\dot{\epsilon}'_{xz} = 4\eta'\dot{\epsilon}'_{xz}{}^2 = 2^{1-n}(\bar{F}L'_z)^{n+1}\left(1 - \frac{z'}{L'_z}\right)^{n+1}e^{\frac{nT'}{1+T'}} \quad (3.15)$$

To determine the first order effects in the stress balance, we derived an extended 1D model and compare its solutions to both the 1D and 2D diffusion model (model 2) solutions. Hence, advection terms are again neglected. We start the derivation by making the assumption of hydrostatic balance. This enable us to obtain the pressure solution and reduce the problem to solving just the x-direction momentum equation given by:

$$\frac{\partial \tau'_{xz}}{\partial z'} \approx -(\bar{F} + 2\frac{\partial \tau'_{xx}}{\partial x'}) \quad (3.16)$$

The hydrostatic assumption combined with the assumption that horizontal gradients of the vertical velocity are small compared to the vertical gradients of horizontal velocity components, corresponds to the so called Blatter-Pattyn model (Blatter, 1995; Pattyn, 2003). Next, we define the following parameter:

$$\beta(x' = \frac{L'_x}{2}, z', t' = t'_0) = 2\frac{\partial \tau'_{xx}}{\partial x'} \quad (3.17)$$

and calculate it from the solution of a model 2 at  $t'_0$  at  $x' = \frac{L'_x}{2}$ . Then this parameter is depth averaged:

$$\bar{\beta} = \frac{2}{L'_z} \int_0^{L'_z} \frac{\partial \tau'_{xx}}{\partial x'} \partial z' \quad (3.18)$$

and to simplify our analysis further we have made an assumption that the longitudinal stress gradient can be well approximated by the introduced depth averaged longitudinal stress gradient  $\bar{\beta}$ . We have further assumed that longitudinal stress is small compared to the shear stress  $\tau'_{xz}$ . It should be stated here that since the rheology is strongly non-linear and strain-rates of all directions are contributing to the effective viscosity, these assumptions do not necessarily

hold. Hence, under given assumptions, we can analytically integrate Equation 3.16 and obtain the explicit expression for the modified shear stress:

$$\tau'_{xz}(x, z) = (\bar{F} + \bar{\beta})L'_z(1 - \frac{z'}{L'_z}) \quad (3.19)$$

The temperature evolution is still governed by Equation 3.14, but  $\bar{F}$  is now substituted with  $\bar{F} + \bar{\beta}$  in Equation 3.15.

### 3.4 Results

The results of a reference model run and model 2 run are presented in Figure 3.2. The left panels show the horizontal velocity component for different times and different model runs, while the right panels show the temperature evolution for different model runs. For readability in all figures, the length scales are rescaled with  $L'_z$  and velocity with the maximum velocity  $V_{sc}$  at  $t'_0$ . At  $t'_0=0$ , the initial temperature deviation is set to 0, and both model runs result in an equivalent output for the velocity and stress fields. The initial scaled velocity of 1 would correspond to approximately 7 m/yr, while the scaled velocity of 3 would correspond to the velocity of 21 m/yr. Temperature deviation of 0.1 would correspond to the temperature increase of 2.87 ° C and the melting temperature would then be reached at temperature deviation of approximately 0.35.

The solutions at  $\frac{x'}{L'_z} = 5$  are shown in more detail in Figure 3.3, where the panels again show the horizontal velocity component on the left and temperature deviation on the right at different times  $t'$ . Times  $t'_1, t'_2$  and  $t'_3$  therefore correspond to 0.27, 1 and 9.97 diffusion time scale. For comparison, using the dimensional values, this would correspond to 250, 950 and  $9.5 \times 10^3$  years. The solutions of three models are shown: 1D model, reference model or model 1 and model 2. As we can see in Figure 3.3, by going further in time both the velocity and the temperature increase until a balance between vertical diffusion and the strain heating term is achieved. Since with a given set of parameters steady state is achievable with a one dimensional model, one can expect that after some time both the temperature deviation and velocity will reach steady state. Depending how far, or close, the parameters are of the critical value, more or less time is needed to achieve this steady state. Usually, the amount of time varies from 2 times to up to 100 times the diffusion time scale. In our case time,  $t'_3$  is around 10 times bigger than the diffusion time scale and the steady state is achieved. One can notice that when the balance is achieved the velocity increases 1.66 times from the initial value, while the temperature deviation from the initial value is 0.196.

Next, we compare the solutions of a one dimensional model with a solution of the two dimensional finite channel without the temperature advection term (model 2). The main differences

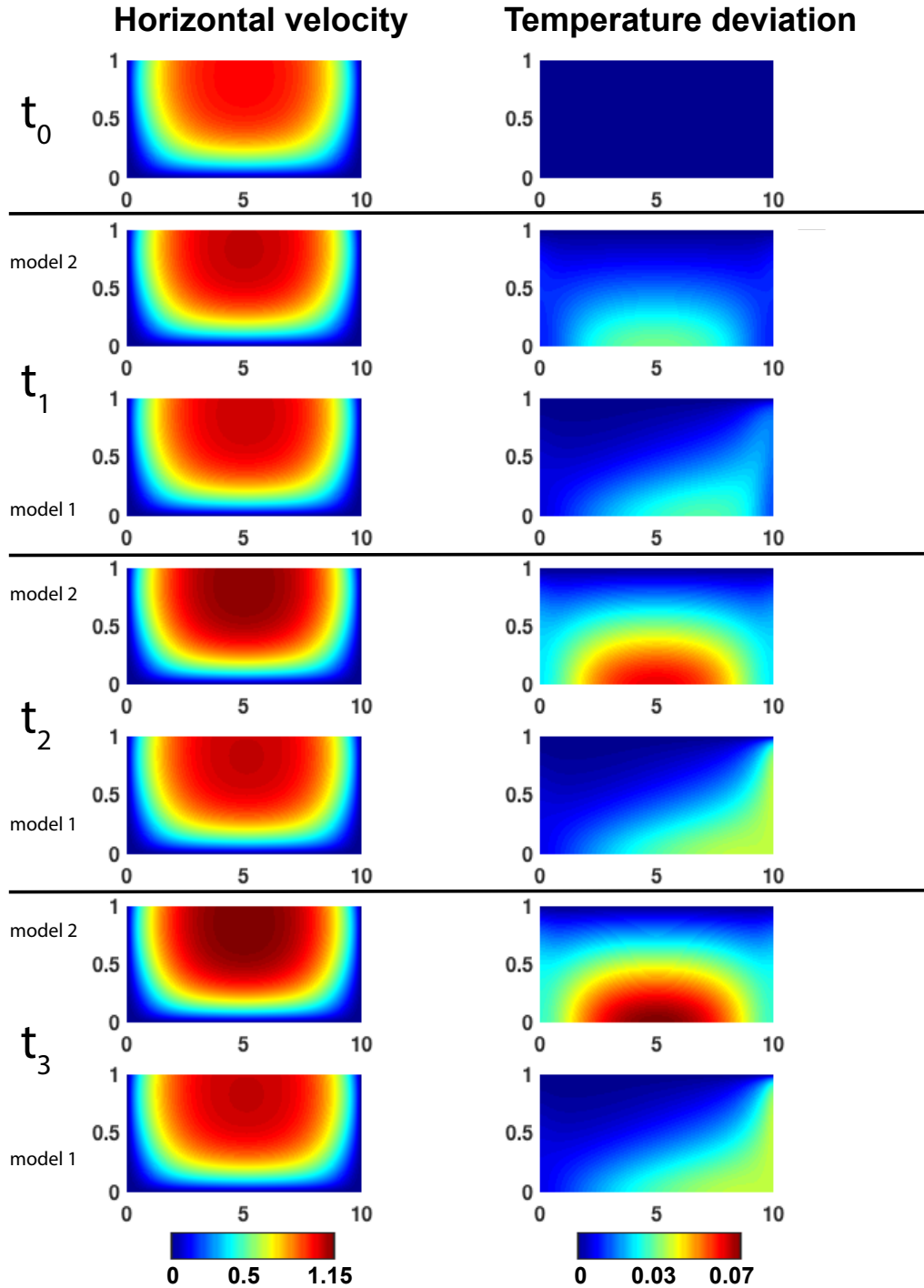


**Figure 3.2:** Non dimensional simulation results at four different time stages for both model 1 and model 2. In the left column the spatial distribution of the horizontal velocity component is shown, while in the right column the temperature deviation from the initial temperature is shown. At  $t_0$  both models return completely the same output, so the simulation result of a single model is shown. For readability, the length scales are rescaled with  $L_z$  and velocity with the maximum velocity  $V_{sc}$  at  $t_0$ . This configuration would correspond to a 2 km long and 200 m thick box inclined for the  $5^\circ$  angle with a initial basal temperature of  $-10^\circ\text{C}$ . The initial scaled velocity of 1 would correspond to approximately 7 m/yr. Temperature deviation of 0.1 would correspond to the temperature increase of  $2.87^\circ\text{C}$ .

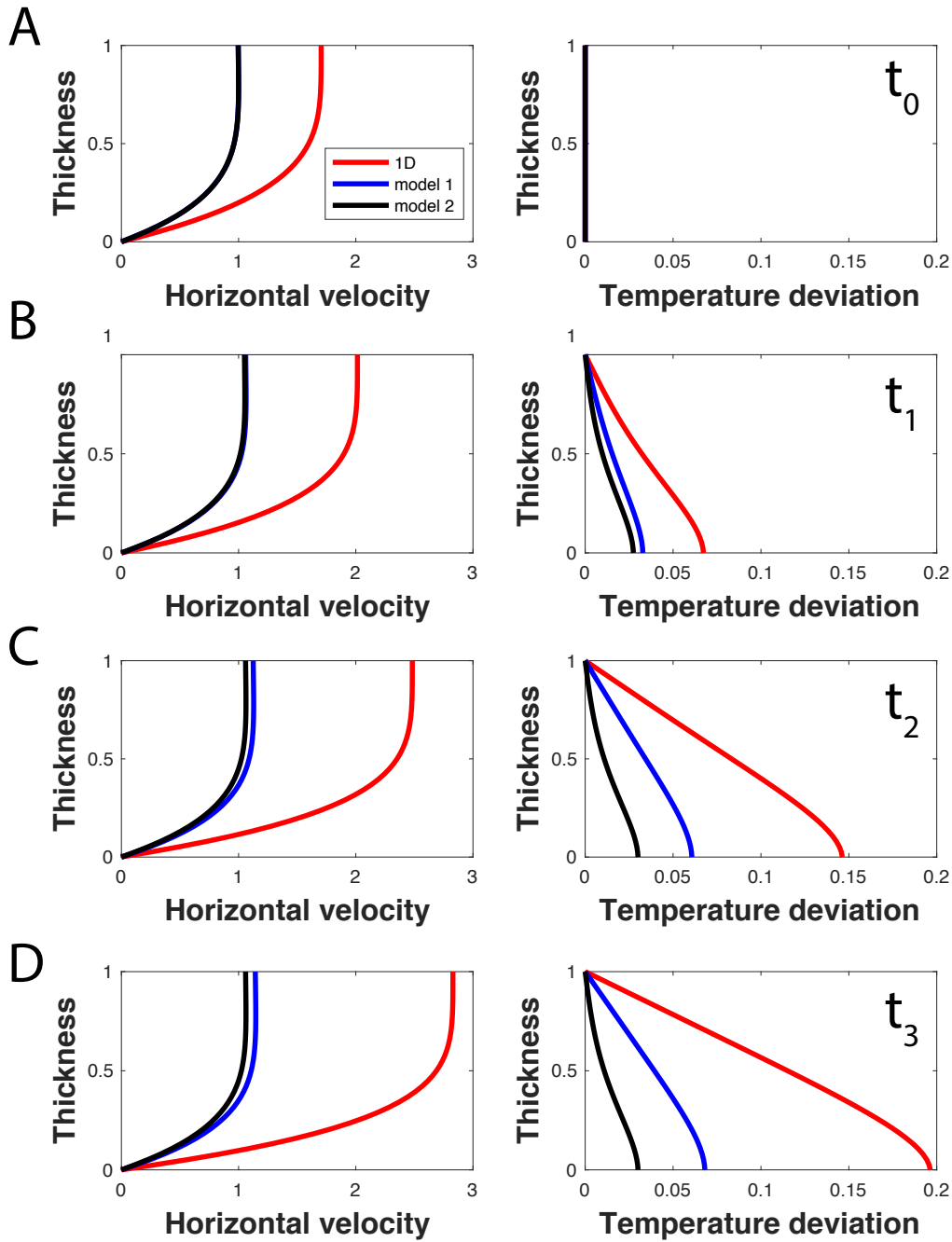


**Figure 3.3:** Simulation results at four different time stages at  $x = \frac{L_x}{2}$  ( $\approx 1$  km) for both model 1 and model 2 and a comparison with 1D model. In the left column the horizontal velocity component as a function of depth is plotted, while in the right column the temperature deviation from the initial temperature is plotted. Solid red line represents the 1D solution, black line model 1 solution and blue line model 2 solution. The initial scaled velocity of 1 would correspond to approximately 7 m/yr, while the scaled velocity of 3 would correspond to the velocity of 21 m/yr. Temperature deviation of 0.1 would correspond to the temperature increase of  $2.87^\circ\text{C}$  and the melting temperature would then be reached at temperature deviation of approximately 0.35.

between the models therefore arise due to the existence of horizontal derivatives, especially due to the longitudinal stress gradient/horizontal pressure gradient in the momentum balance, the horizontal diffusion term in the conservation of energy and different definitions of the strain heating term. At the initial time  $t'_0$ , the maximum horizontal velocity in a finite channel is reduced to 0.59 of the original value for the infinite channel. This effect is mostly because of the effects of longitudinal stress gradient/horizontal pressure gradient that arise in case of a finite channel, since in this case horizontal derivatives are not equal to zero any more. As we advance in time and reach the time  $t'_3$  the velocity increases 1.147 times from its initial value, while temperature increases to 0.068. This is a significant reduction compared to the one dimensional case. In turn, it shows a stabilizing effect of the longitudinal stress gradient and horizontal pressure gradient in the momentum balance.

In case of a two dimensional finite channel with advection (reference model 1) the velocity increases only 1.056 times its initial value, while temperature increases to 0.038, which is again almost a double reduction in value compared to the previous case with no advection included. One striking feature of the results is the depth profile (and spatial distribution) of the temperature, which in both previous cases is linear in the top 85% of ice; while this is not the case when temperature advection is included in the model. This is easily seen in the Figure 3.4, where the temperature depth profile is plotted at time  $t'_3$  at different horizontal positions for both model runs. This confirms the scaling analysis (Baral et al., 2001; Hutter, 1983; Morland, 1984), which shows that, at the first order, the strain heating heat source is primarily balanced by advection of heat and only mildly adjusted by the vertical heat diffusion.

Additionally, in Figure 3.4 the velocity depth profiles of both model runs at different horizontal positions are plotted. We observe that the horizontal velocity component obtained with a model run, including temperature advection, is always equal or smaller than the one obtained with a model not including advection.

In Figure 3.5 the spatial distribution of the strain heating is shown at  $t'_3$  for both model 1 (panel A) and model 2 (panel B). The strain heating term is rescaled, with the maximum value of strain heating  $H_{s_{sc}}$  at  $t'_0$  for model 2. In panel C the difference between the models is shown, where it can be noticed that the model 1 strain heating values are always equal or smaller the values obtained with model 2. The maximum difference is around 10% and are distributed close to the base. In panel D, the spatial distribution of a 1D model is shown, where one can notice that the maximum strain heating values are up to 3 times higher than that in model 1 and model 2.

In Figure 3.6 the results of the model 3 and the extended 1D model are plotted and compared with the previous model runs. One can notice that the difference between model 2 and model 3 is minimal and conclude that the horizontal diffusion has a second order effect on the

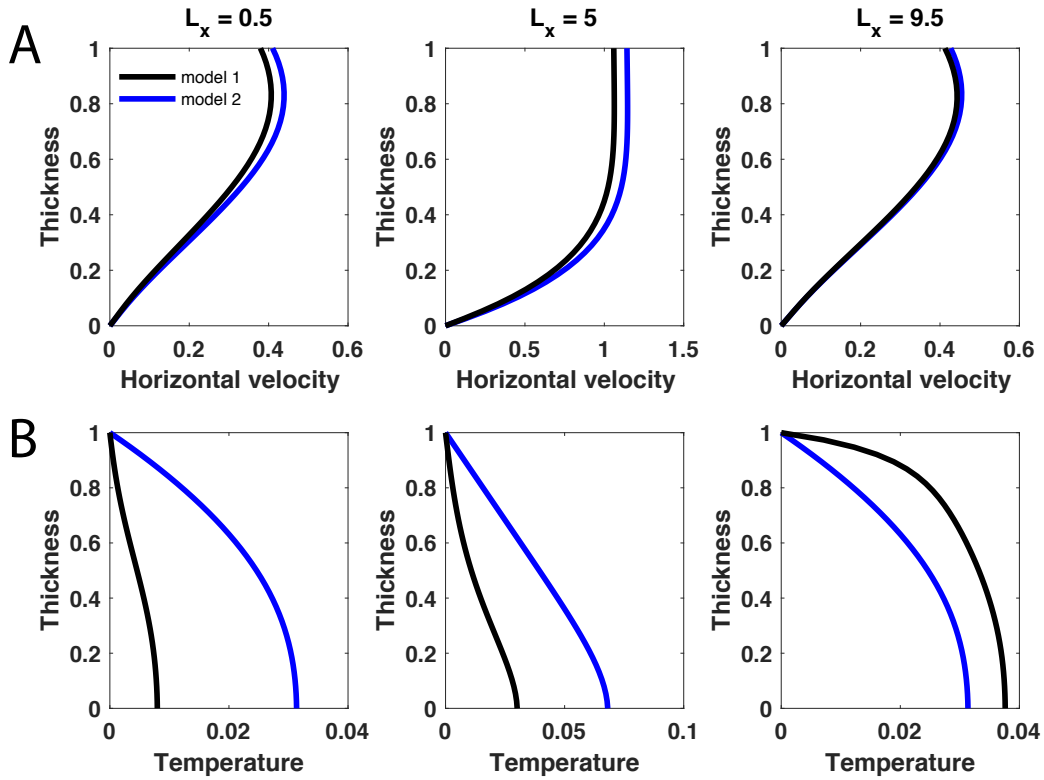


**Figure 3.4:** Simulation results at the last time stage for both model 1 and model 2 at three different horizontal positions (cross-sections). Time  $t_3$  corresponds to 9.97 diffusion time scale or for comparison  $9.5 \times 10^3$  years using dimensional values. In the top panel (A) the horizontal velocity as a function of depth is plotted, while in the bottom panel (B) the temperature deviation as a function of depth is shown. Solid black line represents model 1 solution and blue line model 2 solution.

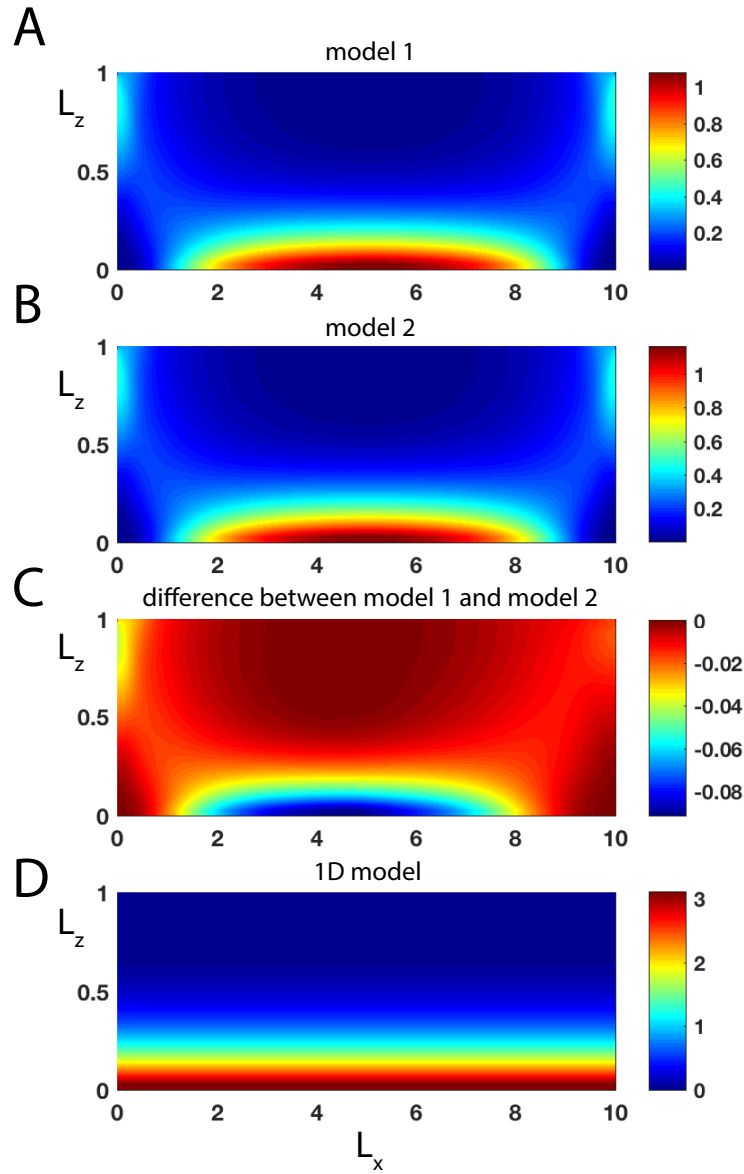


**Figure 3.5:** Spatial distribution of the strain heating term at the time  $t_3$  for (A) model 1, (B) model 2 and (D) the 1D model. Time  $t_3$  corresponds to 9.97 diffusion time scale, or for comparison  $9.5 \times 10^3$  years using dimensional values. The difference between model 1 and model 2 is also shown in panel C. For readability, the length scales are rescaled with  $L_z$ , while the strain heating term is rescaled with the maximum value of strain heating  $Hs_{sc}$  at  $t_0$  for model 1. This configuration would correspond to a 2 km long and 200 m thick box inclined for the  $5^\circ$  angle with a initial basal temperature of  $-10^\circ\text{C}$ .

solution. On the other hand, the inclusion of this simple correction to the basal shear stress in a 1D model enables the approximation of the effects of longitudinal stress gradients. This correction has first order effects on the solution. The extended 1D model and the model 2 are almost indistinguishable from each other and the remaining difference can be assigned to a simple reduction of a function of three variables to a constant.

### 3.5 Parametrization of 1D numerical profiles of velocity and temperature

In the results section it was shown that the 2D behaviour can be properly approximated with the extended 1D model. Here, we return to the initial set of dimensional equations (Equations 3.1 - 3.4) and reduce it to the one dimensional case without advection. Therefore, the temperature evolution is a competition between vertical diffusion (blue term) and the depth dependent strain heating term due to shearing (red term). The temperature evolution in an inclined slab is then governed by the following equation:

$$\frac{\partial T}{\partial t} = \frac{k}{\rho c_p} \frac{\partial^2 T}{\partial z^2} + \frac{2a_0}{\rho c_p} e^{-\frac{Q}{RT_0}} \tau_b^{n+1} \left(1 - \frac{z}{L_z}\right)^{n+1} e^{\frac{Q}{RT_0^2} \left(\frac{T}{1+\frac{T}{T_0}}\right)} \quad (3.20)$$

Additionally, we define the following parameters:

$$\tau_b = \rho g L_z \sin \alpha \quad V_0 = 2a_0 e^{-\frac{Q}{RT_0}} \tau_b^n \frac{L_z}{n+1} \quad t_d = \frac{\rho c_p L_z^2}{k} \quad T_{sc} = \frac{RT_0^2}{Q} \quad (3.21)$$

where  $\tau_b$  is the basal shear stress,  $V_0$  is initial velocity at the surface,  $t_d$  is diffusion time scale and  $T_{sc}$  is the temperature scale. At the start of each simulation the initial basal temperature is set to  $T_0$  everywhere throughout the slab and during the simulation the top surface ( $z = L_z$ ) temperature is kept at  $T_0$ , while at the base ( $z = 0$ ) the heat flux  $q_z$  is set to zero. The physical variables held constant during each simulation are reported in Table 3.2. Next, we define an dimensionless parameter  $\lambda$  as follows:

$$\lambda = \frac{2a_0 Q L_z^2 \tau_b^{n+1}}{k R T_0^2} e^{-\frac{Q}{RT_0}} \quad (3.22)$$

The parameter  $\lambda$  is exactly equivalent to the stability parameter  $\beta$  in (Clarke et al., 1977) where it is used to determine the efficiency and importance of strain heating.

We then vary the mean bed slope from  $4 - 10^\circ$  and slab thickness from  $50 - 200$  m. The initial temperature in the slab is varied from  $253 - 258$  K. The stability parameter  $\lambda$  and the diffusion time scale  $t_d$  are then calculated for every set of parameters and the logarithm of temperature deviation scaled with  $T_{sc}$  is then plotted as a function of stability parameter  $\lambda$

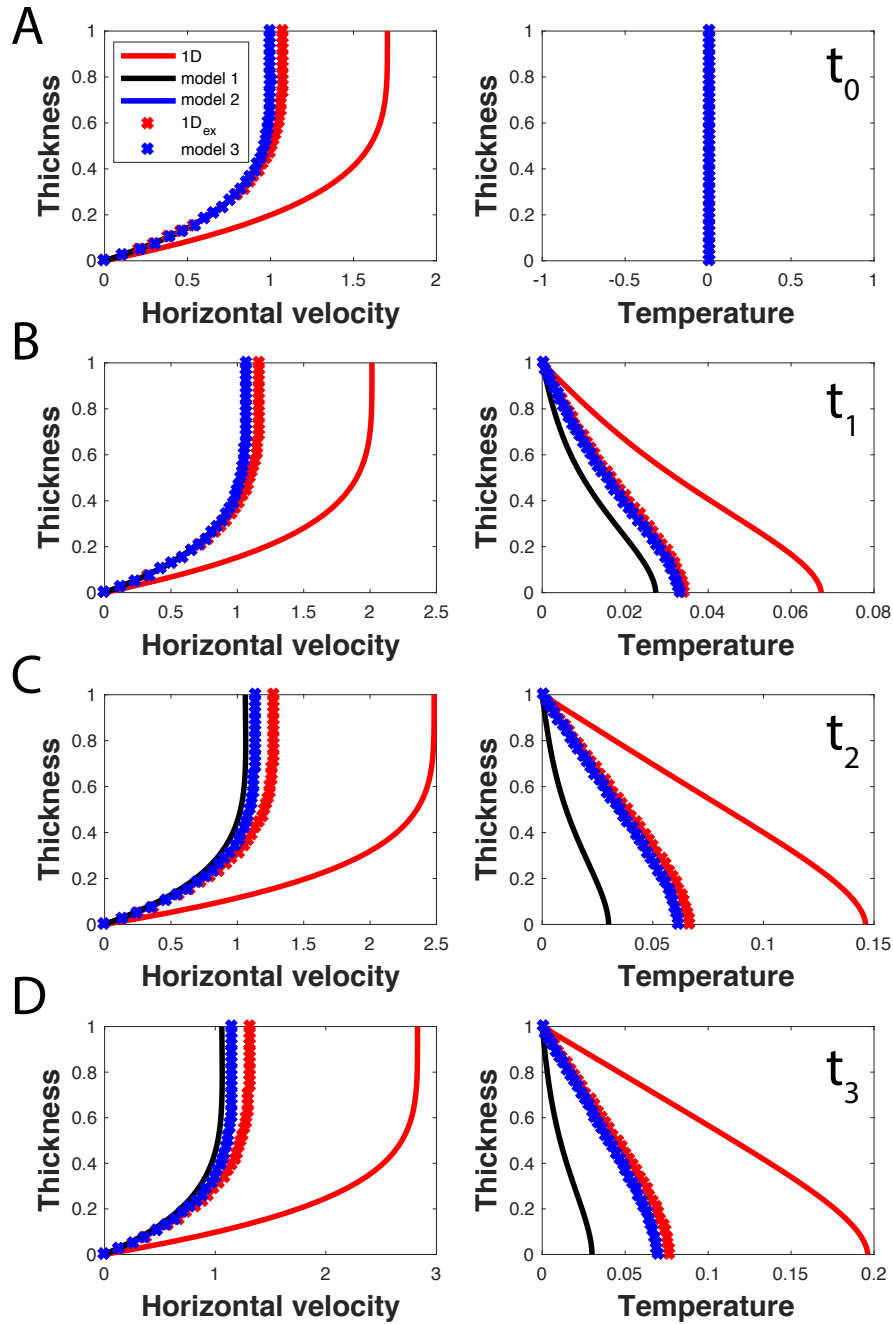


**Figure 3.6:** Simulation results at four different time stages at  $x = \frac{L_x}{2}$  for both model 1, model 2 and model 3 and a comparison with 1D model and 1D extended model. In the left column the horizontal velocity component as a function of depth is plotted, while in the right column the temperature deviation from the initial temperature is plotted. Solid red line represents the 1D solution, black line model 1 solution, blue line model 2 solution, model 3 solution is plotted with blue crosses while the 1D extended solution with red crosses. The initial scaled velocity of 1 would correspond to approximately 7 m/yr, while the scaled velocity of 3 would correspond to the velocity of 21 m/yr. Temperature deviation of 0.1 would correspond to the temperature increase of  $2.87^\circ\text{C}$  and the melting temperature would then be reached at temperature deviation of approximately 0.35.

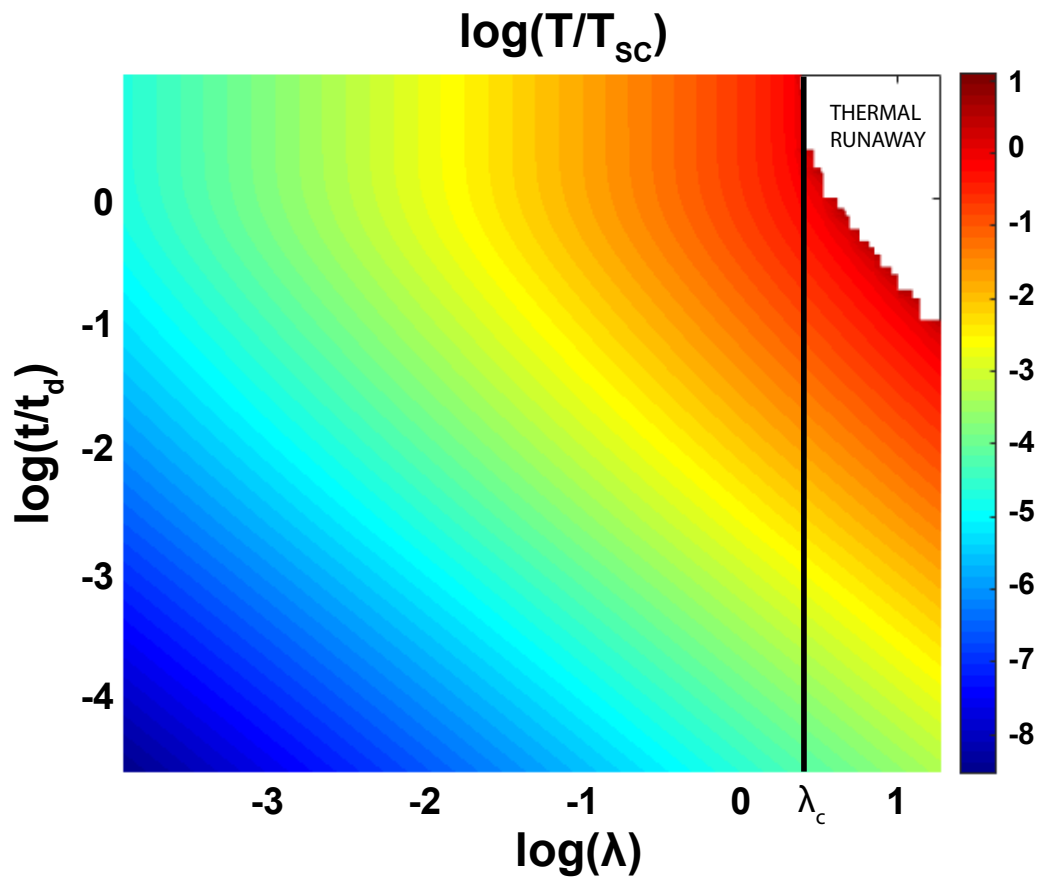


**Figure 3.7:** Contour plots for scaled temperature increase  $\frac{T}{T_{sc}}$  as a function of parameter  $\lambda$  and scaled time  $\frac{t}{t_d}$ . The white color represents the area where thermal runaway occurred. Solid black line indicate the  $\lambda_c$  and separates the diagram on two distinct parts, one where the steady state is reachable and an area where in finite time thermal runaway will occur.

**Table 3.2:** Physical constants

Symbol	Definition	Value	Unit
R	gas constant	8.314	$\frac{J}{molK}$
g	gravity acceleration	9.8	$\frac{m}{s^2}$
$\rho$	ice density	900	$\frac{kg}{m^3}$
k	thermal conductivity	2.51	$\frac{W}{K\eta}$
$\kappa$	thermal diffusivity	$1.33 \times 10^{-6}$	$\frac{m^2}{s}$
$c_p$	specific heat capacity	2096.9	$\frac{J}{kgK}$
n	flow law exponent	3	—
$a_0$	flow law constant	$8.75 \times 10^{-13}$	$Pa^{-3}s^{-1}$
Q	creep activation energy	$60 \times 10^3$	$\frac{J}{mol}$

and scaled time  $\frac{t}{t_d}$ . The results are presented as a filled contour plot in Figure 3.7. It can be seen that when the stability parameter  $\lambda$  reaches some critical value  $\lambda_c$ , thermal runaway occurs in a finite amount of time. Melting temperature is reached, and since melting is not accounted for in our model then the model is not valid any more. As shown by Clarke et al. (1977) the critical value  $\lambda_c$  is approximately equal to  $\frac{\pi^2}{4}$ . This amount of time is always slightly larger than the adiabatic critical time, since diffusion plays an important role, even in the initial transient phase, by slowing down the heating process. It can also be seen that the solution obtained at short times and a larger value of the stability parameter is similar to the solution obtained with a smaller value of the stability parameter and at longer times.

We follow Dold (1985) who argued that the early stages of thermal runaway can be described using a logarithmic expression. Here, we propose the following ansatz as a predictor of maximum temperature at the base of the slab:

$$T_b = T_{sc} \ln \left[ \frac{1}{1 - aBr} \right] \quad (3.23)$$

where we define an additional dimensionless parameter as:

$$Br = \lambda \left( \frac{t}{t_d} \right)^b \quad (3.24)$$

where  $t$  is time and  $t_d$  again represents the diffusion time scale. The parameters  $a$  and  $b$  are derived by fitting the above function to the numerical solution. The obtained values for the fitting parameters are given in Table 3.3.

**Table 3.3:** Fitting parameters valid for  $\lambda < 20$ 

Symbol	Value
$a$	0.3179
$b$	0.7974

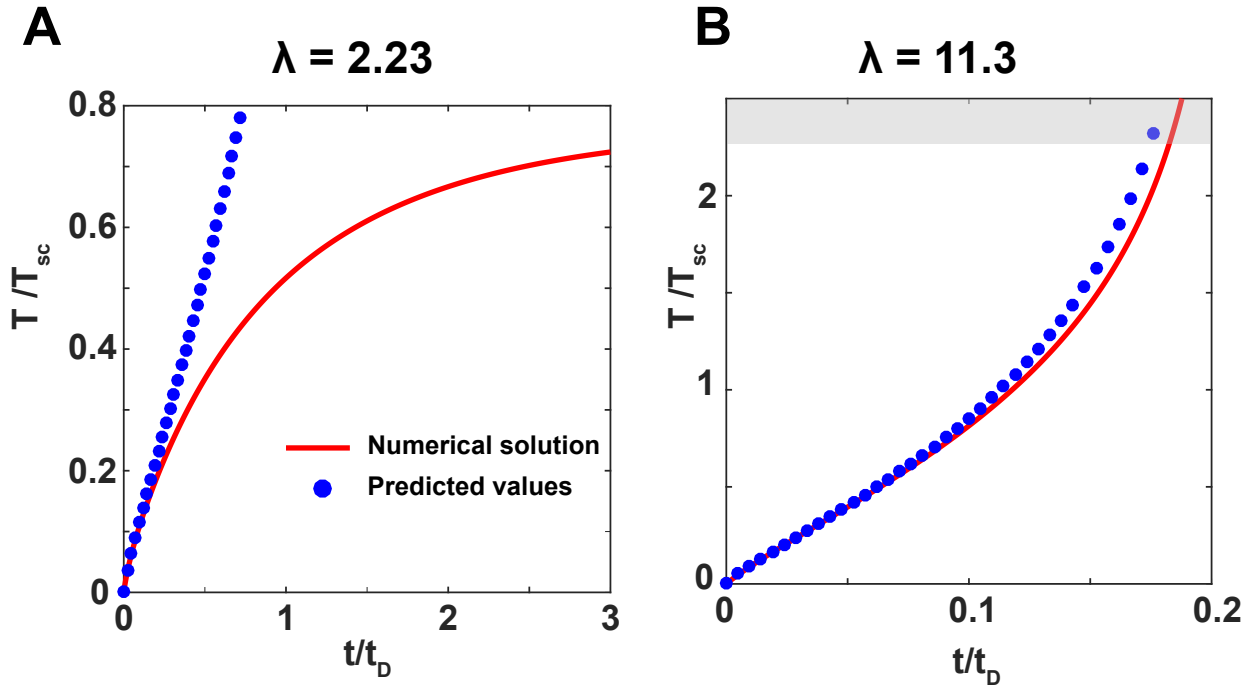


**Figure 3.8:** Comparison between the numerical solution and predicted solution using the ansatz given by Equation 3.23. In both cases the maximum temperature is scaled with  $T_{sc}$ , while time is scaled with  $t_d$ . The maximum temperature in this configuration is located at the base of the slab. A) stability parameter  $\lambda = 2.23$  was obtained by using the ice thickness  $H = 140$  m and initial basal temperature of  $T_0 = -15$  °C B) stability parameter  $\lambda = 11.3$  was obtained by using the ice thickness  $H = 200$  m and initial basal temperature of  $T_0 = -20$  °C . The shaded area in panel B represent area above the melting temperature, an area where the solution is not valid anymore. In both cases the slab was inclined for  $\alpha = 10$  °

One can also immediately notice similarity with the analytical solution obtained in the adiabatic case :

$$T^{AD}(z, t) = T_{sc} \ln \left[ \frac{1}{1 - \lambda \left( \frac{t}{t_d} \right) \left( 1 - \frac{z}{L_z} \right)^{n+1}} \right] \quad (3.25)$$

where  $T^{AD}$  is the temperature increase in the adiabatic case. We continue our derivation by using the first term of the Macularian series for natural logarithm  $\ln[1 - x] \approx -x$  where we obtain:

$$T^{AD}(z, t) \approx T_{sc} \lambda \left( \frac{t}{t_d} \right) \left( 1 - \frac{z}{L_z} \right)^{n+1} \quad (3.26)$$

where  $T_{sc} \lambda \left( \frac{t}{t_d} \right)$  can be recognized as a temperature at the base in the adiabatic case and therefore the temperature profile in the adiabatic case is given by:

$$T^{AD}(z, t) = T_b^{AD} \left( 1 - \frac{z}{L_z} \right)^{n+1} \quad (3.27)$$

We further correct and replace the basal temperature with the temperature given by Equation 3.23 which takes into account diffusion in a boundary layer close to the base and the following temperature ansatz is obtained:

$$T(z, t) = T_b \left( 1 - \frac{z}{L_z} \right)^{n+1} \quad (3.28)$$

To verify that the proposed ansatz can be used to predict the values of the maximum temperature deviation in the slab in early stages ( $\frac{t}{t_d} < 0.2$ ) we compare the numerical solutions and the predicted values in two different examples. The first example is with the value of the stability parameter set to  $\lambda = 2.23$ , a value which is lower than the critical value  $\lambda_c$ , and the second one with the value of the stability parameter  $\lambda = 11.3$ , a value higher then the critical one. The first solution is therefore expected to reach the steady state at some point in time, while the second solution is certain to result in thermal runaway by reaching the melting temperature first. The results are shown in Figure 3.8 and good agreement between the predicted and numerical solution is obtained in the early stages.

Next, we have varied the values of  $\lambda$  from 7 to 20, and values of scaled time  $\frac{t}{t_d}$  from 0.01 to 0.1. The values of maximum temperature increase, scaled with temperature scale  $\frac{T}{T_{sc}}$ , at different times is shown and plotted against the stability parameter  $\lambda$  in the top panel of Figure 3.9. In the bottom panel the same is plotted against the  $Br$  parameter. It can easily be seen that solutions are scattered in the upper figure when plotted against the stability parameter, while solutions collapse when plotted against the  $Br$  parameter. This shows us that the introduced  $Br$  parameter is a good predictor for determining the maximum temperature increase and hence the importance of strain heating.

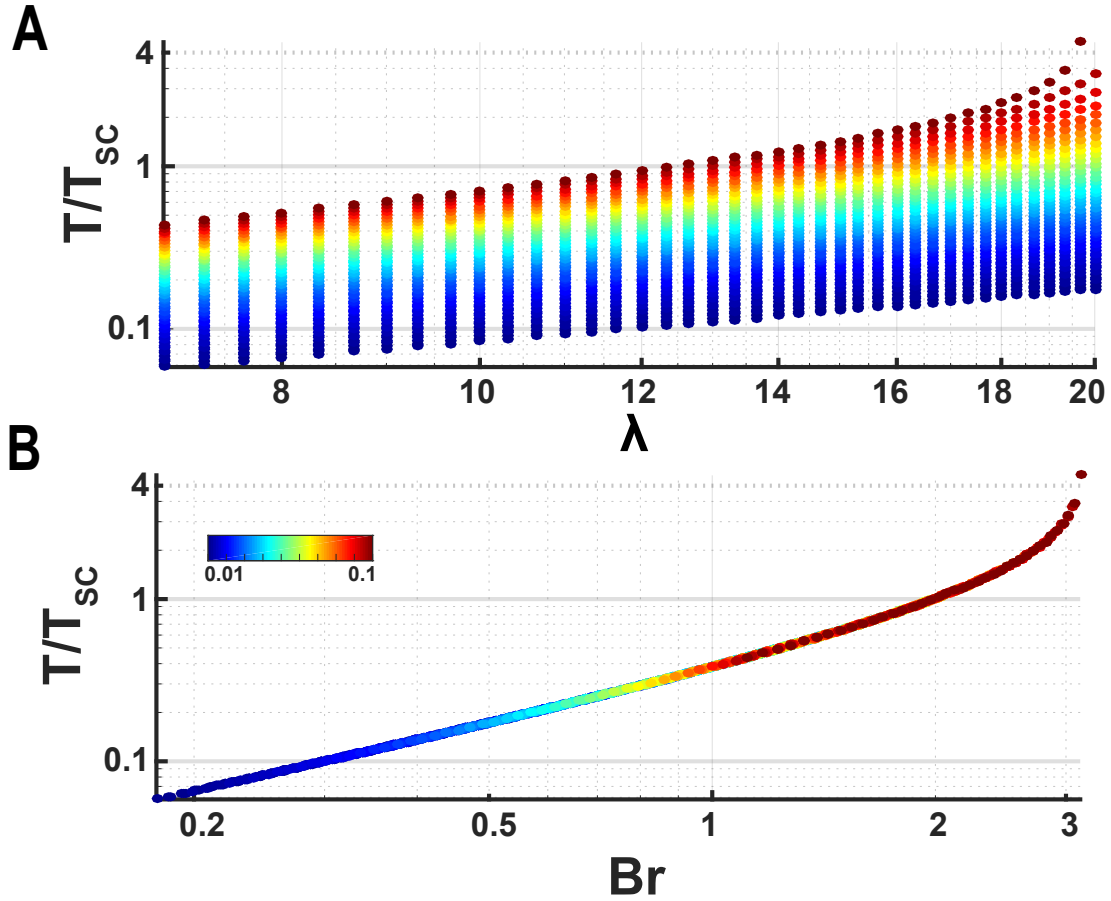


**Figure 3.9:** Comparison between two dimensionless parameters and their usefulness to assess the importance of strain heating and their ability to predict the maximum temperature deviation in the slab. The maximum temperature deviation scaled with  $T_{sc}$  is plotted in upper panel against A) stability parameter  $\lambda$  and in lower panel against B) parameter  $Br$ . The values of  $\lambda$  were varied from 7 to 20, while scaled time  $\frac{t}{t_d}$  was varied from 0.01 to 0.1 in both cases. The colorbar corresponds to the scaled time  $\frac{t}{t_d}$ .

The velocity profile in the slab is given by:

$$V_x(z, t) = 2a_0 \exp\left(-\frac{Q}{RT_0}\right) \tau_b^n \int_0^z \left(1 - \frac{z}{L_z}\right)^n \exp\left(\frac{Q}{RT_0^2} \frac{T(z, t)}{\left(1 + \frac{T(z, t)}{T_0}\right)}\right) dz \quad (3.29)$$

under the assumption of small temperature increases  $\frac{T}{T_0} \approx 0$ , we obtain the following relation for velocity:

$$V_x(z, t) = 2a_0 \exp\left(-\frac{Q}{RT_0}\right) \tau_b^n \int_0^z \left(1 - \frac{z}{L_z}\right)^n \exp\left(\frac{Q}{RT_0^2} T(z, t)\right) dz \quad (3.30)$$

If we further use the fact that temperature in the slab can be approximated well by using Equation 3.28 ( $T(z, t) \approx T_b(1 - \frac{z}{L_z})^{n+1}$ ):

$$V_x(z, t) = 2a_0 \exp\left(-\frac{Q}{RT_0}\right) \tau_b^n \int_0^z \left(1 - \frac{z}{L_z}\right)^n \exp\left(\frac{Q}{RT_0^2} T_b \left(1 - \frac{z}{L_z}\right)^{n+1}\right) dz \quad (3.31)$$

where the integral can be solved analytically to obtain the following:

$$V_x(z, t) = 2a_0 \exp\left(-\frac{Q}{RT_0}\right) \tau_b^n \frac{L_z}{(n+1)} \frac{RT_0^2}{Q} \frac{1}{T_b} \exp\left(\frac{QT_b}{RT_0^2}\right) \left(1 - \exp\left(\frac{QT_b}{RT_0^2} \left(1 - \frac{z}{L_z}\right)^{n+1} - 1\right)\right) \quad (3.32)$$

where we can further recognize initial velocity  $V_0$  from Equation 3.21 and substitute the basal temperature  $T_b$  (Equation 3.23) to obtain:

$$V_x(z, t) = V_0 \left[ \frac{1}{(1 - aBr) \ln\left[\frac{1}{1 - aBr}\right]} \right] \left(1 - \exp\left(\ln[1 - aBr] \left(1 - \left(1 - \frac{z}{L_z}\right)^{n+1}\right)\right)\right) \quad (3.33)$$

Furthermore, velocity at the surface can be obtained by setting  $z = L_z$  which simplifies the above expression to:

$$V_x^S(t) = V_0 \left[ \frac{aBr}{(1 - aBr) \ln\left[\frac{1}{1 - aBr}\right]} \right] \quad (3.34)$$

while the velocity increase due to the shear heating can be formulated as follows:

$$\Delta V(t) = V_0 \left( \frac{aBr}{(1 - aBr) \ln\left[\frac{1}{1 - aBr}\right]} - 1 \right) \quad (3.35)$$

where velocity increase  $\Delta V(t)$  is defined as  $\Delta V(t) = V_x^S(t) - V_0$ .

The proposed ansatz can be used to predict the maximum velocity as a function of time, for a given value of  $\lambda$ . The maximum velocity is always located at the surface of the slab. Due to the approximations of temperature throughout the slab and errors introduced by using the

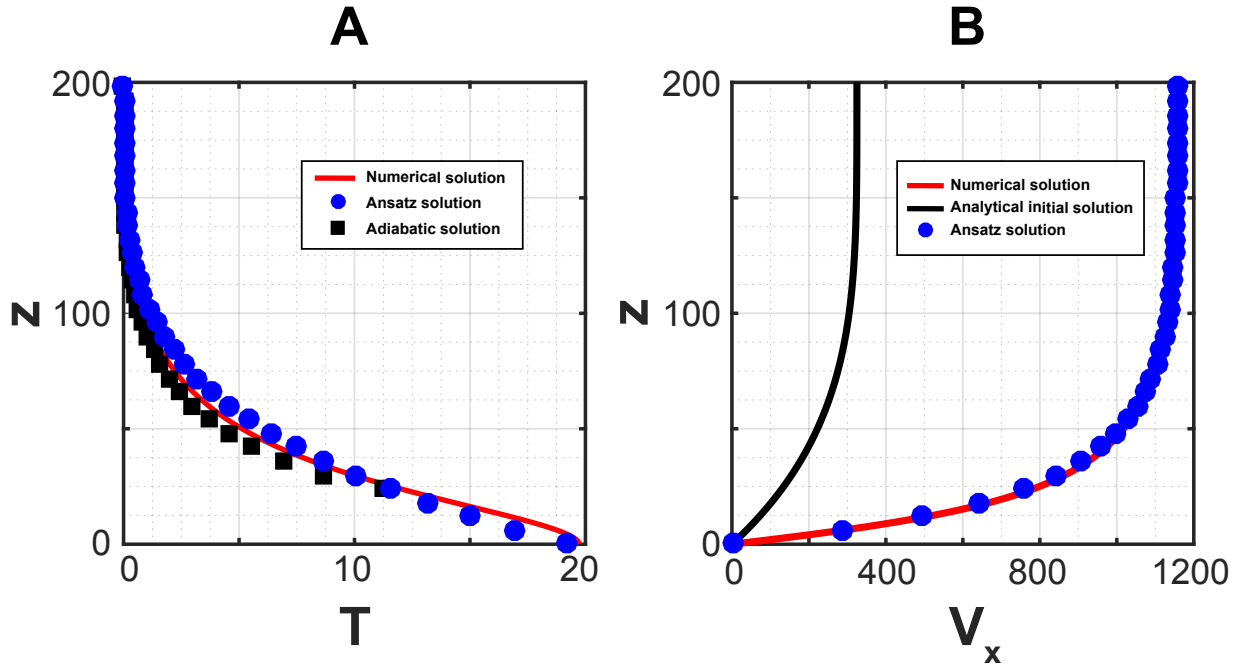


**Figure 3.10:** Comparison between the numerical solution and predicted solution using the ansatz given by Equation 3.28 for A) temperature and by Equation 3.33 for B) velocity. The stability parameter  $\lambda = 113.26$  was obtained by using the ice thickness  $L_z = 200$  m and initial basal temperature of  $T_0 = -20$  °C. The value for the flow law constant  $a_0$  used was  $8.75 \times 10^{-12}$  Pa $^{-3}$ s $^{-1}$ . The slab was inclined for  $\alpha = 10$  ° The model was running for 10.12 years. In panel A we have additionally shown the adiabatic temperature profile (black squares) given by Equation 3.25, but only above the boundary layer  $H > 20$  m in which diffusion significantly influences the solution. In panel B black solid line depicts the velocity profile at the initial time. The value of the fitting parameter  $a$  was reduced to 0.3, while the value of the fitting parameter  $b$  was kept the same.

ansatz for the prediction of maximum basal temperature, errors between the actual numerical solution and the predicted values can be expected. The magnitude of these errors strongly depends on the values of the fitting parameters  $a$  and  $b$ .

To verify the validity of the derived expressions for the temperature and velocity increases due to shear heating, in Figure 3.10 we show depth profiles for both temperature (panel A) and velocity (panel B) increase. We compare the numerical solution and the predicted solution using the ansatz given by Equation 3.28 for A) temperature and by Equation 3.33 for B) velocity. The results show that a good agreement is achieved between the two. Additionally, it can be seen that the error strongly depends on the fitting parameters  $a$  and  $b$ . Adiabatic temperature solution given by the analytical solution (Equation 3.25) represent the numerical solution well in the upper part of the domain, above a boundary layer of thickness  $H = \sqrt{\frac{k}{\rho c p} t}$ , which in our case is approximately 20 m. In the boundary layer, diffusion has significant influence and modifies (slows down) the adiabatic solution by conducting the produced heat. Hence, in this boundary layer the temperature increase is better represented by Equation 3.23 and therefore a combined solution given by Equation 3.28 approximates well the numerical solution for the temperature increase throughout the slab. The same is true for the velocity profile shown in the panel B.

### 3.6 Effects of strain heating for typical ice mass parameters

Here, we investigate the implications of the previous analysis by using realistic dimensions. We have first varied characteristic values of ice thickness  $L_z$  and basal slope  $\alpha$  to investigate temperature and velocity increases due to strain heating over 1 year. The physical variables are reported in Table 3.4. The results are presented in Figure 3.11. The results show that the largest increases in temperature, up to 17 °C, are obtained at high slopes and large ice thickness. The basal temperature of the slab is therefore increased from -20 °C to -3 °C in one year, while the velocity values of order  $1 \frac{km}{yr}$  can be seen. On the contrary, low slope angles and ice thickness are areas where strain heating is insignificant and therefore does not influence neither the temperature or velocity.

**Table 3.4:** Additional physical constants used for Figure 3.11

Symbol	Definition	Value	Unit
$a_0$	flow law constant	$2.7613 \times 10^{-5}$	$Pa^{-3} yr^{-1}$
$Q$	creep activation energy	$60 \times 10^3$	$\frac{J}{mol}$
$T_0$	initial basal temperature	-20	°C
$t$	time	1	yr
$\alpha$	mean bed slope	[1 to 10]	°
$L_z$	ice thickness	[50 to 500]	$m$

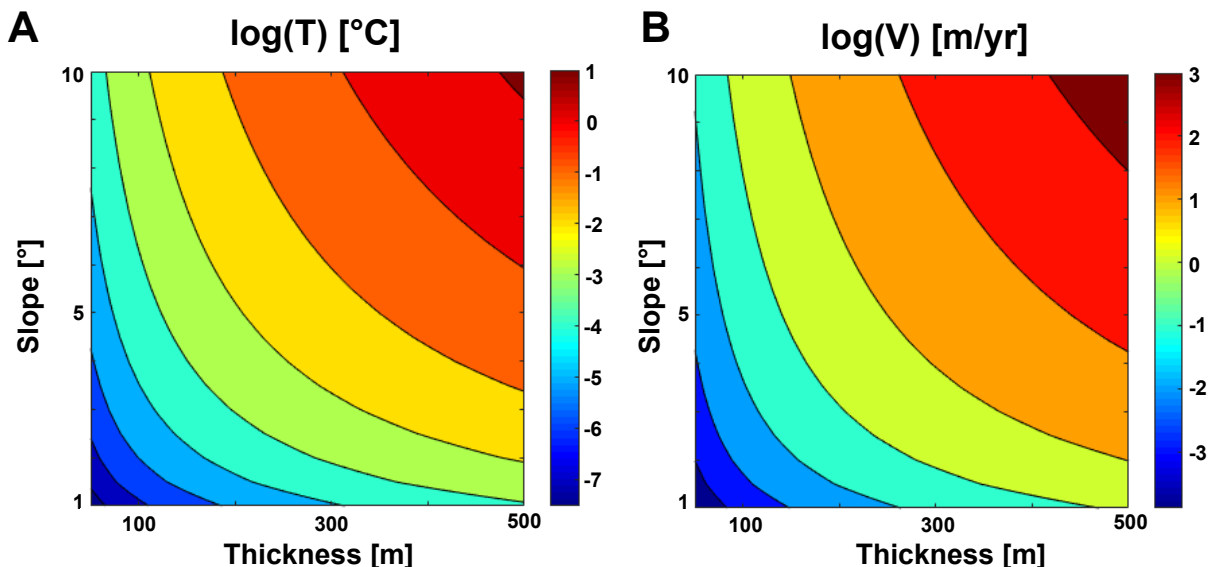


**Figure 3.11:** Dependence of A) the maximum temperature increase and B) velocity as a function of basal slope  $\alpha$  and ice thickness  $L_z$  presented as a contour plot. The dark lines are contour lines. Initial basal temperature  $T_0$  is set to  $-20^\circ\text{C}$ .

Next, we have varied characteristic values of initial basal temperature  $T_0$  and creep activation energy  $Q$  during 1 year for a fixed stress state in the slab. The physical variables are reported in Table 3.5. The results are presented in Figure 3.12. The results show that the largest increases in temperature, up to  $5^\circ\text{C}$ , are obtained at high basal temperature and low values of creep activation energy. The same is true for the velocity, where we can see maximum surface velocities of up to  $1 \frac{\text{km}}{\text{yr}}$ . High creep activation energy, combined with low basal temperature implies low strain heating and minor temperature increase.

**Table 3.5:** Additional physical constants used for Figure 3.12

Symbol	Definition	Value	Unit
$a_0$	flow law constant	$2.7613 \times 10^{-5}$	$\text{Pa}^{-3}\text{yr}^{-1}$
$Q$	creep activation energy	$[60 \text{ to } 120] \times 10^3$	$\frac{\text{J}}{\text{mol}}$
$T_0$	initial basal temperature	$[-40 \text{ to } -5]$	$^\circ\text{C}$
$t$	time	1	$\text{yr}$
$\alpha$	mean bed slope	10	$^\circ$
$L_z$	ice thickness	300	$m$

Finally, we have varied the flow law constant  $a_0$  and time  $t$  for a fixed stress state in the slab. The physical variables are reported in Table 3.6. The results are presented in Figure 3.13. Results show that high values of flow law constant combined with the increased time enables higher values of temperature increase, up to  $12^\circ\text{C}$ , and high velocity values of up to  $1.5 \frac{\text{km}}{\text{yr}}$ .

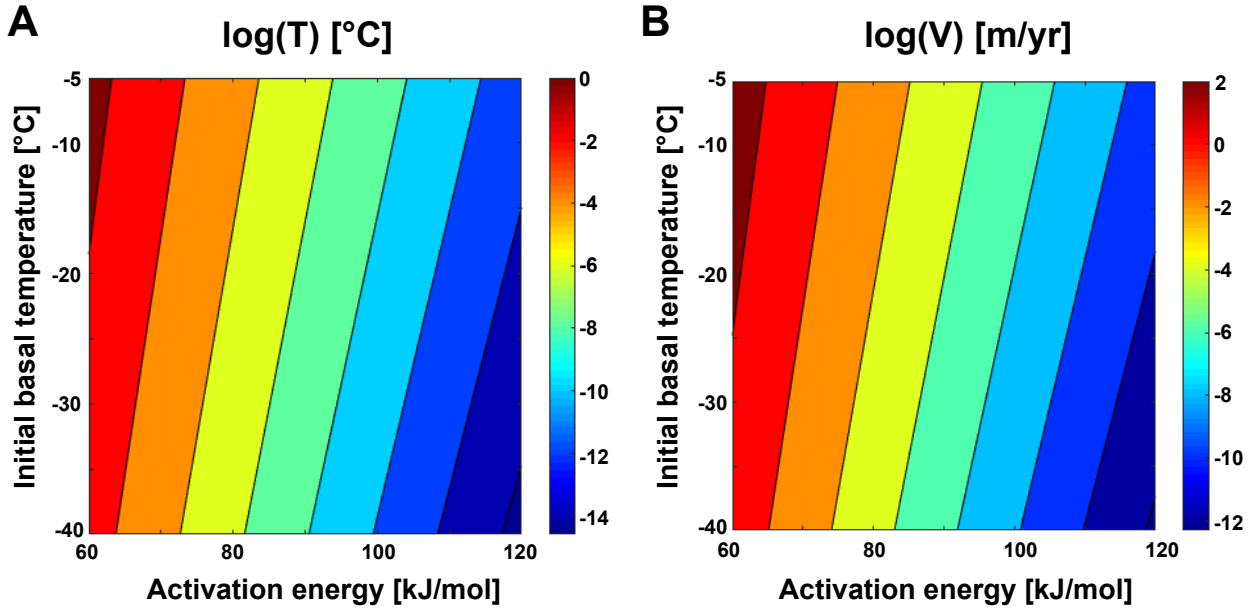


**Figure 3.12:** Dependence of A) the maximum temperature increase and B) velocity as a function of initial basal temperature  $T_0$  and activation energy  $Q$ , presented as a contour plot. The dark lines are contour lines. The slab thickness  $L_z$  is set to 300 m inclined for a basal slope  $\alpha$  of  $10^\circ$ .

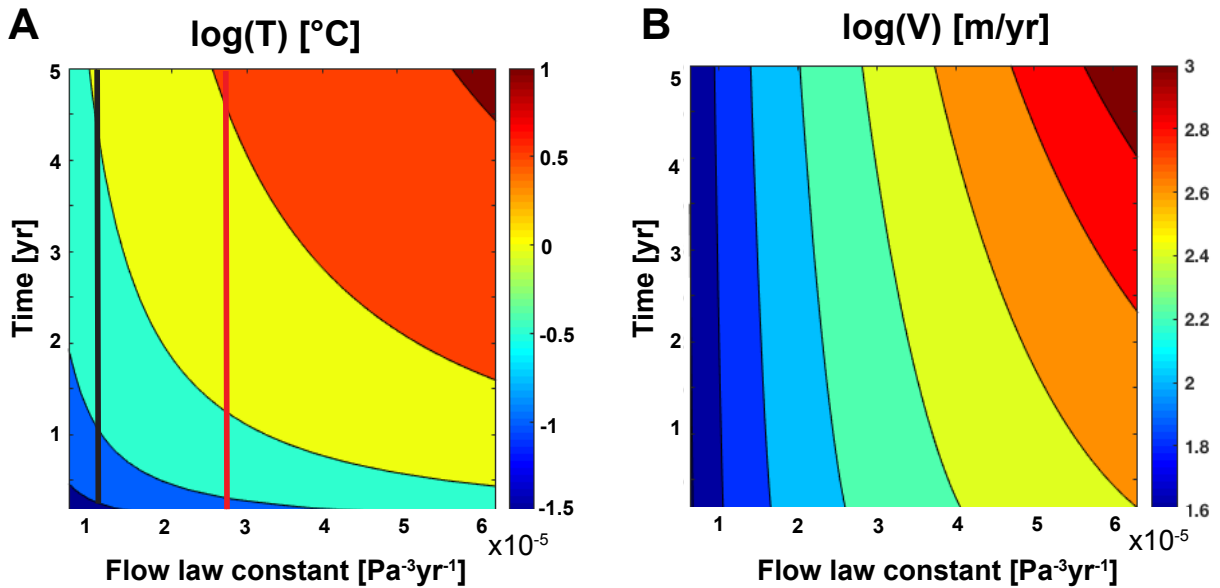


**Figure 3.13:** Dependence of A) the maximum temperature increase and B) velocity as a function of flow law constant  $a_0$  and time  $t$  presented as a contour plot. The dark lines are contour lines. The slab thickness  $L_z$  is set to 300 m inclined for a basal slope  $\alpha$  of  $10^\circ$ . Initial basal temperature  $T_0$  is set to  $-20^\circ\text{C}$ . Black solid line depicts the flow law constant from Paterson (1994), while the red solid line depicts the flow law constant from Clarke et al. (1977)

**Table 3.6:** Additional physical constants used for Figure 3.13

Symbol	Definition	Value	Unit
$a_0$	flow law constant	$[0.6 \text{ to } 6] \times 10^{-5}$	$Pa^{-3}yr^{-1}$
$Q$	creep activation energy	$60 \times 10^3$	$\frac{J}{mol}$
$T_0$	initial temperature	-20	$^{\circ}C$
$t$	time	[0.1 to 5]	$yr$
$\alpha$	mean bed slope	10	$^{\circ}$
$L_z$	ice thickness	300	$m$

Since in most investigations the flow law constant  $a_0$  values reported in Clarke et al. (1977) were used, in Figure 3.13 we highlight this value with a red solid line. Values of the flow law constant  $a_0$  reported in Paterson (1994) are depicted with a black solid line. Both flow law constant values correspond to the values used for cold ice ( $T < -10$ ) $^{\circ}C$ . The maximum temperature increase obtained with the Clarke et al. (1977) values are around 3.5  $^{\circ}C$ , while the maximum temperature increase using the Paterson (1994) values are 1.5  $^{\circ}C$ . Since the value of  $a_0$  is dependent on water content, grain size and the type of ice, and can vary by an order of magnitude, this can provide additional weakening mechanisms and increase the strain heating further.

## 3.7 Discussion and summary

### 3.7.1 Discussion of the results

We have presented the mathematical model suitable for describing the coupled thermo-mechanical fluid flow, in both their dimensional and non dimensional form. We have designed a numerical experiment with the goal of determining the processes occurring in thermo-mechanically coupled problems. The experiment is based around a standard two dimensional inclined box set-up. Three two dimensional and two one dimensional experiments were performed. A reference run, or model 1, is a fully coupled model. In model 2 we have neglected the advection terms in the temperature evolution, while model 3 also neglects the horizontal diffusion. Also, two different one dimensional models were constructed. The standard one dimensional model is obtained by neglecting all horizontal derivatives. This model is best suited for modelling the infinite channel behaviour since it ignores the longitudinal stress and pressure gradients. This model is therefore equivalent to the model used in the studies by Clarke et al. (1977) and Yuen and Schubert (1979b). The second one dimensional model is constructed from the two dimensional model, with the goal of approximating the effects of the longitudinal stress and pressure gradients by modifying the horizontal momentum equation and considering the longitudinal stress and pressure gradients to be constant in time and depth. We named this model the extended 1D model.

The importance of different terms was therefore investigated and compared with a reference model. It was shown that the pressure gradient/longitudinal stress gradient have a first order effect and can significantly alter the temperature distribution in a slab, while the effects of horizontal diffusion are of the second order and the differences between model 2 and 3 are negligible.

It has been shown that the extended 1D model can approximate the results of a more complex two dimensional model. This can be explained easily if one considers the extended 1D horizontal momentum balance and notice that the only change compared to the 1D case is the reduced value of the force term. Therefore, the 1D and 2D diffusion models (models 2 and 3) should give similar results if one consistently reduces the value of the basal shear stress. It should be noted here that an increase of the basal stress is also a possibility.

The results obtained in a reference run with a two way coupled model differ from the above cases, both spatially and in time. At the early stages ( $t < t_1$ ) both models 1 and 2 produce similar results. Since the stress distribution, and therefore strain heating, are almost equal over short time scales this means that the results can deviate only slightly for both temperature increase and velocity. For longer times scales, this does not need to be the case, since both stress and strain heating are spatially distributed differently. The reference model reaches the steady state at much earlier times compared to model 2. Model 2 shows negligible velocity increase and the maximum temperature increase is reduced to almost half of the value in model 2. These results show the stabilizing effect of the heat advection, and shows that at longer times scales advection plays an important role in stabilizing the temperature distribution in the slab.

Thereafter, the solution of a one dimensional model is analysed in more detail. During a single transient run, three separate regimes were identified: (i) transient (or the initial stage), where the temperature rises quickly in a short amount of time (ii) transition phase where the temperature rise is still noticeable, but the temperature rise slows down until the third phase is reached (iii) steady state. We have concentrated our analysis on the initial transient phase. We performed the parametrization of 1D numerical profiles of velocity (Equation 3.33) and temperature (Equation 3.28) using simple two parameter fits utilizing the functional form from the adiabatic solution (Equation 3.25).

Parameters that best describe the maximum temperature in a slab have been determined. The transient phase is best described by a non dimensional number  $Br$  obtained by multiplying the parameter  $\lambda$  and scaled time  $\frac{t}{t_d}$ . This fact also implies the similarity between the two solutions, one at higher value of  $\lambda$  and lower value of scaled time  $\frac{t}{t_d}$ , and the solution obtained with lower value of  $\lambda$  and higher value of scaled time  $\frac{t}{t_d}$ . Since this regime is not diffusion length dependent, the equivalent of this phase would be diffusion in a semi-infinite solid with a transient heat source at the wall. Further confirmation of this fact is the comparison of the

adiabatic solution with a non adiabatic transient phase, and a non adiabatic solution is just a slowed down version of the adiabatic case. This analysis shows that the stability parameter is not sufficient to determine the importance of the strain heating and our results therefore emphasize the importance of recognizing different regimes in thermo-mechanically coupled flow.

The obtained parametrization for the velocity increase (Equation 3.35) represents an increase due to strain heating and can therefore be used as an effective boundary condition that accounts for the coupled processes at scales of interest. The effective boundary condition is therefore a non-linear relationship between basal drag  $\tau_b$  and velocity increase  $\Delta V$  between mechanical model without strain heating and the thermo-mechanically coupled model. This relationship would represent the third type of the boundary conditions or the so called Robin boundary condition. The main difference compared with the more commonly used, linear sliding law, is that no ad hoc parameters, like the slip coefficient  $\beta$  are introduced into the model. Furthermore, the proposed effective boundary conditions arise due to a real physical coupling. In particular, the above analysis shows that a linear relationship between basal drag  $\tau_b$  and velocity increase  $\Delta V$  is not appropriate for describing basal sliding. Moreover, the non-linearity of the suggested functional form is sensitive to and controlled by physics related non-linearities; for example, power law rheology and Arrhenius dependence of viscosity on temperature. It is also consistent with linear stress versus depth dependence due to thin ice approximation of the stress balance.

There are several limitations in our approach which should be investigated further. For example, our analysis considers only the simplest geometrical set-up and boundary conditions. The reasoning behind this is the analysis of solely the viscous heating effects, by reducing the effects of additional factors to a bare minimum. Effects of varying geometry and therefore the effects of additional stress components are mimicked by considering the aspect ratios at which additional stresses have an important influence.

Our analysis is also valid only for the "cold" slab, where the ice temperature is below the melting temperature, and we have therefore not considered the situations where the ice starts to melt. If the melting temperature is reached then the model is not valid any more. Additionally, at the base we have ignored the influence of the geothermal heat flux. Further experiments could therefore involve adding an additional layer below the ice representing the bedrock, since lithosphere thermal inertia is an important physical process (Bueler and Brown, 2009). Furthermore, (Clarke et al., 1977) investigated, under the assumption of quasi-uniform flow, the influence of the vertical advection term and the authors have shown that inclusion of vertical advection can have both stabilizing and destabilizing effects on the flow. In their case, the velocity field is prescribed (approximated as a linear function of depth) and there is no proper feedback/coupling between the velocity (and hence also thickness) and temperature. Here, we have investigated the influence of both horizontal and vertical advection in

a two way coupled system. The results show that inclusion of both horizontal and vertical advection seems to have a stabilizing effect on the flow. We have followed the theoretical approach by Hutter (1983), Morland (1984) and Baral et al. (2001) and included both advection terms, since no shallow scaling justifies the inclusion of just the vertical advection term. An interesting fact, not to be ignored, is also the time needed for the fully coupled problem to converge to a steady state. While the model excluding the advection terms is still in its transient phase, the fully coupled model is already in its steady state phase and the balance between the advection, diffusion and strain heating is achieved. Therefore, in systems where the ratio between advection and the diffusion of temperature is high (high Peclet number), ignoring advection is not justified.

The most severe limitation of our model is probably the inability of the boundaries to evolve in time. The upper, bottom and lateral surfaces should be coupled to their respective kinematic conditions and therefore free to evolve in time. The time scales at which these boundaries can be considered fixed should be further investigated and are of great interest.

### 3.7.2 Comparison to previous literature

Studies investigating the strain heating often reduced the temperature equation to a boundary value problem of the following form:

$$\phi_{\xi\xi} + \lambda(\xi)e^{\frac{\phi}{1+\frac{\phi}{\theta}}} = 0 \quad (3.36)$$

where  $\lambda(\xi) = \lambda_b \xi^{n+1}$  is a function of depth  $\xi$ , while the exponential Arrhenius term is sometimes approximated with the Frank-Kamenetzky(FK) approximation (Frank-Kamenetzky, 1939) i.e  $e^{\frac{\phi}{1+\frac{\phi}{\theta}}} \approx e^{\phi}$  for small values of  $\phi$ .

Equations of this form are mathematically classified as a semilinear elliptic partial differential equation with exponential non linearity. When the exponential term is given by the FK approximation, the above boundary value problem (BVP) reduces to a equation often know across the literature by different names i.e Barenblatt, Bratu, Emden, Fowler, Frank-Kamenetskii, Gelfand or Liouville (Dupaigne, 2011). The arising multiplicity of the boundary value problem solutions is well studied in mathematics (Dupaigne, 2011) and across different fields (fluid dynamics; glaciology; geodynamics; chemical engineering). It is a well known fact that the multiplicity of the solutions is due to a non-linear exponential term arising from temperature dependent viscosity and it is not a result of the non linear dependence of a material rheology on the strain rate (Yuen et al., 1986).

Therefore, it is an established fact that for the values of the stability parameter  $\lambda$  lower than the critical, two solutions of the above BVP exist. They correspond to subcritical and

supercritical branches. Above the critical value of the stability parameter  $\lambda$ , no solution exists.

The thermal runaway, defined as an unbounded growth of temperature in a finite time, is hence associated with the non existence of the solution of the BVP problem. A distinction should therefore be made between the thermal runaway and thermal instabilities caused/induced by small perturbations to steady state solutions of the BVP problem.

Clarke et al. (1977) have argued that the number of solutions can actually depend on the form of the exponential term. They have found that if the exponential term is given by the Arrhenius law, there exists another solution of the BVP problem and they named this solution a hot branch. Hence, the authors concluded that for values of the stability parameter lower than critical, up to three solution of the stated BVP exist (i.e. subcritical, supercritical and hot branch), while above the critical value only one solution (hot branch) exists.

Yuen and Schubert (1979b) obtained two solution with the full Arrhenius term but only because the authors did not explore the whole parameter space, investigating only the ones physically possible. Otherwise the solutions should be equivalent to the ones obtained by Clarke et al. (1977). Since neither of the above studies approximated the  $\lambda(\xi)$ , the solution is only obtainable numerically.

Compared to the previous studies Fowler et al. (2010), reduced the Arrhenius term to the FK approximation and also approximated  $\lambda(\xi) \approx \lambda_b$  across the slab. Therefore, he further reduced the problem to  $\phi_{\xi\xi} + \lambda_b e^{\phi} = 0$ , which is susceptible to a known analytical solution and discussed in detail in Turcotte and Schubert (2014). The authors obtained the solutions on subcritical and supercritical branch. It should also be noted here that even though the analytical solution of the problem exists, the constants of integration (determined by the boundary conditions) can only be obtained numerically, or they can be further approximated like the authors did in the study. By approximating the constants, one is limited on the part of the branch where there is very little shear heating, and the solution is dictated by the basal boundary condition. A similar conclusion was already obtained by investigating the real world example and studying potential heat sources that have a major control on the fast flow of the Vestfonna ice cap, Svalbard (Schäfer et al., 2014).

On the other hand, by approximating the depth dependence of  $\lambda(\xi)$  by its constant maximum value  $\lambda_b$ , the amount of heat generated through the slab is much higher then it should actually be for the same value of  $\lambda$ . Therefore the critical value of the stability parameter reduces even further from  $\lambda_c \approx \frac{\pi^2}{4}$  to  $\lambda_c \approx 0.878$ .

The results in Fowler et al. (2010) also indicated that the supercritical branch is non physical, since its above the melting temperature. This somehow contradicts the results of Clarke et al. (1977) and Yuen and Schubert (1979b) , where it is easily seen that in certain situations the solutions on the supercritical branch can be below the melting temperature of ice. These

differences can be appointed either to the depth dependence of the parameter  $\lambda(\xi)$  or to the approximations made in obtaining the integration constants. Approximating the integration constants leads to a solution which effectively approximates the supercritical branch only at high temperatures above the melting temperature.

Even though the approach taken in Fowler et al. (2010) has the advantage that it is analytically tractable and allows for easy coupling to the thickness evolution equation, unfortunately it is not energy conservative and hence does not approximate the temperature well enough.

Both studies by Fowler et al. (2010) and Clarke et al. (1977) concluded that at the moment when thermal runaway should happen, the switch in boundary condition from cold to temperate stabilizes it and the critical value of the stability parameter changes to a larger value. Since the temperature in a slab is always lower than that at the base, there is no possibility of thermal runaway according to these studies. This is certainly not the case if one also looks at values of the stability parameter larger than the critical one. Compared to a cold based BC where the thermal runaway (first) occurs only at the base, in case of a temperate BC, the thermal runaway (highest temperature) first occurs at some distance above the base.

Contrary to the previous studies, we have here followed the approach of Fujita (1969). Fujita (1969) investigated the above BVP together with an associated initial boundary value problem (IBVP) from a theoretical point of view. A similar approach was also taken by Costa and Macedonio (2003) in their study of viscous heating in fluids with temperature dependent viscosity, where authors investigated the implication of viscous heating on the magma flow.

The associated IBVP is hence given by

$$\phi_\tau = \phi_{\xi\xi} + \lambda(\xi)e^{\frac{\phi}{1+\frac{\phi}{\theta}}} \quad (3.37)$$

Solving the given IBVP requires an initial condition  $\phi = \phi(\xi)$  and a set of boundary conditions to be prescribed (i.e.  $\phi(\xi = 0, t) = 0$  and  $\frac{\partial\phi}{\partial\xi}(\xi = H, t) = 0$ ). If, for example,  $\lambda(\xi)$  is fixed and constant in time, the given IBVP leads to the one of the solutions of the associated BVP:

- if the the values of the stability parameter or the initial condition are below the critical ones, after the transient period the solution of the IBVP will reach a steady state solution on the subcritical branch of the BVP problem.
- if the the value of the stability parameter is below the critical one and the initial condition is equal to the critical value, after the transient period the solution of the IBVP will reach a steady state solution on the supercritical branch of the BVP problem.
- in case the exponential term is the full Arrhenius term, the solution on the "hot branch" will have equivalent meaning to the thermal runaway. Therefore, if either the initial con-

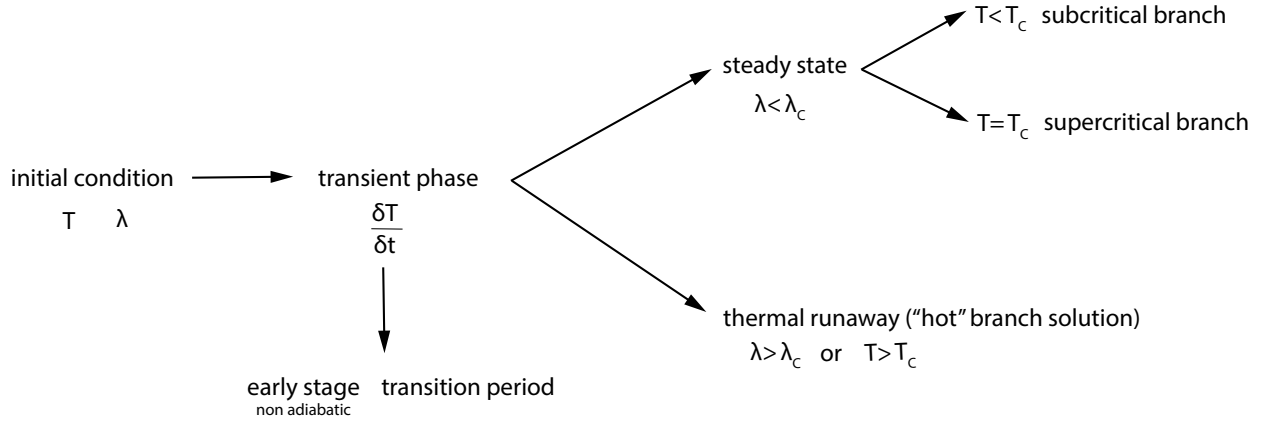


**Figure 3.14:** Schematic of a transient system behaviour.

dition or the stability parameter (or both) have values above critical, thermal runaway occurs after some transient period.

This is shown schematically in Figure 3.14.

In the previous section we have shown the importance of the transient stage, and therefore the importance of solving the IBVP instead of BVP problem. We have also shown the stabilizing effects of the additional stress components. Therefore, in a coupled system the stability parameter  $\lambda(\xi, t)$  actually varies both spatially and in time and it is determined from the mechanical model and the conservation of mass.

### 3.8 Conclusions

Thermal runaway, a physical instability due to a non linear exponential term arising from temperature dependent viscosity, is inherent to all thermo-mechanically coupled flows. Considering only the adiabatic case, which is a severe restriction, it is easily seen that a solution is certain to blow up in a finite amount of time. In the adiabatic case, the stress distribution, the initial temperature condition and the material properties are only factors influencing the efficiency of heat generation and the actual amount of time that is needed for the runaway to occur.

In the non adiabatic case, the diffusion can additionally dissipate the generated heat throughout the slab. How efficiently this can be done will determine either the critical time before

the runaway or the critical stability parameter below which the steady state solution can be reached. Below the critical stability parameter, diffusion is more efficient than the generation of heat by strain heating, while above the critical value the generation of heat is more efficient and the diffusion can again limit it for only a certain amount of time. The time needed for the temperature to reach steady state varies with the stability parameter, and close to the critical stability parameter it can reach values of up to 100 diffusion time scales. Hence there is a high probability that in this specific non realistic example, the change of slab size will occur much sooner than the temperature reaches the steady state.

We have further shown that the stability parameter is not a good predictor for determining the maximum basal temperature increase and hence the importance of strain heating. To establish a parameter useful for predicting basal temperature increase due to the strain heating we have introduced a parameter  $Br$ . This parameter takes into consideration the fact that diffusion has limited time to influence the flow.

The stability parameter, and hence also the introduced  $Br$  parameter, strongly depends on the state of the stress field in the slab, and solving a full mechanical model or their shallow approximations can affect its value. The fact that both velocity and temperature fields can be well approximated with a modified 1D model tells us that shallow approximation has slightly more limited applications, and that both stress models are prone to thermal runaway. Furthermore, the stability parameter greatly depends on material properties, like the flow law constant, which value is still uncertain and often varies by an order of magnitude. The uncertainties in the material properties can significantly affect the actual value of the stability parameter.

Furthermore, the proposed parametrization of 1D numerical profiles of velocity (Equation 3.33) and temperature (Equation 3.28) can be used as an effective boundary condition that accounts for the thermo-mechanically coupled processes at scales of interest. The effective boundary condition is therefore derived as a non-linear relationship between basal drag  $\tau_b$  and velocity increase  $\Delta V$ , where velocity increase  $\Delta V$  represents an velocity increase due to strain heating. Additionally it was shown that the non-linearity of the suggested functional form is sensitive to and controlled by physics related non-linearities. Hence, in cases where strain heating plays an important role, we argue that a linear relationship between basal drag  $\tau_b$  and velocity increase  $\Delta V$  is not appropriate for describing basal sliding.

The slab boundaries evolve due to the velocity field and the prescribed mass balance, and therefore the time evolution of the temperature field is limited by a certain amount of time. Consequently in situations where strain heating is important, one can easily expect the temperature, and hence velocity and the stress state, to be in a transient state.

The limited time also limits the influence of advection, but the effects of advection and the change of the slab size should be further investigated.

## Bibliography

- Aschwanden, A., Bueler, E., Khroulev, C., Blatter, H., 2012. An enthalpy formulation for glaciers and ice sheets. *Journal of Glaciology* 58(209), 441–457.
- Bamber, J. L., Vaughan, D. G., Joughin, I., 2000. Widespread Complex Flow in the Interior of the Antarctic Ice Sheet. *Annals of Glaciology* 287, 1248–1250.
- Baral, D., Hutter, K., Greve, R., 2001. Asymptotic theories of large-scale motion, temperature, and moisture distribution in land-based polythermal ice sheets: A critical review and new developments. *Applied Mechanics Reviews* 54, 215–256.
- Bassis, J., 2010. Hamilton-type principles applied to ice-sheet dynamics: new approximations for large-scale ice sheet flow. *Journal of Glaciology* (56)97, 497–513.
- Blatter, H., 1995. Velocity and stress fields in grounded glaciers: a simple algorithm for including deviatoric stress gradients. *Journal of Glaciology* 5(138), 333–344.
- Bons, P. D., Kleiner, T., Llorens, M., Prior, D. J., Sachau, T., Weikusat, I., Jansen, D., 2018. Greenland Ice Sheet: Higher nonlinearity of ice flow significantly reduces estimated basal motion. *Geophysical Research Letters* 45, 6542–6548.
- Brinkerhoff, D. J., Johnson, J. V., 2013. Data assimilation and prognostic whole ice sheet modelling with the variationally derived, higher order, open source, and fully parallel ice sheet model VarGlaS. *The Cryosphere* 7, 1161–1184.
- Brinkerhoff, D. J., Johnson, J. V., 2015. Dynamics of thermally induced ice streams simulated with a higher-order flow model. *Journal of Geophysical Research: Earth Surface* 120, 1743–1770.
- Brown, J. A. K., 2011. Computational methods for ice flow simulation. Ph.D thesis, ETH Zürich.
- Bueler, E., 2008. Lessons from the short history of ice sheet model intercomparison. *The Cryosphere Discussions* 2, 399–412.
- Bueler, E., Brown, J., 2009. Shallow shelf approximation as a "sliding law" in a thermomechanically coupled ice sheet model. *Journal of Geophysical research* 114, F03008.
- Bueler, E., Brown, J., Lingle, C., 2007. Exact solutions to the thermomechanically coupled shallow-ice approximation: effective tools for verification. *Journal of Glaciology* 53(182), 499–516.

- Burg, J.-P., Gerya, T. V., 2005. The role of viscous heating in Barrovian metamorphism of collisional orogens: thermomechanical models and application to the Lepontine Dome in the Central Alps. *Journal of Metamorphic Geology* 23, 75–95.
- Chandler, D. M., Hubbard, A. L., Hubbard, B. P., Nienow, P. W., 2006. A Monte Carlo error analysis for basal sliding velocity calculations. *Journal of Geophysical Research* 111, F04005.
- Choi, E., Tan, E., Lavier, L. L., Calo, V. M., 2013. DynEarthSol2D: An efficient unstructured finite element method to study long-term tectonic deformation. *Journal of Geophysical Research: Solid Earth* 118(5), 2429–2444.
- Clarke, G. K. C., 2005. Subglacial processes. *Annual Review of Earth and Planetary Sciences* 33, 247–276.
- Clarke, G. K. C., Nitsan, U., Paterson, W. S. B., 1977. Strain heating and creep instability in glaciers and ice sheets. *Reviews of geophysics and space physics* 15 (2), 235–247.
- Cohen, D., Iverson, N. R., Hooyer, T. S., Fischer, U. H., Jackson, M., Moore, P. L., 2005. Debris-bed friction of hard-bedded glaciers. *Journal of Geophysical Research* 110, F02007.
- Cook, S., 2012. *CUDA Programming*. Morgan Kaufmann, Elsevier.
- Costa, A., Macedonio, G., 2003. Viscous heating in fluids with temperature-dependent viscosity: implications for magma flows. *Nonlinear Processes in Geophysics* 10, 545–555.
- Cundall, P., Coetzee, M., Hart, R., Varona, P., 1993. *FLAC users manual*. Itasca Consulting Group, 23–26.
- Dold, J., 1985. Analysis of the early stage of thermal runaway. *The Quarterly Journal of Mechanics and Applied Mathematics* 38(3), 361–387.
- Dupaigne, L., 2011. *Stable solutions of elliptic partial differential equations*. Vol. 1. Chapman and Hall, CRC.
- Duretz, T., Räss, L., Podladchikov, Y., Schmalholz, S., 2019. Resolving thermomechanical coupling in two and three dimensions: spontaneous strain localization owing to shear heating. *Geophysical Journal International* 216, 365–379.
- Egholm, D., M.F., K., Clark, C., Lesemann, J., 2011. Modeling the flow of glaciers in steep terrains: The integrated second-order shallow ice approximation (iSOSIA). *Journal of Geophysical Research: Earth Surface* 116, F02012.
- Fowler, A., 1980. The existence of multiple steady states in the flow of large ice masses. *Journal of Glaciology* 25 (91), 183–184.

- Fowler, A., 1986. Sub-temperate basal sliding. *Journal of Glaciology* 32(110), 3–5.
- Fowler, A., 2013. Correspondence: Thermal convection in ice sheets. *Journal of Glaciology* 59(213), 190–192.
- Fowler, A., Toja, R., Vazquez, C., 2010. Temperature-dependent shear flow and the absence of thermal runaway in valley glaciers. *Proceedings of Royal Society A* 466 (2114), 363–382.
- Fowler, A. C., Johnson, C., 1996. Ice-sheet surging and ice-stream formation. *Annals of Glaciology* 23, 68–73.
- Fowler, A. C., Larson, D., 1980a. The uniqueness of steady state flows of glaciers and ice sheets. *Geophysical Journal International* 63 (1), 333–345.
- Fowler, A. C., Larson, D., 1980b. Thermal stability properties of a model of glacier flow. *Geophysical Journal International* 63 (1), 347–359.
- Frank-Kamenetzky, D. A., 1939. Calculation of thermal explosion limits. *Acta physicochimica U.R.S.S* 10, 365–370.
- Frankel, S. P., 1950. Convergence rates of iterative treatments of partial differential equations. *Mathematical Tables and Other Aids to Computation* 4(30), 65–75.
- Fujita, H., 1969. On the nonlinear equations  $\Delta u + e^u = 0$  and  $\frac{\partial v}{\partial t} = \Delta v + e^v$ . *Bulletin of the American Mathematical Society* 75, 132–135.
- Gagliardini, O., Zwinger, T., 2008. The ISMIP-HOM benchmark experiments performed using the finite-element code Elmer. *The Cryosphere* 2, 67–76.
- Gagliardini, O., Zwinger, T., Gillet-Chaulet, F., Durand, G., Favier, L., de Fleurian, B., Greve, R., Malinen, M., Martín, C., Råback, P., Ruokolainen, J., Sacchetti, M., Schäfer, M., Seddik, H., Thies, J., 2013. Capabilities and performance of Elmer/Ice, a new-generation ice sheet model. *Geoscientific Model Development* 6, 1299–1318.
- Garofalo, F., 1963. An empirical relation defining the stress dependence of minimum creep rate in metals. *Transactions of the Metallurgical Society of AIME* 227, 351–356.
- Gerya, T., 2009. *Introduction to Numerical Geodynamic Modelling*. Cambridge University Press, Cambridge, United Kingdom.
- Gerya, T. V., Yuen, D. A., 2003. Characteristics-based marker-in-cell method with conservative finite-differences schemes for modeling geological flows with strongly variable transport properties. *Physics of the Earth and Planetary Interiors* 140(4), 293–318.

- Gilbert, A., Gagliardini, O., Vincent, C., Wagnon, P., 2014. A 3-D thermal regime model suitable for cold accumulation zones of polythermal mountain glaciers. *Journal of Geophysical Research:Earth Surface* 119, 8761893.
- Glen, J., 1955. The creep of polycrystalline ice. *Proceedings of the Royal Society of London A* 228, 519–538.
- Glen, J. W., 1952. The flow law of ice from measurements in glacier tunnels, laboratory experiments and the Jungfraufirn borehole experiment. *Journal of Glaciology* 2, 111–114.
- Goldberg, D., 2011. A variationally-derived, depth-integrated approximation to the Blatter Pattyn balance. *Journal of Glaciology* 57(201), 157–170.
- Gong, Y., Zwinger, T., Åström, J., Altena, B., Schellenberger, T., Gladstone, R., Moore, J. C., 2018. Simulating the roles of crevasse routing of surface water and basal friction on the surge evolution of Basin 3, Austfonna ice cap. *The Cryosphere* 12, 1563–1577.
- Grigoryan, S., Krass, M., Shumskiy, P., 1976. Mathematical model of a three dimensional non-isothermal glacier. *Journal of Glaciology* 7(77), 401–417.
- Gruntfest, I. J., 1963. Thermal feedback in liquid flow: Plane shear at constant stress. *Transactions of The Society of Rheology* 7, 195–207.
- Harlow, F. H., Welch, E., 1965. Numerical calculation of time-dependent viscous flow of fluid with free surface. *Physics of Fluids* 8(12), 2182–2189.
- Haseloff, M., Schoof, C., Gagliardini, O., 2018. The role of subtemperate slip in thermally driven ice stream margin migration. *The Cryosphere* 12, 2545–2568.
- Hewitt, I. J., Schoof, C., 2017. Models for polythermal ice sheets and glaciers. *The Cryosphere* 11, 541–551.
- Hindmarsh, R. C. A., 2004. Thermoviscous stability of ice-sheet flows. *Journal of fluid mechanics* 502, 17–40.
- Hindmarsh, R. C. A., 2006. Stress gradient damping of thermoviscous ice flow instabilities. *Journal of Geophysical Research:Earth Surface* 111, B12409.
- Hindmarsh, R. C. A., 2009. Consistent generation of ice-streams via thermo-viscous instabilities modulated by membrane stresses. *Geophysical research letters* 36, L06502.
- Hughes, T., 2009. Thermal convection and the origin of ice streams. *Journal of Glaciology* 55(191), 524–536.
- Hughes, T., 2012. Correspondence. Are ice-stream tributaries the surface expression of thermal convection rolls in the Antarctic ice sheet? *Journal of Glaciology* 58(210), 811–814.

- Hutter, K., 1983. Theoretical glaciology: material science of ice and the mechanics of glaciers and ice sheets. Vol. 1. Springer.
- Huybrechts, P., Payne, T., 1996. The EISMINT benchmarks for testing ice-sheet models. *Annals of Glaciology* 23, 1–12.
- Isaac, T., Stadler, G., Ghattas, O., 2015. Solution of Nonlinear Stokes Equations Discretized by High-order Finite Elements on Nonconforming and Anisotropic Meshes, with Application to Ice Sheet Dynamics. *SIAM Journal on Scientific Computing*, B804–B833.
- Jarosch, A., 2008. Icetools: a full Stokes finite element model for glaciers. *Computers and Geosciences* 34, 1005–1014.
- Johns, L. E., Narayanan, R., 1997. Frictional heating in plane Couette flow. *Proceedings of Royal Society A* 453 (1963), 1653–1670.
- Joughin, I., Smith, B., Howat, I., Scambos, T., Moon, T., 2010. Greenland flow variability from ice-sheet-wide velocity mapping. *Journal of Glaciology* 56, 416–430.
- Jouvet, G., Picasso, M., Rappaz, J., Blatter, H., 2008. A new algorithm to simulate the dynamics of a glacier: theory and applications. *Journal of Glaciology* 54, 801–811.
- Kelley, C. T., Keyes, D. E., 1998. Convergence Analysis of Pseudo-Transient Continuation. *SIAM Journal on Numerical Analysis* 35(2), 508–523.
- Kelley, C. T., Liao, L.-Z., 2013. Explicit pseudo-transient continuation. *Pacific Journal of Optimization* 9(1), 77–91.
- Kleiner, T., Rückamp, M., Bondzio, J. H., Humbert, A., 2015. Enthalpy benchmark experiments for numerical ice sheet models. *The Cryosphere* 9, 217–228.
- Krabbendam, M., 2016. Sliding of temperate basal ice on a rough, hard bed: creep mechanisms, pressure melting, and implications for ice streaming. *The Cryosphere* 10, 1915–1932.
- Kyrke-Smith, T. M., Katz, R. F., Fowler, A. C., 2015. Subglacial hydrology as a control on emergence, scale, and spacing of ice streams. *Journal of Geophysical Research:Earth Surface* 120, 1501–1514.
- Landau, L. D., Lifshitz, E. M., 1963. *Fluid Mechanics*. Vol. 1. Pergamon Press.
- Larour, E., Seroussi, H., Morlighem, M., Rignot, E., 2012. Continental scale, high order, high spatial resolution, ice sheet modeling using the Ice Sheet System Model (ISSM). *Journal of Geophysical research* 117, 1–20.

- Leng, W., Ju, L., Gunzburger, M., Price, S., 2014. A Parallel Computational Model for Three-Dimensional, Thermo-Mechanical Stokes Flow Simulations of Glaciers and Ice Sheets. *Computer Physics Communications* 16(4), 1056–1080.
- Leng, W., Ju, L., Gunzburger, M., Ringler, T., 2012. A parallel high-order accurate finite element nonlinear Stokes ice sheet model and benchmark experiments. *Journal of Geophysical Research* 117, F01001.
- Lliboutry, L. A., 1987. *Very Slow Flows of Solids: Basics of Modeling in Geodynamics and Glaciology*. Vol. 7. Springer Netherlands.
- MacAyeal, D. R., 1992. The basal stress distribution of Ice Stream E, Antarctica, inferred by control methods. *Journal of Geophysical Research: Earth Surface* 97, 595–603.
- Moore, P., Iverson, N., Cohen, D., 2009. Ice flow across a warm-based/cold-based transition at a glacier margin. *Annals of Glaciology* 50 (52), 1–8.
- Morland, L., 1984. Thermomechanical balances of ice sheet flows. *Geophysical and Astrophysical Fluid Dynamics* 29, 237–266.
- Nye, J. F., 1953. The flow law of ice from measurements in glacier tunnels, laboratory experiments and the Jungfraufirn borehole experiment. *Proceedings of Royal Society A* 219, 477–489.
- Ogawa, M., Schubert, G., Zebib, A., 1991. Numerical simulations of three-dimensional thermal convection in a fluid with strongly temperature dependent viscosity. *Journal of Fluid Mechanics* 233, 299–328.
- Omlin, S., 2017. Development of massively parallel near peak performance solvers for three-dimensional geodynamic modelling. Ph.D thesis, University of Lausanne.
- Patankar, S., 1980. *Numerical Heat Transfer and Fluid Flow*, Comput. Methods Mech. Thermal Sci. Ser. CRC Press, Boca Raton, Fla.
- Paterson, W., 1994. *The physics of glaciers*. Third edition. Elsevier.
- Pattyn, F., 2003. A new three-dimensional higher-order thermomechanical ice sheet model: basic sensitivity, ice stream development and ice flow across subglacial lakes. *Journal of Geophysical Research* 108(B8), 2382.
- Pattyn, F., Perichon, L., Aschwanden, A., Breuer, B., de Smedt, B., Gagliardini, O., Gudmundsson, G. H., Hindmarsh, R. C. A., Hubbard, A., Johnson, J. V., Kleiner, T., Konovalov, Y., Martin, C., Payne, A. J., Pollard, D., Price, S., Rückamp, M., Saito, F., Soucek, O., Sugiyama, S., , Zwinger, T., 2008. Benchmark experiments for higher-order and full-Stokes ice sheet models (ISMIP- HOM). *The Cryosphere* 2, 95–108.

- Payne, A., Dongelmans, P., 1997. Self-organization in the thermomechanical flow of ice sheets. *Journal of Geophysical research* 102(B6), 219–233.
- Payne, T., Baldwin, D., 2000. Analysis of ice-flow instabilities identified in the EISMINT intercomparison exercise. *Annals of Glaciology* 30, 204–210.
- Payne, T., Huybrechts, P., Abe-Ouchi, A., Calov, R., Fastook, J., Greve, R., Marshall, S., Marsiat, I., Ritz, C., Tarasov, L., Thomassen, M., 2000. Results from the EISMINT model intercomparison: the effects of thermomechanical coupling. *Journal of Glaciology* 46(153), 227–238.
- Perego, M., Gunzburger, M., Burkardt, J., 2012. Parallel finite element implementation for higher order ice-sheet models. *Journal of Glaciology* 58(207), 76–88.
- Poliakov, A. N. B., Cundall, P. A., Podladchikov, Y. Y., Lyakhovsky, V. A., 1993. An explicit inertial method for the simulation of viscoelastic flow: An evaluation of elastic effects on diapiric flow in two- and three-layers models. *Flow and Creep in the Solar Systems: Observations, Modeling and Theory*, 175–195.
- Pollard, D., DeConto, R. M., 2012. Description of a hybrid ice sheet-shelf model, and application to Antarctica. *Geoscientific Model Development* 5, 1273–1295.
- Räss, L., Simon, N., Podladchikov, Y., 2018. Spontaneous formation of fluid escape pipes from subsurface reservoirs. *Scientific Reports* 8 (11116).
- Robin, G. d. Q., 1955. Ice movement and temperature distribution in glaciers and ice sheets. *Journal of Glaciology* 2 (18), 523–532.
- Saito, F., Abe-Ouchi, A., Blatter, H., 2006. European Ice Sheet Modelling Initiative (EISMINT) model intercomparison experiments with first-order mechanics. *Journal of Geophysical Research* 111, F02012.
- Schäfer, M., Gillet-Chaulet, F., Gladstone, R., Pettersson, R., Pohjola, V., Strozzi, T., Zwinger, T., 2014. Assessment of heat sources on the control of fast flow of Vestfonna ice cap, Svalbard. *The Cryosphere* 8, 1951–1973.
- Schoof, C., 2005. The effect of cavitation on glacier sliding. *Proceedings of Royal Society A* 461, 609–627.
- Schoof, C., Hewitt, I. J., 2016. A model for polythermal ice incorporating gravity-driven moisture transport. *Journal of fluid mechanics* 797, 504–535.
- Schoof, C., Hindmarsh, R., 2010. Thin film flows with wall slip: an asymptotic analysis of higher order glacier flow models. *The Quarterly Journal of Mechanics and Applied Mathematics* 63(1), 73–114.

- Schubert, G., Yuen, D., 1982. Initiation of ice ages by creep instability and surging of the East Antarctic ice sheet. *Nature* 296 (5853), 127–130.
- Shapiro, D. R., Joughin, I., Poinar, K., Morlighem, M., Gillet-Chaulet, F., 2016. Basal resistance for three of the largest Greenland outlet glaciers. *Journal of Geophysical Research: Earth Surface* 121, 168–180.
- Shin, D., Strikwerda, J. C., 1997. Inf-Sup conditions for finite-difference approximations of the Stokes equations. *Journal of the Australian Mathematical Society. Series B. Applied Mathematics* 39(01), 121–134.
- Solomon, S., Qin, D., Manning, M., Chen, Z., Marquis, M., Averyt, K., Tignor, M., Miller, H., 2007. The physical science basis p.235–337, IPCC report AR4 . New York and Cambridge: Cambridge University Press.
- Stearns, L. A., Van der Veen, C. J., 2018. Friction at the bed does not control fast glacier flow. *Science* 361(6399), 273–277.
- Steinemann, S., 1958. Experimentelle Untersuchungen zur Plastizität von Eis. *Beiträge zur Geologie der Schweiz. Hydrologie* 10.
- Suckale, J., Platt, J., Perol, T., Rice, J., 2014. Deformation-induced melting in the margins of the West Antarctic ice streams. *Journal of Geophysical Research:Earth Surface* 119, 1004–1025.
- Tezaur, I. K., Perego, M., Salinger, A. G., Tuminaro, R. S., Price, S. F., 2015. Albany/FELIX: a parallel, scalable and robust, finite element, first-order Stokes approximation ice sheet solver built for advanced analysis. *Geoscientific Model Development* 8, 1197–1220.
- Turcotte, D., Schubert, G., 2014. *Geodynamics* 3rd Edition. Vol. 1. Cambridge University Press.
- Van der Veen, C., Oerlemans, J., 1984. Global thermodynamics of a polar ice sheet. *Tellus* 36A, 228–235.
- Wong, W. A., Jonas, J. J., 1968. Aluminum extrusion as a thermally activated process. *Transactions of the Metallurgical Society of AIME* 242, 2271–2280.
- Yang, X. I., Mittal, R., 2014. Acceleration of the Jacobi iterative method by factors exceeding 100 using scheduled relaxation. *Journal of Computational Physics* 274, 695–708.
- Yuen, D., Saari, M., Schubert, G., 1986. Explosive growth of shear heating instabilities in the down-slope creep of ice sheets. *Journal of Glaciology* 32 (112), 314–320.

- Yuen, D., Schubert, G., 1977. Asthenospheric shear flow: thermally stable or unstable. *Geophysical research letters* 4 (11), 503–506.
- Yuen, D., Schubert, G., 1979a. On the stability of frictionally heated shear flows in the asthenosphere. *Geophysical Journal International* 57 (1), 189–207.
- Yuen, D., Schubert, G., 1979b. The role of shear heating in the dynamics of large ice masses. *Journal of Glaciology* 4 (90), 195–212.
- Zhang, T., Ju, L., Leng, W., Price, S., Gunzburger, M., 2015. Thermomechanically coupled modelling for land-terminating glaciers: a comparison of two-dimensional, first-order and three-dimensional, full-Stokes approaches. *Journal of Glaciology* 61(228), 702–711.
- Zoet, L. K., Iverson, N. R., 2016. Rate-weakening drag during glacier sliding. *Journal of Geophysical Research: Earth Surface* 121, 1206–1217.
- Zwinger, T., Greve, R., Gagliardini, O., Shiraiwa, T., Lyly, M., 2007. A full Stokes-flow thermo-mechanical model for firn and ice applied to the Gorshkov crater glacier, Kamchatka. *Annals of Glaciology* 45, 29–37.



## CHAPTER 4

---

Perspectives

---

## 4.1 General remarks

In many instances it is seen that algorithms are not well adapted to the current trends in hardware industry, i.e. massive parallelism. Furthermore, algorithms can be limited by the memory restriction imposed by the usage of the direct methods or relatively poor performance of the iterative solvers in three dimensions. Therefore, due to computational limitations three dimensional modelling of the physical processes is generally restricted to low numerical resolution or is reserved to the usage of supercomputers.

We have addressed these challenges by developing an numerical model based on the iterative pseudo-transient (PT) continuation method. The same method was already successfully applied by Duretz et al. (2019) for studying spontaneous strain localisation in geodynamical applications and Räss et al. (2018) in studying spontaneous channelling of porous fluids. Method relies on the usage of matrix-free stencil based method, therefore ensuring minimal, local and regular memory access. These algorithm properties are well suited for modern massively parallel hardware accelerators like the computer graphic cards (GPU). The performance of which strongly depends on the memory access and transfer speed and not the actual speed of calculations.

In this thesis, we have reported the performance of the developed algorithm on various graphic cards. We have shown that the usage of high end gaming graphic cards have enabled us to perform high resolution three dimensional modelling of the thermo-mechanically coupled ice flow, where we have further established that a high numerical (spatial and temporal) resolution is needed to capture the non linearities associated with the ice flow rheology. Unfortunately, the need to recognise moderate enhancements of gradients near the base is numerically achieved only by a small number of computationally tractable shallow ice models, while some more complete continuum models often use very low vertical numerical resolution while modelling coupled flow. We have further shown that implicit coupling results in a slightly more localized solution and its in better agreement with a referent solution. The coupling method can hence have significant influence in a more complete thermal model when advection is allowed to operate and the flow problem becomes even more non linear and two way coupled.

We have further investigated localization and temporal evolution of strain heating on synthetic cases using a numerical approach. Strain heating is the main internal volumetric heat source in the conservation of energy. Its influence is dynamic and it is dependent on the distribution of stress and strain rate. Hence it can vary significantly both in space and time. It can be a significant heat source in some situations, while non important in others.

Additionally, strain heating can operate on different time scales and it can therefore limit the influence of diffusion. We have determined that two distinctive regimes are usually associated

with the strain heating; transient and steady state, and we have determined that in a steady state regime strain heating can significantly influence the ice flow only in situations when diffusion is close to balance the strain heating term. In other words, close to the so-called critical stability parameter. Furthermore, our results show that large stress gradients in the momentum balance can have first order influence on the strain heating distribution and therefore significantly slow down the process. Therefore, it can be said that the distribution of stress in an ice slab affects the time scale on which strain heating operates.

Our results therefore corroborates conclusions of many previous studies (Grigoryan et al., 1976; Van der Veen and Oerlemans, 1984; Yuen et al., 1986; Yuen and Schubert, 1979b) where authors identified that a first order balance is between temperature evolution, ice advection and strain heating while diffusion is often important only in a varying conductive boundary layer.

## 4.2 Future work

In future work it would be interesting to continue with the research on numerical properties and behaviour of the model. Specifically, investigating the influence of the numerical coupling method when advection and the change of material properties (evolution of the boundaries) are included in the model. Therefore, simultaneous, implicit, solution of velocity, temperature and material properties (i.e. geometry change) should be sought. Additionally, the magnitude of numerical errors introduced by the first order upwind scheme compared to flux conservative schemes like total variation diminishing (TVD) type should be investigated for an advection dominated system. Furthermore, since velocity and stress change on the time-scale governed by the temperature evolution the change of geometry can therefore occur very localized in time and space and can further evolve across the boundary. It is imperative that this kind of behaviour is not filtered out by the use of overly diffusive numerical schemes.

One additional aspect that should be considered in future investigation is the introduction of conservation laws due to their geometrical structure into the model and therefore the conservation of total energy. For example, for single phase model, conservation of mass, energy and momentum requires variations of density with temperature. The importance of which is still discussed in the literature (Fowler, 2013; Hughes, 2009, 2012). Change of density over time implies that fluid had either compressed or expanded. This can introduce additional gradients in the system and their influence should be investigated. Therefore enforcing that the divergence of flow velocity vanishes in a coupled model can easily lead to errors in mass conservation. Magnitude and significance of this errors should be quantified.

The main theme across this thesis is numerical modelling of thermo-mechanically coupled ice flow. The problem of determining the thermal field consistent with the current flow condi-

tions is a complementary and closely related to the problem of determining basal boundary conditions. By prescription of the slip/no slip transition into the continuum formulation we introduce non-physical singularities into the model (Brown, 2011). The physically based basal boundary condition should satisfy conservation laws (linear momentum, mass, energy and momentum of momentum) and should therefore be thermodynamically admissible. To address this problem a sub-temperate sliding law, like the one proposed in (Fowler, 1986) should be investigated further and results should be compared with different sliding laws currently used across the literature.

In this thesis we have investigated only the viscous rheology. Different rheologies should be further investigated. For example visco-elasto-plastic rheology.

---

## Curriculum vitae

---

### Education

- Master in physics and geophysics, University of Zagreb, Croatia, 2012.
- Bachelor in geophysics, University of Zagreb, Croatia, 2009.
- Secondary school graduation, Pazinski kolegij, Pazin, Croatia, 2004.

### Fields of Research Interest

Glaciology, ice flow, TMC coupling, Numerical modelling, High-Performance Computing, GPU.

### Memberships

- Member of the Swiss Geocomputing Centre (SGC)
- Member of the European Geoscience Union (EGU)

### Teaching Experience

- BSc, Numerical Modelling, Unil 2016.



### Contributions to international conferences

- Licul, A., Herman, F., Podladchikov, Y., Räss, L. and Omlin, S. (2015). Full Stokes glacier model on GPU. EGU2015-4958, Geophysical Research Abstracts, *submitted to EGU General assembly, 2015, Vienna, Austria*
- Licul, A., Herman, F., Podladchikov, Y., Räss, L. and Omlin, S. (2015). Full Stokes glacier modeling on graphic cards, Platform Geosciences, Swiss Academy of Science, *submitted to Swiss Geoscience Meeting, 2015*
- Licul, A., Herman, F., Podladchikov, Y., Räss, L. and Omlin, S. (2016). Multi-GPU three dimensional Stokes solver for simulating glacier flow. EGU2016-13008, Geophysical Research Abstracts, *submitted to EGU General assembly, 2015, Vienna, Austria*
- Räss, L., Omlin, S., Licul, A., Podladchikov, Y. and Herman, F. (2016). Efficient development of memory bounded geo-applications to scale on modern supercomputers. EGU2016-13605, Geophysical Research Abstracts, *submitted to EGU General assembly, 2016, Vienna, Austria*
- Visnjevic, V., Herman, F. and Licul, A. (2016). Insight into glacier climate interaction: reconstruction of the mass balance field using ice extend data. EGU2016-13243, Geophysical Research Abstracts, *submitted to EGU General assembly, 2016, Vienna, Austria*

**Summer schools and workshops**

- Karthaus Summer School on Ice Sheets and Glaciers in the Climate System, September 2014, Italy
- Elmer/Ice course: Glacier modelling using Elmer/ICE, October 2016, University of Oslo, Norway

---

## Acknowledgements

---

Firstly, I would like to express my sincere gratitude to my advisor Prof. Dr. Frédéric Herman for his continuous support during my PhD study. His guidance helped me in all the time of research and writing of this thesis. I am very grateful for the given opportunity to work on this project.

I am also very grateful to Prof. Dr. Yury Podladchikov (also the internal expert of my thesis committee) for his guidance during my PhD study and constant feedback on all the aspects of this project. Without your ideas and help this thesis would not have been achievable.

Additionally, I would like to thank the external expert of my thesis committee Dr. Thomas Zwinger for his insightful comments which further improved my PhD thesis. A special thanks to Prof. Dr. Christian Kull for presiding over my thesis defence.

I am very grateful to Dr. Ludovic Räss from whom I have learned a great deal about programming, computer graphic cards and science in general. I really enjoyed our discussions and collaboration. I greatly appreciate the time and work you have invested in this project.

I would also like to thank to Dr. Thibault Duretz and Dr. Samuel Omlin for theirs scientific advices and discussions which significantly contributed to the work presented in this thesis.

Further, I would like to express my immense gratitude to Prof. Mario Turić and Prof. Dr. Giuliana Verbanac with a few words in Croatian. Hvala Vam što ste već tokom mog ranog školovanja prenijeli na mene ljubav prema znanosti i istraživanju.

Lastly, I am especially thankful to my family. Hvala Vam na beskrajnoj podršci i iskazanom povjerenju. There is no words to express my gratitude to my wife Ivana. You are always being there for me and for supporting me. Thank you for helping me to follow my dreams.